MODELING OF TURBULENT PARTICULATE FLOW IN THE RECIRCULATION ZONE DOWNSTREAM OF A BACKWARD FACING STEP PRECEDING A POROUS MEDIUM

By

ALOK DANGE

Bachelor of Science in Mechanical Engineering

University of Mumbai

Mumbai, India

2005

Submitted to the Faculty of the
Graduate College of the
Oklahoma State University
in partial fulfillment of
the requirements for
the Degree of
MASTER OF SCIENCE
December, 2010

MODELING OF TURBULENT PARTICULATE FLOW IN THE RECIRCULATION ZONE DOWNSTREAM OF A BACKWARD FACING STEP PRECEDING A POROUS MEDIUM

Thesis Approved:

Dr. F. W. Chambers

Thesis Adviser

Dr. D. G. Lilley

Dr. K. A. Sallam

Dr. Mark E. Payton

Dean of the Graduate College

ACKNOWLEDGMENTS

I would like to thank my academic adviser Dr. Chambers, for guiding me throughout the project. It was an amazing learning experience to work under his guidance. His emphasis on minute details has been instrumental in successfully completing this study.

My sincere thanks to Dr. Lilley and Dr. Sallam who spent time to review my thesis and attend my presentation.

I would also like to thank my room-mates, my friends and my family back home in India who supported me in every aspect.

TABLE OF CONTENTS

Chapter Page

1. INTRODUCTION 1

1.1 Background 1
1.2 Objective 3

2. REVIEW OF LITERATURE 4

2.1 Flow over a backward facing step 4
2.2 Backward facing step flow with porous medium 10
2.3 Backward facing step flow with particle injections 15

3. TURBULENCE MODELING 19

3.1 Introduction 19
3.2 Reynolds averaged Navier Stokes (RANS) 19
3.3 Classification of Turbulence models 20
3.4 Two equation models 21
3.4.1 *k*-ω model 22
3.4.2 *k*-ε model 23
3.4.3 *k*-ω SST model 24
3.4.4 *k*-ε RNG model 25
3.4.5 Large eddy simulation 27
3.4.6 Direct numerical simulation 27
3.5 Near wall treatment 28
3.5.1 Near wall treatment for *k*-ω and *k*-ε models 29

Chapter page

3.6 Modeling the discrete phase....31
3.6.1 Saffman lift force....33

4. METHODOLOGY AND BOUNDARY CONDITIONS....34

4.1 Introduction....34
4.2 Grid generation and adaption....35
4.3 Boundary conditions....36
4.3.1 Velocity inlet....36
4.3.2 Wall....36
4.3.3 Outflow....36
4.3.4 Porous medium....36
4.4 Discrete phase modeling....38
4.5 Solution controls....39

5. RESULTS AND DISCUSSION....40

5.1 Grid independence....40
5.2 Fully developed flow....43
5.3 Velocity field analysis for no filter case....46
5.3.1 Location at the step....46
5.3.2 Location at X=3.75h from the step....47
5.3.3 Location at X=6.25h from the step....49
5.3.4 Velocity contours....50
5.4 Velocity field analysis for filter at X=4.25h....52
5.5 Velocity field analysis for filter at X=6.75h....55
5.6 Discrete phase modeling analysis....59
5.6.1 Monodispersed particles....59
5.6.2 Polydispersed particles....68

Chapter page

6. CONCLUSIONS AND RECOMMENDATIONS ……..…….……73

6.1 Conclusions…….. 73

6.2 Recommendations for future work……...74

References……75

LIST OF TABLES

Table Page

3.1 Closure coefficients for standard and RNG *k*-ε turbulence models 26
4.1 Porous medium parameters as given by Yao (2000) 37
4.2 Discretization schemes.....39
5.1 Mesh size 40
5.2 Reattachment length for different meshes 40
5.3 Variation of power law parameter with the Reynolds number - Schlichting (2000) 43

LIST OF FIGURES

Figure Page

1.1 Backward facing step geometry 2

2.1 Location of detachment and reattachment of the flow at center of test section from Armaly et al. (1983) 6

2.2 Backward facing step flow experimental geometry and inlet conditions from Driver and Seegmiller (1985) 7

2.3 Reattachment location vs top wall deflection angle from Driver and Seegmiller (1985) 7

2.4 Variation of R_{EH} with X_r from Lee and Mateescu (1998) 9

2.5 Reynolds number as a function of reattachment from Kim and Moin (1985) 10

2.6 Comparison of streamlines between linear and non-linear *k*-ε models for backward facing step flow with porous insert, $k = 10^{-6}$ m^2, $\varphi = 0.65$, from Assato et al. (2005) 11

2.7 Comparison of streamlines between linear and non-linear *k*-ε models for backward facing step flow with porous insert, $k = 10^{-6}$ m^2, $\varphi = 0.85$, from Assato et al. (2005) 12

2.8 Comparison of streamlines between linear and non-linear *k*-ε models for backward facing step flow with porous insert, $k = 10^{-7}$ m^2, $\varphi = 0.65$, from Assato et al. (2005) 12

Figure Page

2.9 Sensitivity of flow field to changes in Darcy number from Chan and Lien (2005).....14

2.10 Sensitivity of flow field to changes in Forchheimer constant from Chan and Lien (2005).....14

2.11 Sensitivity of flow field to changes in thickness of porous insert from Chan and Lien (2005).....15

2.12 Contour plot of particle number density distribution from Fessler and Eaton (1997).....17

3.1 Near wall treatment.....29

4.1 2-D backward facing step 35

5.1 Comparison of velocity profiles at step for different mesh sizes for Re = 10000.....41

5.2 Comparison of velocity profiles at X = 3.75h for different mesh sizes for Re = 10000.....42

5.3 Comparison of velocity profiles at X = 6.25h for different mesh sizes for Re = 10000.....42

5.4 Velocity profile comparison at step with different locations behind step for Re = 6550.....44

5.5 Velocity profile comparison at step with the power law profile for Re = 6550.....44

5.6 Velocity profile comparison at step with different locations behind step for Re = 10000.....45

5.7 Velocity profile comparison at step with the power law profile for Re = 10000.....45

5.8 Comparison of velocity profiles at step for Re = 6550 for no filter case.....46

5.9 Comparison of velocity profiles at step for Re = 10000 for no filter case.....47

5.10 Comparison of velocity profiles at X = 3.75h for Re = 6550 for no filter case 48

Figure Page

5.11 Comparison of velocity profiles at X = 3.75h for Re = 10000 for no filter case 48

5.12 Comparison of velocity profiles at X = 6.25h for Re = 6550 for no filter case 49

5.13 Comparison of velocity profiles at X = 6.25h for Re = 10000 for no filter case 50

5.14 Velocity contours for Re = 6550 for no filter case 51

5.15 Velocity contours for Re = 10000 for no filter case 51

5.16 Comparison of velocity profiles at X = 3.75h for Re = 6550 with filter at X=4.25h 53

5.17 Comparison of velocity profiles at X = 3.75h for Re = 10000 with filter at X=4.25h 53

5.18 Velocity contours for Re = 6550 for filter at X=4.25h 54

5.19 Velocity contours for Re = 10000 for filter at X=4.25h 54

5.20 Comparison of velocity profiles at X = 6.25h for Re = 6550 with filter at X=6.75h 55

5.21 Comparison of velocity profiles at X = 6.25h for Re = 10000 with filter at X=6.75h 56

5.22 Velocity contours for Re = 6550 for filter at X=6.75h 56

5.23 Velocity contours for Re = 10000 for filter at X=6.75h 57

5.24 Comparison of velocity profiles for “no filter’ and “filter” case at X=3.75h for Re = 6550 58

5.25 Comparison of velocity profiles for “no filter’ and “filter” case at X=6.25h for Re = 6550 58

5.26 Particle residence time for 10μm particles for Re = 6550 with filter at X=4.25h.....59

5.27 Velocity tracks for 10μm particles for Re = 6550 with filter at X=4.25h.....60

5.28 Particle residence time for 40μm particles for Re = 6550 with filter at X=4.25h.....60

Figure Page

5.29 Velocity tracks for 40μm particles for Re = 6550 with filter at X=4.25h.....61

5.30 Particle residence time for 10μm particles for Re = 10000 with filter at X=4.25h.....62

5.31 Velocity tracks for 10μm particles for Re = 10000 with filter at X=4.25h.....62

5.32 Particle residence time for 40μm particles for Re = 10000 with filter at X=4.25h.....63

5.33 Velocity tracks for 40μm particles for Re = 10000 with filter at X=4.25h.....63

5.34 Particle residence time for 10μm particles for Re = 6550 with filter at X=6.75h.....64

5.35 Velocity tracks for 10μm particles for Re = 6550 with filter at X=6.75h.....65

5.36 Particle residence time for 40μm particles for Re = 6550 with filter at X=6.75h.....65

5.37 Velocity tracks for 40μm particles for Re = 6550 with filter at X=6.75h.....66

5.38 Particle residence time for 10μm particles for Re = 10000 with filter at X=6.75h.....66

5.39 Velocity tracks for 10μm particles for Re = 10000 with filter at X=6.75h.....67

5.40 Particle residence time for 40μm particles for Re = 10000 with filter at X=6.75h.....67

5.41 Velocity tracks for 40μm particles for Re = 10000 with filter at X=6.75h.....68

5.42 Trajectories for polydispersed particles based on diameter for Re = 6550 with filter at X=4.25h.....70

5.43 Trajectories for polydispersed particles based on diameter for Re = 6550 with filter at X=6.75h.....70

5.44 Trajectories for polydispersed particles based on diameter for Re = 10000 with filter at X=4.25h.....71

5.45 Trajectories for polydispersed particles based on diameter for Re = 10000 with filter at X=6.75h.....71

NOMENCLATURE

a	Distance from step to the location of porous medium
C_2	Pressure jump coefficient
C_D	Drag coefficient
C_μ	Modeling constant for *k*-ε model
D	Diameter of dispersed particles
D_h	Hydraulic diameter
E	Wall roughness function
F1 and F2	Blending functions for SST *k*-ω model
F_D	Drag force
F_i	External force
h	Step height
k	Turbulent kinetic energy
k	Von Karman constant
n	Power law parameter
p	Pressure
P_k	Production
R_e	Reynolds number based on maximum velocity used in the current study
S_{ij}	Strain rate
S_t	Stokes number
u	Velocity of the continuous phase (air)
u_i	Velocity in horizontal direction

U	Mean velocity in horizontal direction
u'_i	Velocity fluctuation in horizontal direction
u'_j	velocity fluctuation in vertical direction
U_{max}	Maximum velocity at the inlet
U_p	Time average velocity of the fluid at point p above the wall
v	Velocity of dispersed particles
X_r	Reattachment length
y	Vertical distance from the wall
α	Permeability of porous medium
ΔP	Pressure drop across the porous medium
Δt	Thickness of porous medium
ε	specific dissipation
μ_c	Dynamic Viscosity of air
μ_T	Eddy viscosity or turbulent viscosity
υ	Kinematic viscosity of air
ρ	Density of air
ρ_p	Density of dispersed particles
τ_{ij}	Stress tensor
τ_p	Particle response time
τ_v	Momentum response time
τ_w	Wall shear stress
$\tau_{p,\ Stokes}$	Particle time constant
φ	Porosity of the porous medium
ω	Dissipation per unit kinetic energy
ω^2	Enstrophy

CHAPTER 1

INTRODUCTION

1.1 Background

Flow separation and its subsequent reattachment to a solid surface are evident in many systems and structures. Some of the examples are turbulent flows over aerofoils with large angles of attack, flow past a cylinder and bluff bodies, flow through a sudden expansion etc. Air filter housings in automobiles is one such case where, due to sudden expansion, the flow tends to separate and then reattach at some distance. These filter housings are designed in a way that they would be accommodated in the least amount of space due to space restrictions; rather than being designed for providing maximum filter efficiency. Due to such design complexities, the flow is not delivered uniformly over the filter surface. The separated flow results in large velocity fluctuations and a prominent recirculation zone, which further results in poor performance of the filter. While in some cases, the flow separation and reattachment may improve momentum transfer, in most of the cases it results in an unsteady and a non-uniform flow which hampers the efficiency.

Predicting the flow characteristics in such complex geometries which incorporate flow separation and reattachment and a recirculation zone is always a difficult task, mainly due to the fact that the mean flow in the domain might be laminar, transitional or turbulent. The real flow field, considered with all its geometrical parameters, is extremely intricate and expensive to simulate even with today's advanced technologies. It is also very difficult to analyze all the

minute details in a real flow field. In order to study such flow characteristics, a *backward facing step geometry* serves as a useful prototype which delivers similar flow separation and reattachment as other complex systems. The current study focuses on a turbulent flow past backward facing step geometry with a pleated filter modeled as a porous medium at different locations in the domain. In the later part, dust particles with different diameters and Stokes number are injected and the recirculation zone is analyzed to study the particulate precipitation. The backward facing step geometry used in the current study is depicted in Figure 1.1

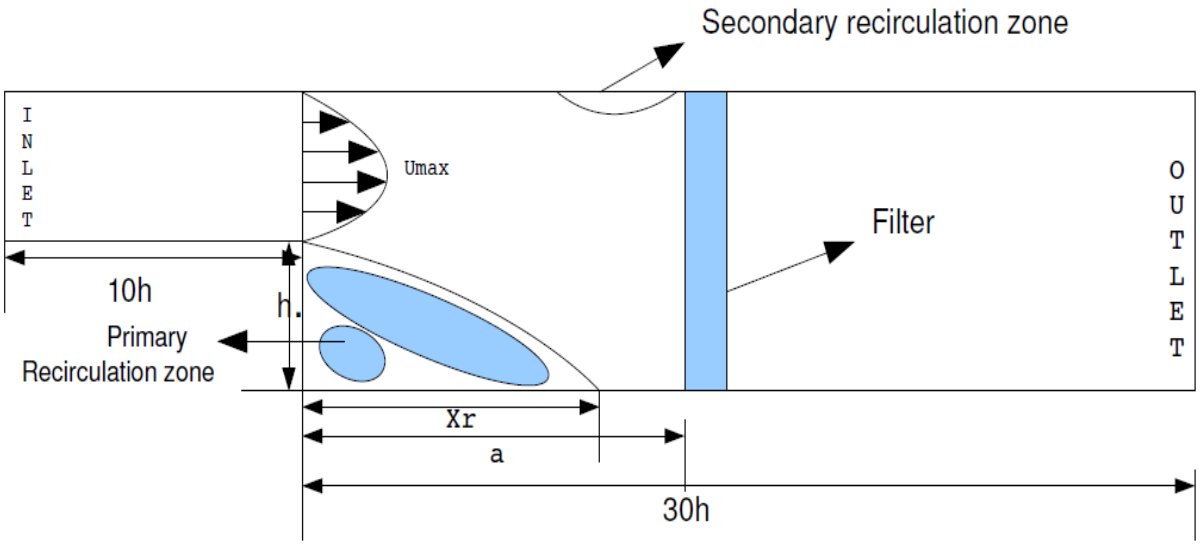

Figure 1.1: Backward facing step geometry

- "h" is the step height while the total channel height is 2h
- Inlet channel length is taken as 10h
- Channel length from the step until the outlet is taken as 30h
- Xr is the reattachment length
- "a" is the distance from the step to the location of the porous medium. In the current study, "a" is taken as 4.25h and 6.75h from the step.

Reynolds number used for this study is based on the hydraulic diameter (step height) and centerline or the maximum velocity at inlet, which is analogous to experiments of Yao (2000)

$$\mathrm{Re} = \frac{\rho U_{max} D_h}{\mu_c}$$

- Re = Reynolds number at the inlet
- ρ = Density of air (1.22 kg/m^3)
- U_{max} = max velocity at the inlet or the centerline velocity
- D_h = Hydraulic diameter (step height)
- μ_c = Kinematic viscosity of air (1.8 X 10^{-5} m^2/s)

Considering the above definition of Reynolds number, inlet velocity at the step for Re = 6550 is 3.865m/s and for Re = 10000 is 5.901m/s

1.2 Objective

The main objective of the current study is to analyze flow characteristics and particle motion in the recirculation zone downstream of a backward facing step and to determine the effect of the recirculation zone on the filtration of an automotive air filter. Very few studies have been made on particle injections in a backward facing step flow preceding a porous medium. The current study focuses on monodispersed and polydispersed particulate flow over a backward facing step with a pleated filter modeled as a porous medium. A turbulent flow has been modeled for two different Reynolds numbers of 6550 and 10000 with a porous medium placed at two different locations in the domain. Test dust particles ranging from Stokes number of about 0.1 to 10 are then injected in order to obtain the flow domain similar to a real flow field encountered in many multi-phase flow applications and the effect of recirculation zone on these particles is then analyzed.

.

CHAPTER 2

REVIEW OF LITERATURE

The turbulent flow over a backward facing step has been studied for many decades and has proven to be a useful tool in analyzing flow characteristics in many industrial applications. It is also used to study various aspects of turbulence modeling because of its simple geometry yet it provides flow characteristics similar to many complex systems. The aim of this chapter is to review and understand various numerical and experimental studies on backward facing step turbulent flow and the flow through a porous medium. The studies on particulate flow are also reviewed in detail in the later part followed by conclusions of the review

2.1 Flow over a backward facing step

The numerical and experimental studies on flow over a backward facing step have been carried out for many decades. Kim et al. (1980) performed experiments to study an incompressible flow over a backward facing step. They used two different step heights with $h/\delta = 2.2$ and 3.3, where h and δ were step height and boundary layer thickness respectively. These step heights gave aspect ratios of 16 and 24. The reference speed was set at 18.2 m/s and Reynolds number depending on momentum thickness was 1.3×10^3. The mean distance to reattachment from the step was found to be $7 \pm 1h$. The authors found that the flow characteristics remain almost identical for different step heights. The effect of changing Reynolds number over a limited range was also minimal. This was in accordance with the previous experimental results of Tani et al. (1961), Abbott and Kline (1961) and Chandrsuda (1975). The authors also concluded that the case for laminar flow is altogether different for the flow characteristics change with step height.

Maximum values of turbulent intensities and shear stress were found to be in the reattachment zone followed by a rapid drop after reattachment. It was also found that as the flow moves downstream of the reattachment; it slowly develops into an ordinary turbulent boundary layer flow

Durst and Tropea (1981) did the experimental analysis of backward facing step flow and found the effect of expansion ratio and Reynolds number on the reattachment length. The authors found that the reattachment length increases with the increase in both expansion ratio and Reynolds number. Their experimental results with an expansion ratio of 20 were similar to those of Johnston and Eaton (1980) with an expansion ratio of 16.6

Armaly et al. (1983) performed experimental and theoretical studies on a backward facing step flow. LDA was applied for velocity measurements and velocity distribution and reattachment lengths were reported downstream of a single backward facing step. The Reynolds number range considered was $70 < Re < 8000$ which covers laminar, transitional and turbulent flow regimes. Reynolds number defined was related to the maximum centerline velocity at the inlet and was given by $Re = \frac{2}{3}U_{max}\ D / \upsilon$, where D was the hydraulic diameter and υ was the kinematic viscosity of air. An expansion ratio of 1:1.94 was used. Because of the longer inlet channel length, the flow was fully developed at the inlet. The authors found that the flow was two dimensional only at Reynolds number $Re < 400$ and $Re > 6000$. In between these numbers, the flow was highly three dimensional. The reattachment length was reported to increase for the laminar regime and then decrease as the flow became turbulent at higher Reynolds numbers. The authors also found a small secondary recirculation zone downstream of the step which originated at the start of the transitional flow regime ($1200 < Re < 6600$) where the reattachment length experienced a sharp drop in its magnitude. Figure 2.1 displays the change in reattachment with the Reynolds number.

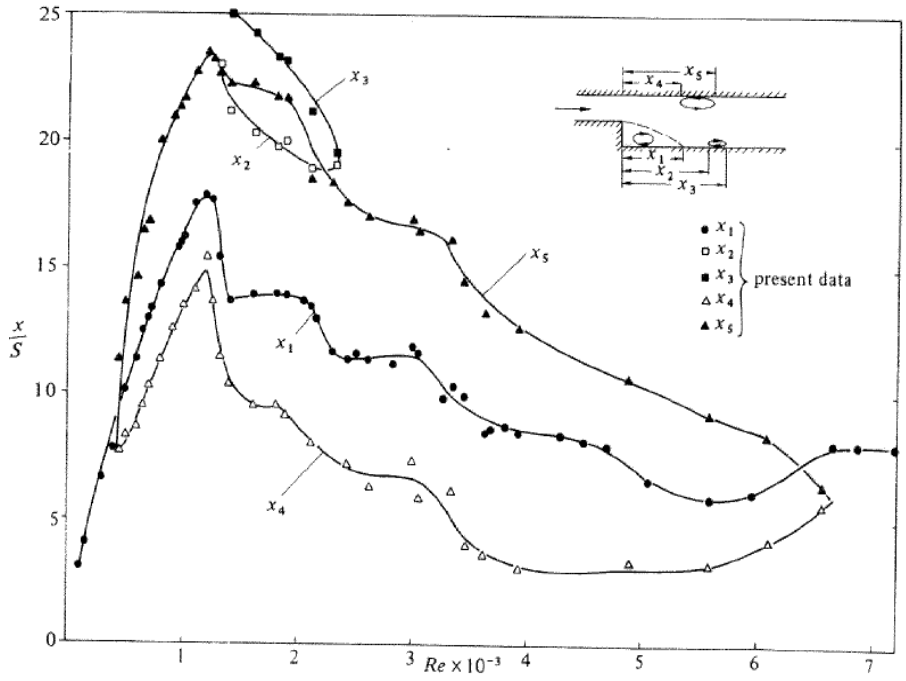

Figure 2.1: Location of detachment and reattachment of the flow at center of test section from Armaly et al. (1983)

The experimental results of Armaly et al. (1983) were similar to the results of Sinha et al. (1981) who had also experimentally analyzed laminar and turbulent flow regimes for a backward facing step flow. Reynolds number range used in their study was $100 < Re < 12000$. The reattachment length was found to increase until $Re = 800$, then fall gradually until reaching a constant value for $Re > 10000$

Driver and Seegmiller (1985) analyzed experimentally as well as numerically, the effect of pressure gradients on the reattachment. The experiments were conducted in an incompressible, high Reynolds number flow and a laser doppler velocimeter was used for mean velocity and turbulence measurements throughout the flow-field. The experimental setup was built in such a way that a pressure gradient was imposed by deflecting a wall opposite to the step. Figure 2.2 displays their experimental setup

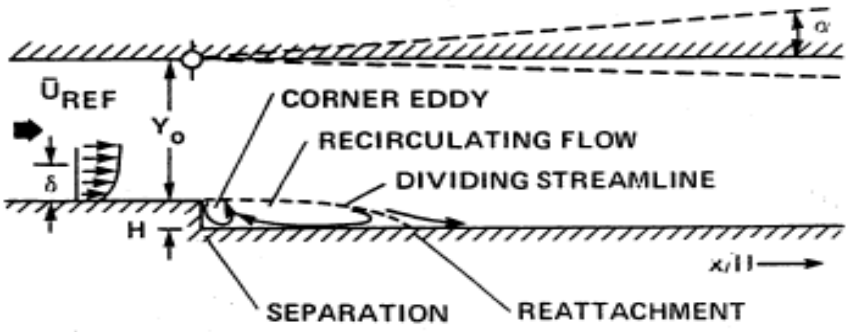

Figure 2.2: Backward facing step flow experimental geometry and inlet conditions from Driver and Seegmiller (1985)

The authors found that as the wall is deflected, the spreading rate of the shear layer increases hence increasing the reattachment length. This delays the pressure recovery after reattachment. It was also found that there is no significant change in Reynolds stresses with the change in wall deflection angle. The authors compared their experimental data with their numerical analysis of the same case and found that the numerical model under predicts the reattachment length. Figure 2.3 depicts their results for wall deflection angle and reattachment length for both experimental and numerical analysis.

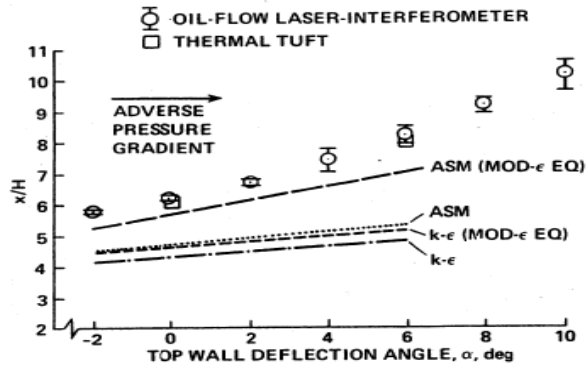

Figure 2.3: Reattachment location vs top wall deflection angle from Driver and Seegmiller (1985)

Adams and Johnston (1988 a, b) experimentally measured the reattachment length of a separated flow past a backward facing step for Reynolds numbers $8000 < Re < 40000$. The expansion ratio used was 1.25. The authors concluded that the reattachment for the case of laminar boundary layers upstream of the step was about 30% smaller than when the upstream boundary layers were turbulent. This decrease in the reattachment length was found to be prominent due to the increased entrainment of the free shear layer.

Chung and Sung (1996) performed an experimental study on a flow over a backward facing step in which the separated flow was given external excitations with a sinusoidally oscillating jet. The main objective behind their study was to get an in-depth knowledge of the characteristics of large scale vortex development in bounded flows and to reduce the unsteadiness in separated and reattached flows. The Reynolds number based on step height was $13000 < Re < 33000$ and the expansion ratio used was 1.5. The free stream turbulent intensity used was about 0.6% at the speed of 4 – 14 m/s. The authors found that due to the external force applied, there was an increase in the shear layer growth rate which produced a large vortex at the separation edge. This enhanced the rate of entrainment thus reducing the reattachment length as compared to the natural unforced flow. At a higher forcing level and a specific forcing frequency, the reattachment had a single minimum value.

Lee and Mateescu (1998) performed both experimental and numerical analysis of the backward facing step flow. The Reynolds number range used was $Re \leq 3000$ and the expansion ratios used were 1.17 and 2.0. The transitional flow regime for $1150 \leq Re \leq 3000$ was also taken into consideration. The authors found that their results were in good agreement with the literature. Figure 2.4 gives a comparison of their data for the effect of variation of separation length on Reynolds number for an expansion ratio of 1.17, with that of Goldstein et al. (1970) and Armaly et al. (1983)

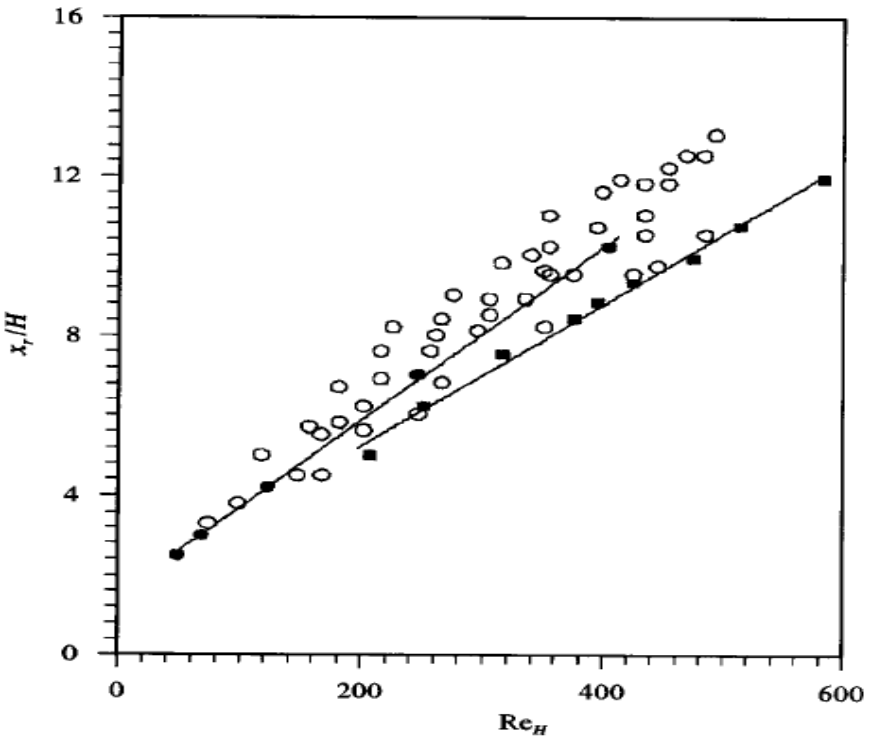

Figure 2.4: Variation of R_{EH} with X_r from Lee and Mateescu (1998).■-Lee and Mateescu, ●-Armaly et al., ○-Goldstein et al.

Kim and Moin (1985) devised a numerical method for computing three dimensional, time dependent incompressible flows which is based on fractional step methodology. They applied this technique to study the backward facing step flow with a parabolic profile prescribed at the step and the outlet at a distance of "30h" from the step, where "h" is the step height. The authors found that the dependence of reattachment length on the Reynolds number was in good agreement with experimental results in the literature until Re = 500, but from Re = 600, the computational results start to deviate from the experimental results. As pointed by Armaly et al. (1983) and as cited by the authors, the deviation was due to three dimensionality of the experimental flow. Figure 2.5 below shows the dependence of Reynolds number with the reattachment length for the numerical results of Kim and Moin (1985) and the experimental results of Armaly et al. (1983)

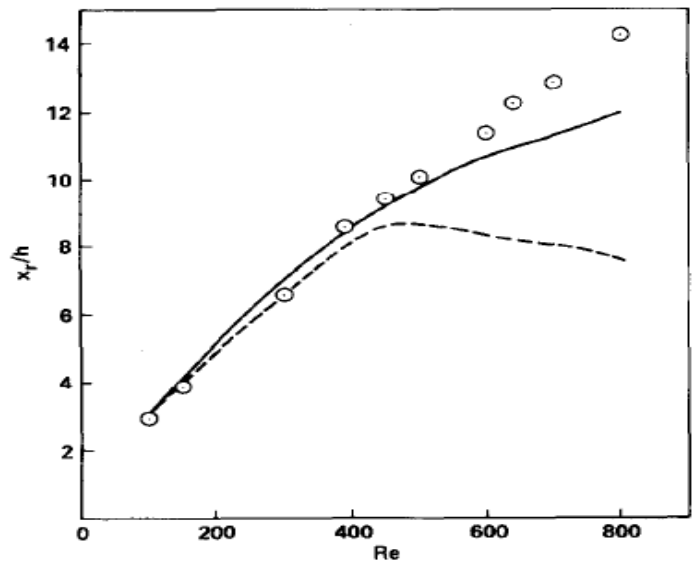

Figure 2.5: Reynolds number as a function of reattachment from Kim and Moin (1985). ○-exp. Data of Armaly et al., ---numerical data of Armaly et al., ─-numerical data of Kim and Moin

Biswas et al. (2004) numerically studied the flow over a backward facing step for different expansion ratios (1.9423, 2.5 and 3.0) and a wide range of Reynolds numbers ($10^{-4} \leq Re \leq 800$). The geometry used by the authors was in accordance with the experimental set-up of Armaly et al. (1983). Authors found that their two dimensional and three dimensional computations are in good agreement with the respective experimental results of Armaly et al. (1983). The authors also studied the pressure loss throughout the channel for various expansion ratios and Reynolds numbers and found that the pressure losses increase with increase in step height while the losses reduce with increasing Reynolds numbers.

2.2 Backward facing step flow with porous medium

The flow through a porous media is encountered in a variety of engineering applications which include flow through packed beds, perforated plates, filters etc. and it is always important to predict the flow field to optimize a given design. This section reviews some of the studies performed for a backward facing step flow with a porous medium insert.

Assato et al. (2005) performed a numerical analysis of a turbulent flow past a backward facing step with a porous medium insert using linear and non-linear *k*-ε models. The properties of the porous medium such as permeability, porosity and thickness were varied to study their effect on flow pattern. In this case, the porous medium was located right at the step. The authors found that both linear and nonlinear models underpredict the reattachment length, though non-linear models gave slightly better results due to their ability to simulate important flow characteristics which linear models failed to do. The experimental value for reattachment was found to be 7.0, whereas linear and non-linear models used by the authors gave reattachment length to be 5.55 and 6.45 respectively. The authors also found that as the thickness of the porous insert is increased, the difference in the value of reattachment length calculated by both models is reduced. This was due to the fact that inside the porous medium, additional forces exerted by the solid on the fluid cause the Darcy region velocity profiles to flatten. Figures 2.6 – 2.8 compares the streamlines for various values of permeability and porosity for linear and nonlinear *k*-ε models.

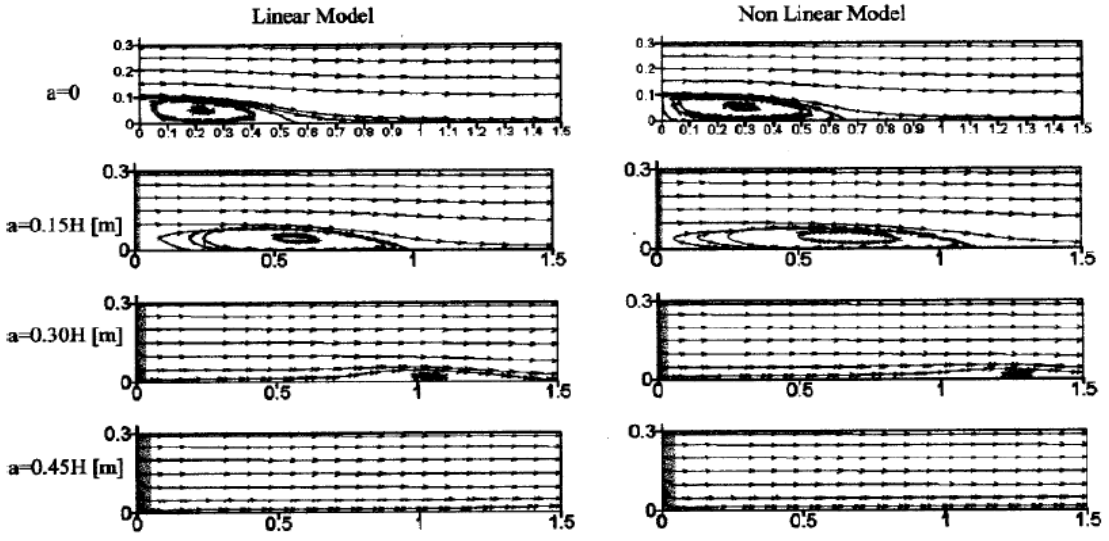

Figure 2.6: Comparison of streamlines between linear and non-linear *k*-ε models for backward facing step flow with porous insert, $k = 10^{-6}$ m^2, $\varphi = 0.65$, from Assato et al. (2005)

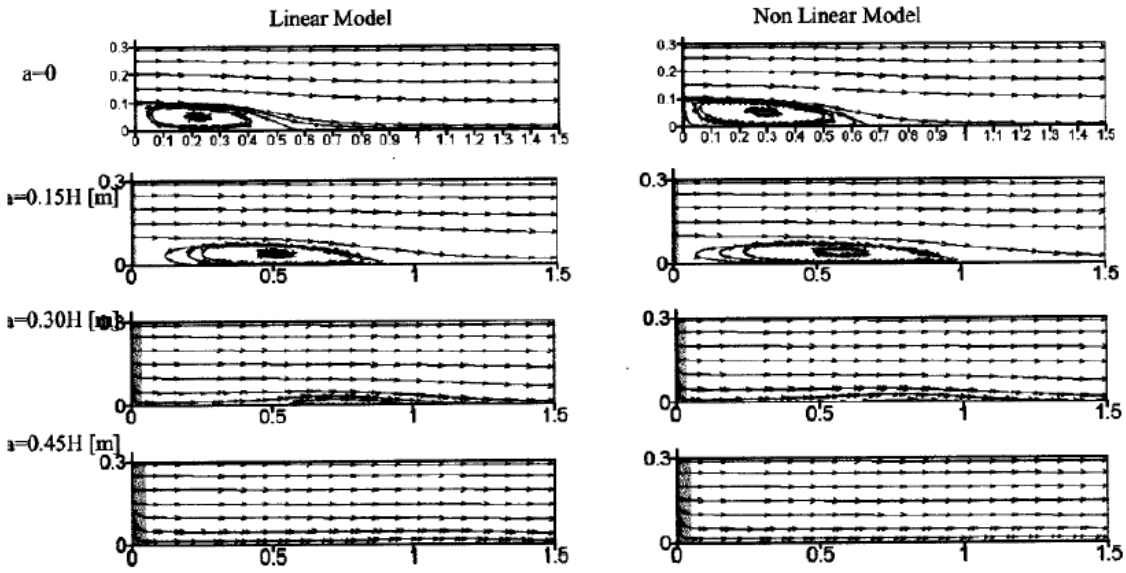

Figure 2.7: Comparison of streamlines between linear and non-linear *k*-ε models for backward facing step flow with porous insert, $k = 10^{-6}$ m^2, $\varphi = 0.85$, from Assato et al. (2005)

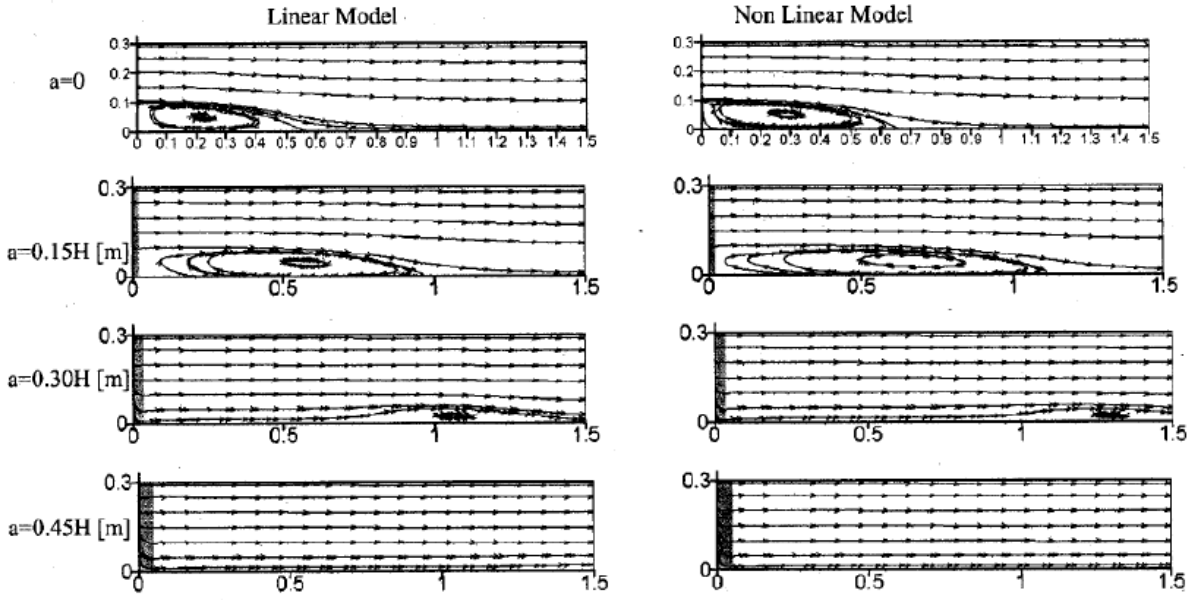

Figure 2.8: Comparison of streamlines between linear and non-linear *k*-ε models for backward facing step flow with porous insert, $k = 10^{-7}$ m^2, $\varphi = 0.65$, from Assato et al. (2005)

Chan and Lien (2005) derived a *k*-ε model by time averaging the Navier-Stokes equations and used it to study the backward facing step flow with porous insert. The aim of their study was to analyze the effect of change in various parameters like permeability, Forchheimer's constant and the thickness of the porous medium on the resulting mean flow and turbulent kinetic energy distributions. The flow geometry used by the authors was the same as the experimental set-up of Driver and Seegmiller (1985). Reynolds number used was Re = 37000 and a higher expansion ratio of 9:1 was used. The total channel length was 32h, h being the step height, ensuring a fully developed velocity profile at the expansion point and the outlet. The porous medium was modeled using the Darcy's equation with an additional term for inertial effects of the porous medium

$$\Delta p = -\left(\frac{\vartheta}{\alpha} v + F\alpha^{\frac{-1}{2}} v|v|\right) b.$$

The first term on the right hand side is the Darcy term while the second term is the inertial term, F being the Forchheimer's constant. α and b were the permeability and the thickness of the porous medium respectively. The authors used the experimental data for inlet velocity. K and ε at the inlet and near wall region were assumed to obey law of the wall. After a detailed analysis, the authors discovered that by decreasing permeability or the Darcy number ($Da = \alpha/b^2$), and thereby increasing its resistance, the recirculation zone keeps on reducing until it is eliminated. Similar results were found with the increase in Forchheimer's constant and the thickness. Figures 2.9 – 2.11 shows the above mentioned effects of all the three parameters on the flow field.

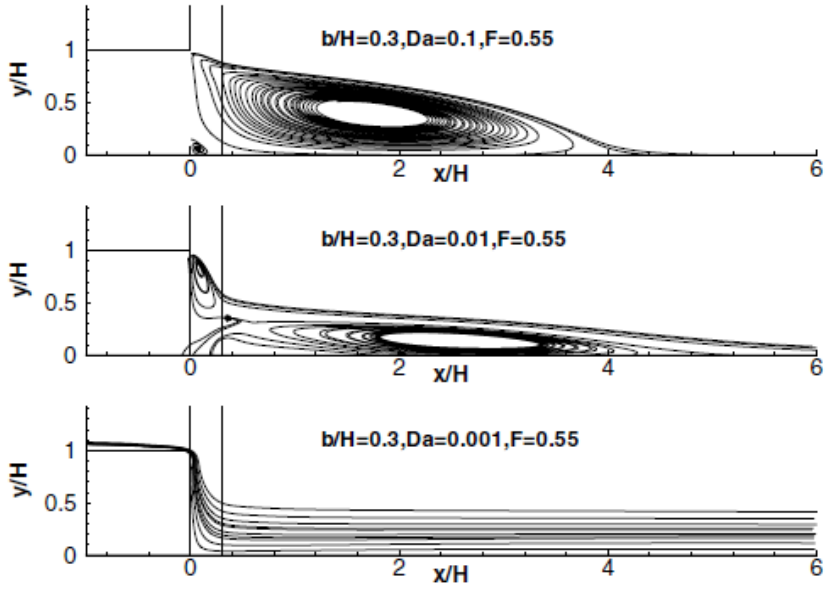

Figure 2.9: Sensitivity of flow field to changes in Darcy number from Chan and Lien (2005)

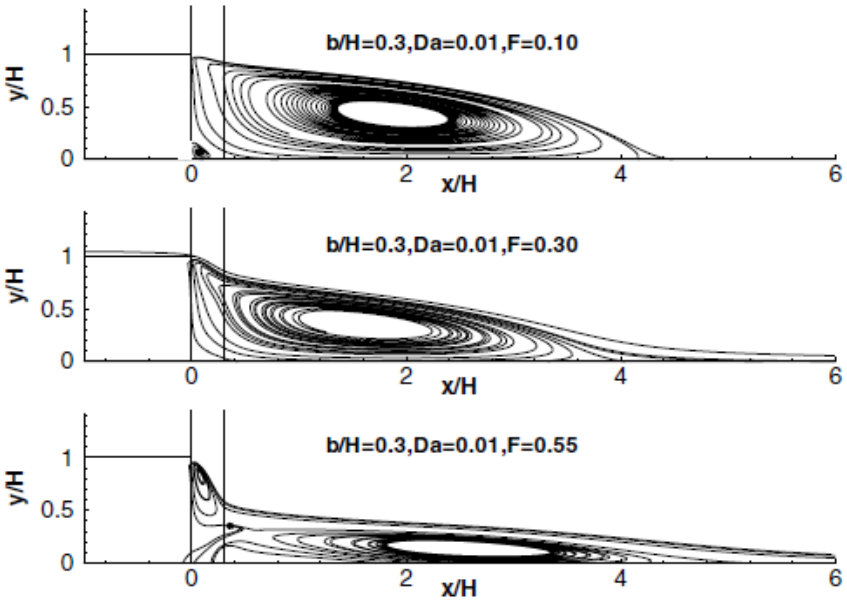

Figure 2.10: Sensitivity of flow field to changes in Forchheimer constant from Chan and Lien (2005)

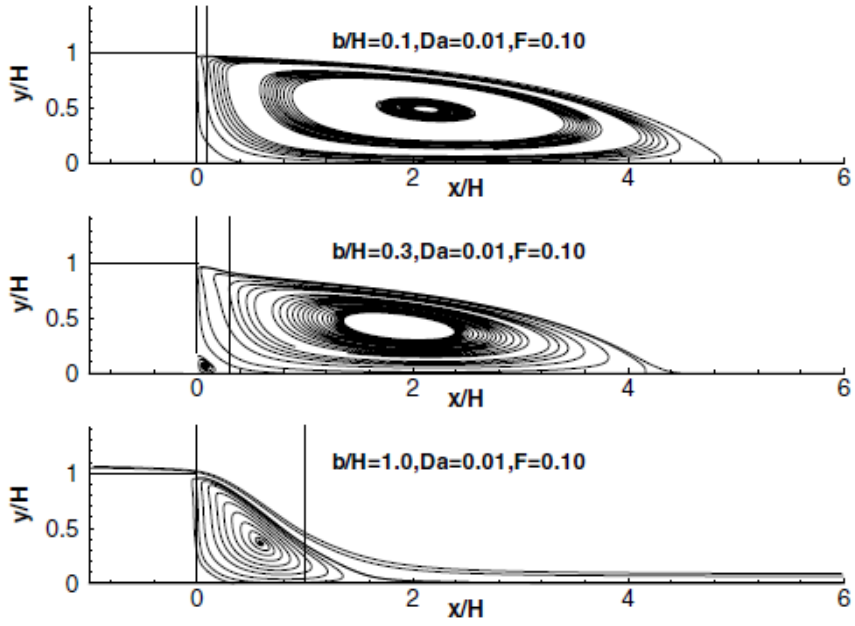

Figure 2.11: Sensitivity of flow field to changes in thickness of porous insert from Chan and Lien (2005)

Krishnamoorthy (2007) performed a numerical analysis of a backward facing step flow past a porous medium. Numerical simulations were performed in FLUENT and the performance of various turbulence models was compared. The numerical data obtained was compared with experimental results of Yao (2000). It was observed that the numerical results did not compare well with the experimental results for lower Reynolds numbers. However, the reattachment length was predicted well. As the Reynolds number was increased, the results were in good agreement with experiments. Amongst various turbulence models, the realizable *k*-ε model was found to provide good results.

2.3 Backward facing step flow with particle injections

Particle dispersion in a flow over a backward facing step was studied by Ruck and Makiola (1988). The particles encountered were in a size range of 1 to 70 μm with a density of 1500 kg/m^3 and Laser Doppler Anemometry (LDA) was used to measure particle motion over the step. To

trace the continuous fluid phase, small oil particles of diameter 1μm and density 810 kg/m3 were used. Three different sizes (15, 30 and 70 μm) of starch particles were used which were spherical in shape and were insoluble in cold water. The size and particle number concentration was such that the air flow was not affected by particle motion. The Reynolds numbers based on the step height used were 15000 and 64000. The authors found that the difference between the particle velocity field and continuous phase velocity field increases with the increase in particle size. The bigger particles were found to have smaller recirculating velocities and hence a smaller recirculation zone.

Chan et al. (2001) simulated a gas particle flow over a backward facing step using a stochastic separated flow model. The gas phase or continuous phase used was air and the particle phase included a mixture of 150μm glass particles and 70μm copper particles. The *k*-ε turbulence model was implemented to describe the turbulent motion of the continuous phase. The authors found that the predicted streamwise mean velocities as well as the fluctuating velocities of both the phases were in good agreement with experimental results of Fessler and Eaton (1999). The reattachment length of 7.6h was also found to be close to experimental value of 7.4h, h being the step height.

Fessler and Eaton (1997) studied the particle response in a flow passing through a sudden expansion. The particles used were in a Stokes number range of 0.5 to 7.4. It was noted that the particles with Stokes number higher than 3 did not enter the recirculation zone of the expansion. The expansion ratio used was 5.3. The inlet Reynolds number was 13800 and the back step Reynolds number was 18400 based on centerline velocity. Three different types of particles were used: 90μm glass, 150μm glass and 70μm copper particles. Particle velocities were measured using LDA. The authors observed that particle mean streamwise velocities were higher than the fluid velocity at the expansion. This difference between the velocities increased downstream of the step due to the higher response of fluid to adverse pressure gradients. Whereas in shear layer

where the fluid fluctuations were maximum, the wall normal fluctuating velocities of particles were less than fluid fluctuating velocities due to the fact that particles are unresponsive to fluid fluctuations because of their higher inertia. It was observed that the particle response was unaltered with change in Reynolds number.

Fessler and Eaton continued their study in 1999, studying the turbulence modification by particles in a turbulent flow over a backward facing step with a fully developed flow at the inlet. Similar conditions were used as in Fessler and Eaton (1997) with three different diameter particles (90μm and 150μm glass particles and 70μm copper particles). The authors observed very small number of particles in the recirculation zone due to higher Stokes number in use. It was found that the degree of turbulence modification for the continuous phase fluid increases with an increase in particle's Stokes number and Reynolds number. But the particles were not able to have any significant effect on turbulence just behind the step where the flow is mainly governed by the shear layer at separation point. Figure 2.12 gives an insight of the particle number density for 70μm copper particles. It can be seen that very few particles are present in the recirculation zone.

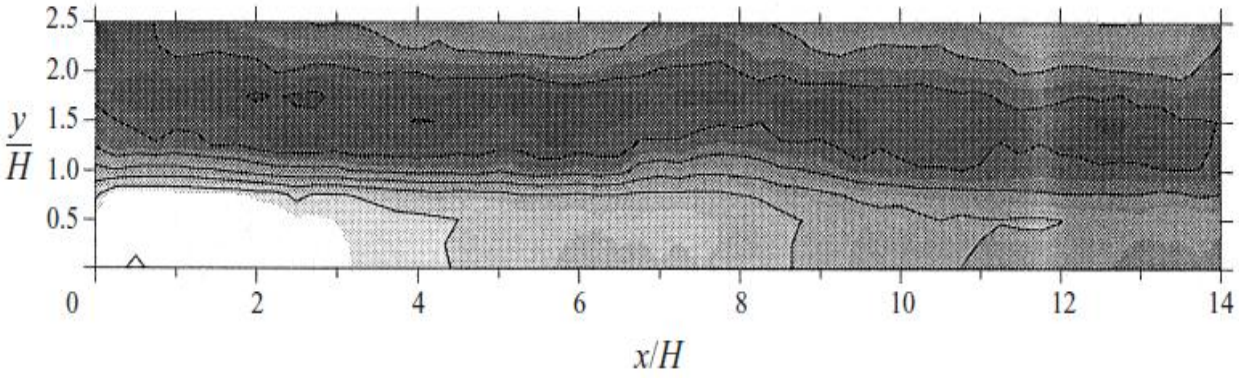

Figure 2.12: Contour plot of particle number density distribution from Fessler and Eaton (1997)

After the reattachment point which was about x/H = 7.4, the number of particles increase below y/H = 1. At about x/H = 14, the particle number density becomes more uniform.

Previous Studies at OSU

Yao (2000), Yao et al. (2007) performed an experimental and numerical analysis of the backward facing step flow with a pleated filter for Reynolds numbers 2000, 3750, 6550 and 10000. It was observed that the recirculation zone is highly affected when the filter is placed in the recirculation zone. But as the filter is moved farther downstream of the step, negligible effect was found on the recirculation zone.

Krishnamoorthy et al. (2009) did the numerical analysis of the backward facing step flow, comparing the various turbulence models of FLUENT. The authors used the same Reynolds numbers of 2000, 3750, 6550 and 10000 and the results were validated with the experimental results of Yao (2000). It was observed that the numerical results were in good agreement with the experimental results for Reynolds numbers 6550 and 10000 but the turbulent models in FLUENT were unable to simulate the flow for Reynolds numbers 3750 and 6550 due to the transitional nature of the flow.

The current study is continuation of the work by Ravi (2010), who did a numerical analysis of a particulate flow with monodispersed particles past a backward facing step preceding a porous medium. The author used a shorter inlet channel length of "2h" (where h is the step height) as compared to the length of "10h" used in the current study. The longer inlet channel length ensures a nearly fully developed flow at the step as described in a later section. The numerical results of the current study are in good agreement with the author's results except for some cases near the wall. This may be due to the different wall functions used.

CHAPTER 3

TURBULENCE MODELING

3.1 Introduction

One of the core problems in fluid dynamics is the prediction of turbulence in fluid flows. Although analyzing the turbulent motion of a fluid is less complicated than using the governing Navier-Stokes equations of fluid dynamics, the task becomes difficult due to limitations of computational power. To solve this problem, various turbulence models are developed to approximate the physical effects of turbulent flows and to analyze desired flow characteristics. As cited by Wilcox (2006), turbulence modeling is one of the three key elements of Computational Fluid Dynamics; the other two being grid generation and algorithm development. Many mathematical models have been developed to approximate the physics of turbulent flows, but none of them have been truly accurate. This is due to the extremely complex nature of turbulence. These mathematical models consist of differential equations and the related algebraic equations and constants, the solutions of which, combined with the solutions of Navier-Stokes equations, simulate the real turbulent flow field.

3.2 Reynolds averaged Navier Stokes (RANS)

The Reynolds averaged Navier Stokes equations as described in Wilcox (2006) are given as

$$\rho\frac{\partial U_i}{\partial t} + \rho\, U_j \frac{\partial U_i}{\partial x_j} = -\frac{\partial P}{\partial x_i} + \frac{\partial}{\partial x_j}(2\mu S_{ij} - \overline{\rho u'_i u'_j}) \tag{3.1}$$

The terms in brackets on right hand side represent stress. The first term, which contains the strain rate (S_{ij}), is the viscous stress, while the second term represents Reynolds stress, which

contributes to acceleration. These stresses are to be related to the mean motion before solving the equations, to match the number of unknowns with the number of equations. The absence of these additional equations results in the closure problem of turbulence. So the function of turbulence modeling is to relate the unknown quantities with the mean flow properties that are known, in order to get sufficient number of equations. By making such approximations, the closure problem is solved.

For the turbulence models which solve for turbulent kinetic energy and which are of interest for the current study; the Boussinesq approximation is used, which gives the Reynolds stress tensor as,

$$\overline{-\rho u'_i u'_j} = 2\mu_T S_{ij} - \frac{2}{3}\rho k \delta_{ij} \tag{3.2}$$

where μ_T is the turbulent viscosity (eddy viscosity) and S_{ij} is the mean strain rate tensor given by,

$$S_{ij} = \frac{1}{2}\left[\frac{\partial U_i}{\partial x_j} + \frac{\partial U_j}{\partial x_i}\right] \tag{3.3}$$

3.3 Classification of Turbulence models

Modeling a turbulent flow is always a difficult task, mainly due the presence of different length scales and time scales throughout the flow field. For instance, the smaller scale eddies encountered in turbulent flows have a length scale of millimeters while the actual flow-field may extend to a few kilometers like the flows in long pipes. Besides these different length scales, there are shear stresses near the wall which need to be resolved precisely, to obtain accurate results. There does not exist any uniform methodology to develop turbulence models which will approximate a wide range of flows. The turbulence models are thus developed according to the differing requirements of the flow-field (Hanjalic (2008)).

The flows may be computed using several approaches; either by solving the Reynolds averaged Navier-Stokes equations with appropriate models for turbulent quantities or by computing them directly. The main approaches as given by Pope (2000) are as follows:

- RANS based models
    - Linear eddy viscosity model
        - Algebraic models
        - One equation and two equation models
    - Non-linear eddy viscosity models
    - Reynolds stress transport models (RSM)
- Large eddy simulation
- Detached eddy simulation
- Direct numerical simulation

The selection criteria for turbulence models, as described by Pope (2000) are listed below

- Level of description
- Completeness
- Cost and ease of use
- Range of applicability
- Accuracy

3.4 Two equation models

These are the most widely used turbulence models and are considered to be the cornerstone of turbulence model research. The two equation models compute turbulent kinetic energy (k) and turbulence length scale or its equivalent and are considered to be complete in nature as no prior

knowledge of turbulence structure is required. Almost all two equation models start with the Boussinesq approximation, given in Eqn. 3.2 and the turbulent kinetic energy in the form of

$$\rho\frac{\partial k}{\partial t} + \rho U_j \frac{\partial k}{\partial x_j} = \tau_{ij}\frac{\partial U_i}{\partial x_j} - \rho\varepsilon + \frac{\partial}{\partial x}\left[\frac{\partial k}{\partial x_j}(\mu + \frac{\mu_T}{\sigma_k})\right] \quad (3.4)$$

where μ_T is the eddy viscosity given by $\mu_T = \rho k/\omega$ and ω - dissipation per unit kinetic energy

According to Wilcox (2006) the greatest amount of uncertainty about two equation models lies in the transport equation for *k*. Also, it is difficult to make an appropriate choice for the second variable. Thus the two equation models can be expected to be inaccurate for many non-equilibrium turbulent flows.

3.4.1 *k* – ω model

Wilcox (2006) indicates that Kolmogorov proposed this model in 1942. This is the first ever two equation model of turbulence. The first transported variable is the turbulent kinetic energy, while the second transported variable "ω" is dissipation per unit turbulent kinetic energy$\left(\frac{\varepsilon}{k}\right)$. "ω" determines scale of turbulence while "*k*" determines energy of turbulence. Equations for the two transported variables are given by Wilcox.

Turbulence Kinetic energy (*k)*

$$\rho\frac{\partial k}{\partial t} + \rho U_j \frac{\partial k}{\partial x_j} = \tau_{ij}\frac{\partial U_i}{\partial x_j} - \rho k\omega\beta^* + \frac{\partial}{\partial x_j}\left[(\mu + \sigma^*\mu_T)\frac{\partial k}{\partial x_j}\right] \quad (3.5)$$

Specific dissipation rate (ω)

$$\rho\frac{\partial \omega}{\partial t} + \rho U_j \frac{\partial \omega}{\partial x_j} = \alpha\frac{\omega}{k}\tau_{ij}\frac{\partial U_i}{\partial x_j} - \rho\beta\omega^2 + \frac{\partial}{\partial x_j}\left[(\mu + \sigma\mu_T)\frac{\partial \omega}{\partial x_j}\right] \quad (3.6)$$

Eddy viscosity $\mu_T = \rho k/\omega$

Wilcox (2006) gives the values of closure coefficients:

$\alpha = 5/9$, $\beta = 3/40$, $\beta^* = 9/100$, $\sigma = 1/2$, $\sigma^* = 1/2$.

Auxiliary relations

$\varepsilon = \beta^* \omega k$ and $l = k^{1/2}/\omega$

3.4.2 $k - \varepsilon$ model

This is the most widely used two equation turbulence model, developed by Jones and Launder (1972) and further modified by Launder and Sharma (1974). The first transported variable is turbulent kinetic energy (k), which determines the energy of turbulence and the second transported variable is turbulent dissipation (ε), which determines the scale of turbulence. As described by Bardina et al. (1997), this model gives good results for free shear layer flows as well as wall bounded and internal flows with relatively small pressure gradients. The $k - \varepsilon$ model formulation as described in Wilcox (2006) is given as follows

Turbulent kinetic energy (k)

$$\rho \frac{\partial k}{\partial t} + \rho U_j \frac{\partial k}{\partial x_j} = \tau_{ij} \frac{\partial U_i}{\partial x_j} - \rho \varepsilon + \frac{\partial}{\partial x_j} \left[(\mu + \mu_T/\sigma_k) \frac{\partial k}{\partial x_j} \right] \quad (3.13)$$

Dissipation rate (ε)

$$\rho \frac{\partial \varepsilon}{\partial t} + \rho U_j \frac{\partial \varepsilon}{\partial x_j} = C_{\varepsilon 1} \frac{\varepsilon}{k} \tau_{ij} \frac{\partial U_i}{\partial x_j} - C_{\varepsilon 2} \rho \frac{\varepsilon^2}{k} + \frac{\partial}{\partial x_j} \left[(\mu + \mu_T/\sigma_\varepsilon) \frac{\partial \varepsilon}{\partial x_j} \right] \quad (3.14)$$

Eddy viscosity $\mu_T = \rho C_\mu k^2/\varepsilon$

Wilcox (2006) gives the values of closure coefficients:

$$C_{\varepsilon 1} = 1.44, C_{\varepsilon 2} = 1.92, C_\mu = 0.09, \sigma_k = 1, \sigma_\varepsilon = 1.3$$

With auxiliary relations $\omega = \varepsilon/(C_\mu k)$ and $l = C_\mu k^{3/2}/\varepsilon$

3.4.3 $k - \omega$ SST model

The SST (Shear stress transport) $k - \omega$ turbulence model is a modified form of the original $k - \omega$ model. It is a combination of $k - \omega$ and $k - \varepsilon$ turbulence models. It uses standard k-ω approach in the inner parts of the boundary layer, which makes the model useful in the near wall region. The SST formulation uses k-ε approach in the free-stream, thereby avoiding the standard k-ω problem that the model is too sensitive in the free stream region. $k - \omega$ SST model is found to give good results in adverse pressure gradients and separating flows.

The SST $k - \omega$ formulation as given by Menter (1994) is as follows

Turbulent Kinetic energy:

$$\rho \frac{\partial k}{\partial t} + \rho U_i \frac{\partial k}{\partial x_i} = P_k - \rho k \omega \beta^* + \frac{\partial}{\partial x_i}\left[(\mu + \sigma_k \mu_T)\frac{\partial k}{\partial x_i}\right] \tag{3.7}$$

Specific dissipation rate

$$\rho \frac{\partial \omega}{\partial t} + \rho U_i \frac{\partial \omega}{\partial x_i} = \alpha \rho S^2 - \rho \beta \omega^2 + \frac{\partial}{\partial x_i}\left[(\mu + \sigma_{w1} \mu_T)\frac{\partial \omega}{\partial x_i}\right] +$$

$$2(1 - F_1)\rho \sigma_{w2} \frac{1}{\omega}\frac{\partial k}{\partial x_i}\frac{\partial \omega}{\partial x_i} \tag{3.8}$$

Where F1 is the blending function given by

$$F_1 = tanh\left\{\left\{min\left[max\left(\frac{\sqrt{k}}{\beta^* \omega y}, \frac{500\vartheta}{y^2 \omega}\right), \frac{4\rho \sigma_{\omega 2} k}{CD_{k\omega} y^2}\right]\right\} \text{^} 4\right\} \tag{3.9}$$

With $CD_{k\omega} = max\left(2\rho\sigma_{\omega 2}\frac{1}{\omega}\frac{\partial k}{\partial x_i}\frac{\partial \omega}{\partial x_i}, 10^{-10}\right)$ and "y" is the distance from the wall

The value of the blending function F_1 is zero away from the wall, where the $k - \varepsilon$ model is applicable while it is one in the boundary layer where $k - \omega$ is applicable

The turbulent eddy viscosity for the SST model is defined as follows

$$\vartheta_T = \frac{a_1 k}{\max(a_1\omega, SF_2)} \tag{3.10}$$

Where S is the invariant measure of strain rate and F_2 is a second blending function defined by

$$F_2 = tanh\left[\left[max\left(\frac{2\sqrt{k}}{\beta^*\omega y}, \frac{500\vartheta}{y^2\omega}\right)\right]\text{^}2\right] \tag{3.11}$$

A production limiter, used to prevent turbulence in stagnation regions, is given by

$$P_k = \mu_T \frac{\partial U_i}{\partial x_i}\left(\frac{\partial U_i}{\partial x_j} + \frac{\partial U_j}{\partial x_i}\right) \tag{3.12}$$

The constants are calculated by the combination of corresponding constants of $k - \omega$ and $k - \varepsilon$ models. Wilcox (2006) gives the values of constants for this model as:

$\beta^* = .09$, $\alpha_1 = 5/9$, $\beta_1 = 3/40$, $\sigma_{k1} = 0.85$, $\sigma_{\omega 1} = 0.5$, $\alpha_2 = 0.44$, $\beta_2 = 0.0828$, $\sigma_{k2} = 1$, $\sigma_{\omega 2} = 0.856$

3.4.4 $k - \varepsilon$ RNG model

This is the modified form of standard $k - \varepsilon$ model developed using renormalization group (RNG) methods by Yakhot et al. (1992). In this method, the Navier-Stokes equations are renormalized to consider the effects of smaller scales of turbulent motion. In the standard $k - \varepsilon$ model, eddy viscosity is evaluated by a single turbulence length scale. Thus the calculated diffusion is only for a specified scale, whereas in a real flow-field, all the length scales account for turbulent diffusion.

The RNG model accounts for different scales of motion through changes to the production term. The equation for turbulent kinetic energy is unchanged as in the standard $k - \varepsilon$ model. The formulation of RNG model is given as follows

Turbulent kinetic energy (k)

$$\rho \frac{\partial k}{\partial t} + \rho U_j \frac{\partial k}{\partial x_j} = \tau_{ij} \frac{\partial U_i}{\partial x_j} - \rho\varepsilon + \frac{\partial}{\partial x_j}\left[(\mu + \mu_T/\sigma_k)\frac{\partial k}{\partial x_j}\right] \qquad (3.15)$$

Dissipation rate

$$\rho \frac{\partial \varepsilon}{\partial t} + \rho U_j \frac{\partial \varepsilon}{\partial x_j} = C_{\varepsilon 1} \frac{\varepsilon}{k} \tau_{ij} \frac{\partial U_i}{\partial x_j} - C^*_{\varepsilon 2} \rho \frac{\varepsilon^2}{k} + \frac{\partial}{\partial x_j}\left[(\mu + \mu_T/\sigma_\varepsilon)\frac{\partial \varepsilon}{\partial x_j}\right] \qquad (3.16)$$

Where $C^*_{\varepsilon 2}$ is given by,

$$C^*_{\varepsilon 2} = C_{\varepsilon 2} + \frac{C_\mu \eta^3 (1 - \frac{\eta}{\eta_0})}{1 + \beta\eta^3}$$

$$\eta = \frac{Sk}{\varepsilon} \quad and \quad S = (2S_{ij}S_{ij})^{1/2}$$

In the current study, the $k - \varepsilon$ RNG model with standard wall functions is used and compared with the corresponding experimental data

The values for closure coefficients for standard $k - \varepsilon$ and RNG model are tabulated below

coefficients	C_μ	σ_k	σ_ε	$C_{1\varepsilon}$	$C_{2\varepsilon}$	β	η_0
Std. $k - \varepsilon$	0.09	1	1.3	1.44	1.92	---	---
RNG	0.0845	0.7194	0.7194	1.42	1.68	0.012	4.38

Table 3.1: Closure coefficients for standard and RNG k-ε turbulence models

3.4.5 Large eddy simulation

Large eddy simulation (LES), is a turbulence model in which large eddies are computed directly while smaller eddies are modeled computationally. It is based on Kolmogorov's theory of self-similarity which states that the larger eddies in a flow depend on the geometry while the smaller eddies are independent of the geometry and are more universal. Thus in LES, larger eddies are solved explicitly while the smaller ones are solved implicitly by using a sub-grid scale model. In order to remove small scale eddies from the Navier-Stokes equations, a filtering approach is implemented. The LES filter operation is low-pass, which means it filters out the scales associated with high frequencies. The filtered form of the continuity equation is then represented by

$$\frac{\partial \overline{v_i}}{\partial x_i} = 0 \tag{3.17}$$

And the filtered form of Navier-Stokes equation is

$$\frac{\partial \overline{u_i}}{\partial t} + \overline{u_j}\frac{\partial \overline{u_i}}{\partial x_j} = -\frac{1}{\rho}\frac{\partial \overline{p}}{\partial x_i} + \frac{\partial}{\partial x_j}\left[(\vartheta + \vartheta_T)\frac{\partial \overline{u_i}}{\partial x_j}\right] \tag{3.18}$$

where $\overline{p}$ is the filtered pressure and υ_T is the sub-grid scale turbulent viscosity

As described by Wilcox (2006), since LES involves modeling smaller eddies, the smallest finite difference cells in use can be larger than Kolmogorov length and hence larger time steps can be used which makes it possible to reach higher Reynolds numbers

3.4.6 Direct numerical simulation

Direct numerical simulation (DNS), considered as the most powerful computing approach, is a simulation technique in which complete time dependent Navier-Stokes equations and the

continuity equation are solved numerically. This implies that when using DNS, all the scales of turbulence, right from the smallest eddies (Kolmogorov length scale) to the largest integral eddies which contain most of the kinetic energy are to be resolved. As described by Wilcox (2006), the number of operations in DNS increases as Re^3, and thus the computational cost of DNS is very high even for moderate Reynolds numbers. Due to this, DNS is used only for the fundamental turbulence research. The current research is limited to the RANS modeling approach, and thus DNS is not discussed in more detail.

3.5 Near wall treatment

Turbulent flows are found to be significantly affected by the presence of walls. Hence an appropriate wall treatment is required to predict wall bounded turbulent flows. The near-wall treatment significantly affects the accuracy of numerical solutions, as walls are the main source of mean vorticity and turbulence. It is in this region that the turbulence parameters like velocity and pressure have large gradients, and the momentum transport occurs most strongly. Therefore, precise representation of the flow in the regions near the wall is important in successfully approximating the wall-bounded turbulent flows.

There are fundamentally three types of wall treatments as described in the FLUENT user manual

- The high y+ wall treatment, in which it is assumed that the near-wall cell is in the outermost layer (logarithmic region) of the boundary layer.
- The low y+ wall treatment, in which it is assumed that the innermost layer (viscous sublayer) is suitably resolved.
- The all y+ wall treatment, which is a combination of the above two approaches, uses the high y+ wall treatment for coarse meshes and the low y+ wall treatment for fine meshes.

The wall treatments are developed according to each turbulence model, since assumptions specific to that model are made for wall boundary conditions for turbulence parameters.

3.5.1 Near wall treatment for $k - \omega$ and $k - \varepsilon$ models

As described in the FLUENT user manual (2010), the wall boundary conditions for the k equation in the $k - \omega$ model are similar to the k equation for enhanced wall treatment with the $k - \varepsilon$ model. This indicates that all boundary conditions for wall function meshes will correspond to the wall function approach, while for the fine meshes, the appropriate low Reynolds number boundary conditions will be applied.

The popular near wall treatment for k – ε models has been proposed by Launder and Spalding (1974). The wall function method developed by the authors has been widely used for many practical applications. In Figure 3.1 "p" is a point in the domain at a distance of y_p from the wall surface.

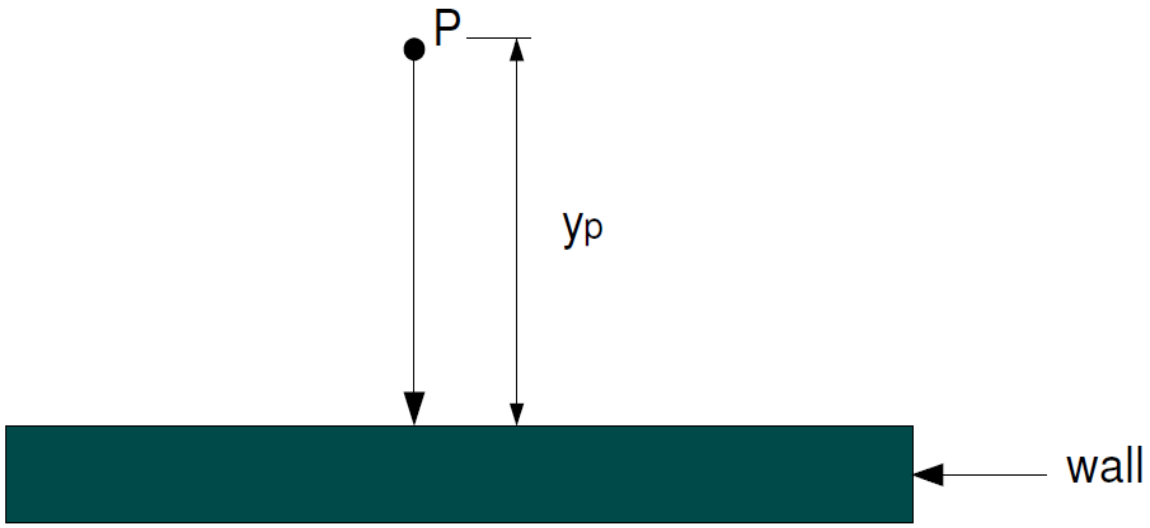

Figure 3.1: Near wall treatment

When using this wall function method, it is important to make sure that point "p" is at a sufficient distance from the wall so that the viscous effects there are completely dominated by the turbulent ones. The formulation given by Launder and Spalding (1974) is as follows.

The momentum flux to the wall is given by,

$$\frac{U_p}{(\tau/\rho)_w} C_\mu^{1/4} k_p^{1/2} = \frac{1}{k}\, ln\left[E_{yp} \frac{\left(C_\mu^{1/2} k_p\right)^{1/2}}{\vartheta}\right] \tag{3.17}$$

Where U_p is the time average velocity of the fluid at point P, τ_w is the wall shear stress in the direction of U_p, K_p is the turbulent kinetic energy at point P, E is the wall roughness function, whose value is approximately 0.9 for smooth walls, C_μ is the modeling constant for $k - \varepsilon$ model, k is the Von Karman constant and υ is the kinematic viscosity of the fluid.

When evaluating the value of K_p, it is important to assign a value for average energy-dissipation rate over the control volume, which is inferred from the assumption that

$$\int_0^{y_p} \varepsilon dy = C_\mu \frac{k_p^{3/2}}{k} ln\left[E_{yp} \frac{\left(C_\mu^{1/2} k_p\right)^{1/2}}{\vartheta}\right] \tag{3.18}$$

A comparison of near wall treatment methods using various turbulence models was done by Kim et al. (2005) for the flow over a backward facing step. The Reynolds number based on the step height was 38000 with the free stream velocity of 44.2m/s. They used standard wall functions and non-equilibrium wall functions of the *k*-ε turbulence model and compared their results with the experimental results of Driver and Seegmiller (1985). The authors found that the non-equilibrium wall functions with some modifications in the *k*-ε model gave the results closest to the experimental results. Thus the authors concluded that a proper combination of turbulence models and the appropriate near wall treatment gives reliable results.

3.6 Modeling the discrete phase

There are primarily two ways of describing the motion of a fluid. First is the Lagrangian approach, where the fluid is stationary and the motion is described by a moving particle in the fluid. The second approach is the Eulerian, in which, the particle is stationary and the motion is described by the moving fluid around the particle. In the discrete phase model, particle trajectories are computed in a Lagrangian frame, while the continuous phase is modeled in Eulerian frame. The discrete phase model does not take in to account the particle interactions in the domain. Hence it is always recommended to have a maximum value for volume fraction of about 10%. If higher value of volume fraction is used, then particle interaction becomes significant and it might affect the accuracy of results. The discrete phase model accounts for effects of turbulence on particle trajectories, which are computed by integrating the force balance equation

$$\frac{dv}{dt} = F_D(u - v) + g\left(1 - \frac{\rho}{\rho_p}\right) + \frac{F_i}{\rho_p} \tag{3.19}$$

Where

- u and v are the continuous phase and discrete phase particle velocities
- ρ and ρ_p are the continuous phase and discrete phase particle densities
- F_D is the drag force given by $\frac{18\mu_c}{\rho_p D^2} C_D \frac{R_e}{24}$
- C_D is the drag coefficient
- D is the particle diameter and Re, the Reynolds number
- F_i is the external force, which includes pressure or temperature gradient, Brownian motion, Saffman lift force etc.

For the current study, as mentioned earlier, particles with varying Stokes number are injected in the domain.

Fessler and Eaton (1999) describes how the drag coefficient, and hence the Stokes number for the particles, changes with increasing Reynolds number. By definition, Stokes number is the ratio of particle time response to a representative time scale in the domain.

$$S_t = \frac{\tau_p}{\tau_f}$$

And the particle time constant is $\tau_{p,stokes} = \frac{\rho_d D^2}{18\mu_c}$

But this time constant is valid only for creeping flow. As the Reynolds number increases, the drag coefficient is corrected to

$$C_D = \frac{24}{R_e}[1 + 0.15R_e^{0.687}]$$

The increase in drag coefficient with Reynolds results in shorter particle response time.

As described in the FLUENT user manual (2010), the turbulent dispersion can be modeled either by stochastic particle tracking, in which particle trajectories are predicted using the mean continuous phase velocity or by particle cloud tracking, where, the turbulent dispersion of particles about a mean trajectory is calculated using statistical methods. In the current study, stochastic particle tracking is used and the effects of turbulence are added by adjusting the number of tries. If the value for the number of tries is set to zero, then the particle trajectory is computed based on mean continuous phase velocity field, ignoring the effects of turbulence. The turbulent velocity fluctuations are included when the input value for the number of tries is set to one or more. Each number of tries represents a different particle trajectory and every trajectory includes a new stochastic representation. For the current study, gravity effects are not included on the particle motion. When the gravity effects are considered, some of the particles in the flow might reach their settling velocity and they might settle down at the bottom wall.

3.6.1 Saffman lift force

This is a lift force due to shear, which is mainly encountered when considering small particle Reynolds numbers and is valid only for submicron particles. The equation for Saffman lift force, as represented in the FLUENT user manual (2010) is given by

$$F = \frac{2k\vartheta^{\frac{1}{2}}\rho d_{ij}}{\rho_p D(d_{lk}d_{lk})^{\frac{1}{4}}}(u - v) \tag{3.20}$$

Where k=2.594 and d_{ij} is the deformation tensor. u and v are the velocities of continuous phase and discrete phase respectively.

In the current study, this force is used as an additional force on the injected particles.

Thus for the current study, the continuous phase is modeled using *k*-ε RNG turbulence model with standard wall functions. The grid adaptation near the wall, as described in the subsequent chapter, is done using the gradient approach. The particle injections are modeled using the Discrete phase model of FLUENT with the Stochastic approach. The subsequent chapter describes the detailed methodology and the boundary conditions used for the current study.

CHAPTER 4

METHODOLOGY AND BOUNDARY CONDITIONS

4.1 Introduction

In computational fluid dynamics, convergence of the solution is a major issue, and it has to be considered with utmost care. It is very difficult to simulate a detailed flow where an unsteady phenomenon like turbulence dominates other flow characteristics. Thus a choice of proper turbulence model, which will simulate an extremely complex flow and resemble a real flow-field with precision, is of prime importance. It is also important to ensure that the geometry under consideration extends far enough to ensure a fully developed flow. A shorter outlet or inlet section may result in a non-converging solution. A proper choice of grid is also essential to ensure that it resolves the variations in flow, arising because of the geometry or other flow characteristics. An improper grid can affect the convergence as well as the accuracy of results. The flow separation and reattachment encountered in the current study are largely dependent on the prediction of near wall turbulence. Thus near wall treatment is extremely important to deal with flow separation and reattachment, and the selected mesh should be able to resolve this near wall region with a high level of accuracy. In order to obtain an accurate solution for iterative convergence, as described by Roache (2002), the value of residual error should be set to a very low value. In the present study, this value is set to $1e^{-6}$, which is low enough to achieve proper convergence. The subsequent sections of this chapter deal with creating geometry, grid generation and adaptation, the modeling process and the boundary conditions applied for the current study

4.2 Grid generation and adaption

The 2-D backward facing step geometry is created in ICEM CFD. Selection of a two dimensional geometry is mainly due to the fact that the experimental flow by Yao (2000) was primarily 2-D due to a high aspect ratio. While creating the grid in ICEM CFD, units are not important, but while simulating the flow in FLUENT, all the parameters must be in SI units. For 2-D geometries, *z* co-ordinates are set to a default value of zero. An inlet channel length of 10h before the step and outlet channel length of 30h after the step are used. In ICEM CFD, both structured and unstructured meshes are available. In the current study, a fully structured quadrilateral mesh is used. Grid adaption based on velocity gradients with a refine threshold value of 0.5 (as described in FLUENT user manual (2010)) is then employed for near wall treatment to achieve an appropriate value of y+. In the current study, *k*-ε RNG turbulence model with standard wall functions is used and the gradient grid adaption ensures y+ value between 30 - 60 for both Reynolds number of 6550 and 10000. Figure 4.1 below depicts the mesh created, with a number of cells equal to 44801.

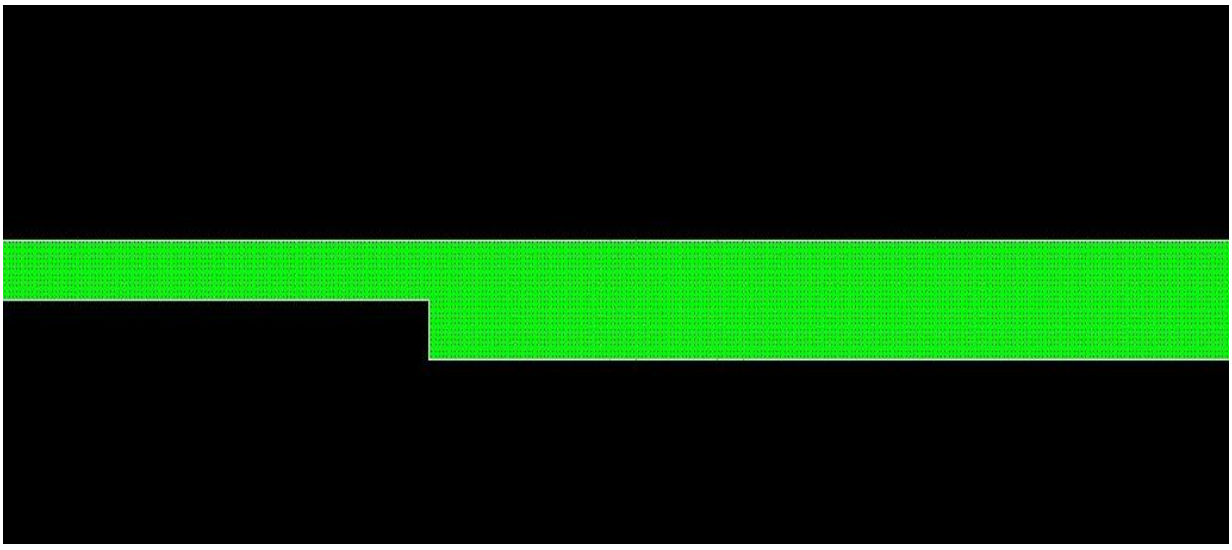

Figure 4.1: 2-D backward facing step

4.3 Boundary conditions

4.3.1 Velocity inlet

This boundary condition has been applied to the inlet section of the step. The velocity values are based on Reynolds number calculations described in Chapter 1. The turbulence intensity of 5% is used and the hydraulic diameter of 25mm (equal to step height) is used.

4.3.2 Wall

The wall boundary condition is applied to the top and bottom surfaces of the geometry. A stationary wall is considered with no slip condition. Default value of 0.5 as given by FLUENT for wall roughness constant is considered.

4.3.3 Outflow

The outflow boundary condition is used for the channel outlet. Basically there are two different types of boundary conditions, the *outflow* and the *pressure outlet*, which can be used for channel outlet. The main difference between these two conditions, as described in Poinsot and Lele (1992), is that for pressure outlet, the flow at the exit is monitored with some specified pressure. In this case, the flow may or may not reach fully developed condition. The outflow boundary condition on the other hand is consistent with the fully developed flow assumption and assumes a zero diffusion flux for all flow parameters. In the current study, the outflow condition is applied since the flow at the exit is fully developed.

4.3.4 Porous medium

The fundamental relation for a flow through a porous medium is given by Darcy's equation

$$\Delta p = -\frac{\mu}{\alpha} v \, \Delta t \tag{4.1}$$

Where Δp is the pressure drop, μ is the fluid viscosity, α is the constant of proportionality called the permeability of the porous medium, v is the mean velocity and Δt is the thickness of the medium. Porous jump boundary condition, as described in FLUENT user manual (2010), may be used to model membranes that have known velocity or pressure drop characteristics. This condition is mainly used to model flow through screens and filters, especially where heat transfer is not important. The user manual suggests that it is advisable to use porous jump instead of full porous medium model because of its robustness and ability to yield better convergence. Pressure drop across the porous medium, used for the porous jump boundary condition, may be defined as a combination of Darcy's law and an additional inertial loss term

$$\Delta p = -\left(\frac{\mu}{\alpha} v + C_2 \frac{1}{2} \rho v^2\right) \Delta t \tag{4.2}$$

Where,

- μ is the fluid viscosity
- α is the permeability of the porous medium
- C_2 is the pressure jump coefficient
- v is the fluid velocity normal to the porous medium
- Δt is the thickness of porous medium

For the current study, the values for porous medium variables, obtained by Yao (2000) are used. They are given in the following table

Parameter	Value	units
Permeability (α)	$1.17 * 10^{-9}$	m^2
Pressure jump coefficient (C_2)	$4.533 * 10^{3}$	1/m
Thickness	15	mm

Table 4.1: Porous medium parameters as given by Yao (2000)

4.4 Discrete phase modeling

The Discrete phase model of FLUENT is used to study the impact of the recirculation zone on particulate injections. The particles used for the current study are fine Arizona test dust particles of class A2 given by "Powder Technology Inc.". The density of particles is 500 kg/m^3.depending on the diameter used. Input diameter of the particles is adjusted according to their Stokes number, which is given by

$$S_t = \frac{\tau_v U}{h} \tag{4.3}$$

Where U is the fluid velocity, h is the step height and τ_v is the momentum or velocity response time. This response time for the particles is the time taken to react to momentum transfer. The response time is given by the following equation. (Crowe, Sommerfeld and Tsuji (1998))

$$\tau_v = \frac{\rho_d D^2}{18\,\mu_c} \tag{4.4}$$

Where ρ_d is the density of dispersed phase, particles in this case, D is the particle diameter and μ_c is the viscosity of the continuous phase, which is air in this case. The response time given above assumes low particle Reynolds number. Three different Stokes numbers ranging from 0.1 to 10 are used in the current study. Input velocity for particles is given as 2.5 m/s for the Reynolds number of 6550 and 4m/s for the Reynolds number of 10000. The input velocity for discrete phase is kept close to that of the continuous phase. The Discrete random walk model is used for turbulent dispersion which includes the effect of instantaneous turbulent velocity formulations on particle trajectories through a stochastic method. In this method, the turbulent dispersion of the particles is calculated by integrating the trajectory equations for individual particles using the instantaneous velocities of the continuous phase. As described in the FLUENT user manual (2010), the random walk model determines the instantaneous velocity of the continuous phase. The fluctuating velocity components are constant functions of time and their random value is kept

constant over an interval of time specified by the characteristic lifetime of the eddies. In this way, the random effects of turbulence on the particle dispersion are taken into consideration. To study polydispersed particles, the Rosin Rammler diameter distribution is used with minimum diameter corresponding to Stokes number of 0.1 and maximum diameter corresponding to Stokes number of 10. The number of particles is adjusted by adjusting the number of tries in turbulent dispersion section. The time scale constant, which is a Lagrangian time scale, is found iteratively such that the particle trajectories are dispersive.

4.5 Solution controls

The pressure – velocity coupling method used for the current study is SIMPLE which is the default method given by FLUENT. The discretization schemes used for pressure, momentum, turbulent kinetic energy and turbulent dissipation are tabulated below

parameter	scheme
pressure	standard
momentum	Second order
Turbulent kinetic energy	Second order
Turbulent dissipation	Second order

Table 4.2: Discretization schemes

The second order discretization scheme is used because of the complexity of the flow. Due to flow separation and reattachment, the flow is not properly aligned with the grid. In such cases, the second order scheme results in better convergence than the first order scheme, as described in the FLUENT User manual (2010)

.

CHAPTER 5

RESULTS AND DISCUSSION

5.1 Grid independence

Grid independence is one of the most important parameters in computational fluid dynamics. The results obtained without performing grid independence studies might prove costly, in that the engineering designs can be made based on inappropriate data. In the present study, grid independence is carried out for the higher Reynolds number of 10000 with three different mesh sizes. The velocity profiles at three different locations in the domain are compared for all the three meshes. The details of the meshes used is tabulated in table 5.1

Mesh Quality	Number of cells
Coarse	20576
Medium	44801
Fine	79390

Table 5.1: Mesh size

and the lengths of reattachment for each mesh are given in Table 5.2

Mesh	Recirculation zone length
Coarse	7.38h
Medium	7.11h
Fine	6.93h

Table 5.2: Reattachment length for different meshes

The reattachment lengths found for different mesh sizes are in good agreement with the experimental results of Yao (2000), which gave the reattachment length of about 7h, and with the numerical analysis of Krishnamoorthy (2007), which gave a reattachment length of 6.6h, using the realizable *k*-ε turbulence model

Figure 5.1 shows the comparison of velocity profiles at the step for the Reynolds number of 10000 for the above mentioned mesh sizes, while Figures 5.2 and 5.3 show the velocity profiles at X = 3.75h and X = 6.25h from the step.

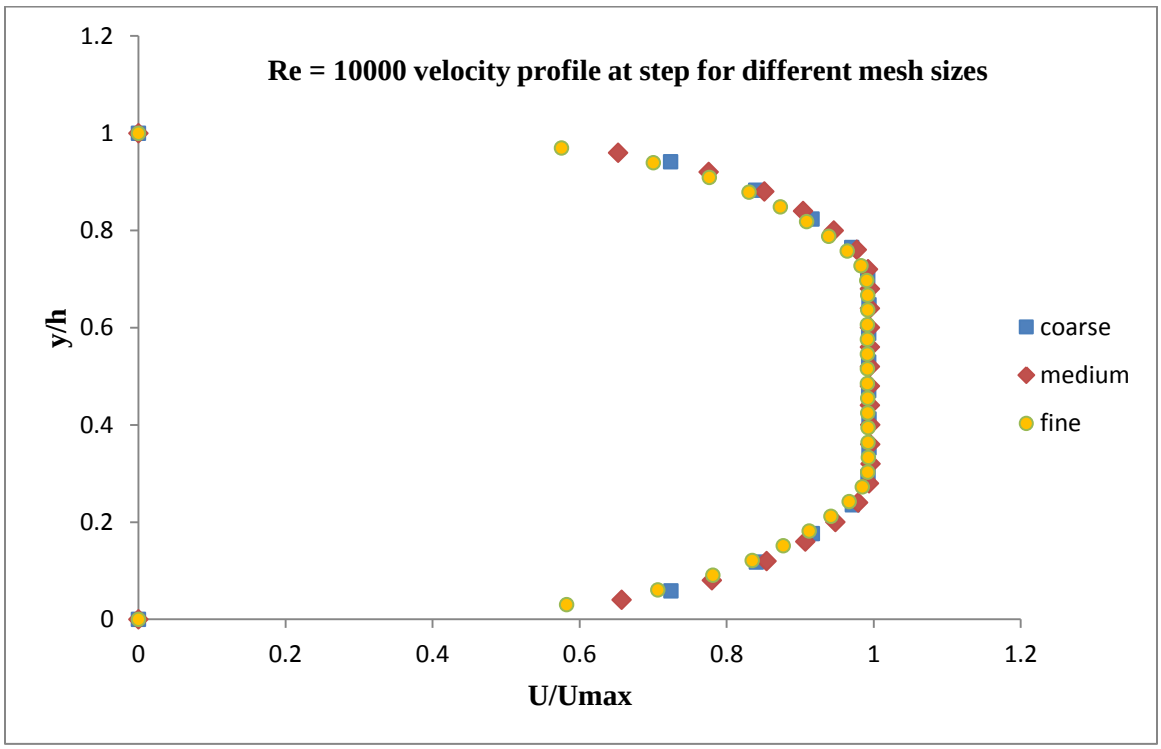

Figure 5.1: Comparison of Velocity profiles at step for different mesh sizes for Re = 10000

It can be seen from the figure that the velocity profiles at each location are independent of the mesh size. For the current study, in order to reduce the computational time, the medium size mesh is used with k – ε RNG turbulence model and standard wall functions

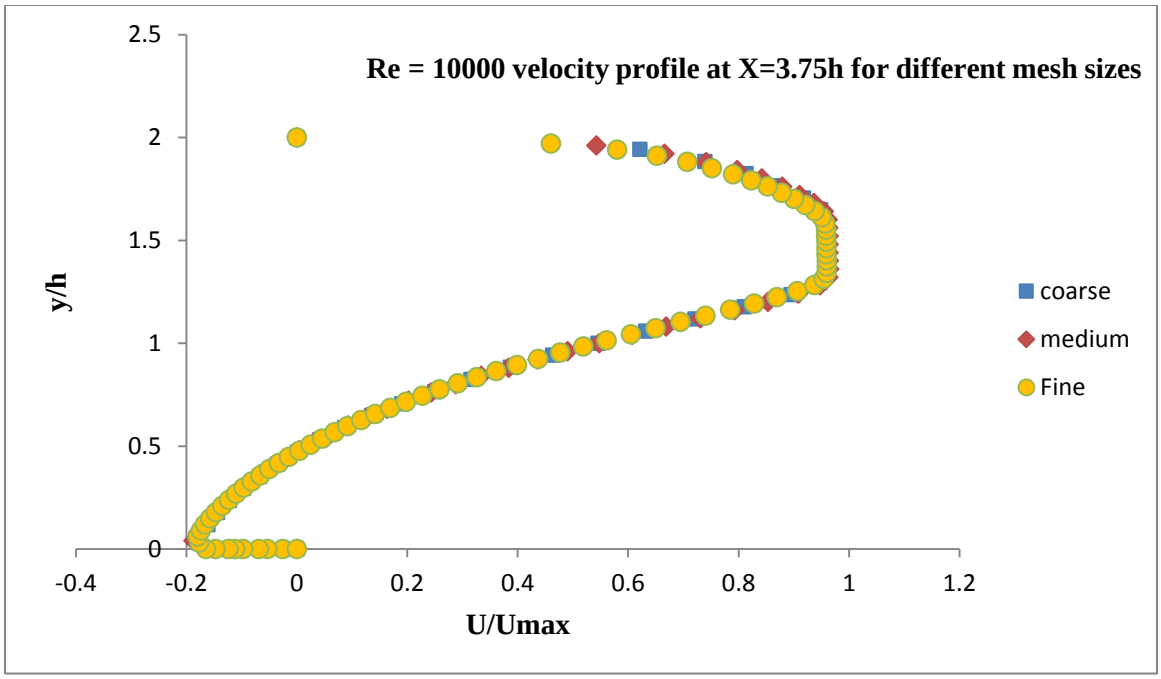

Figure 5.2: Comparison of velocity profiles at X = 3.75h for different mesh sizes for Re = 10000

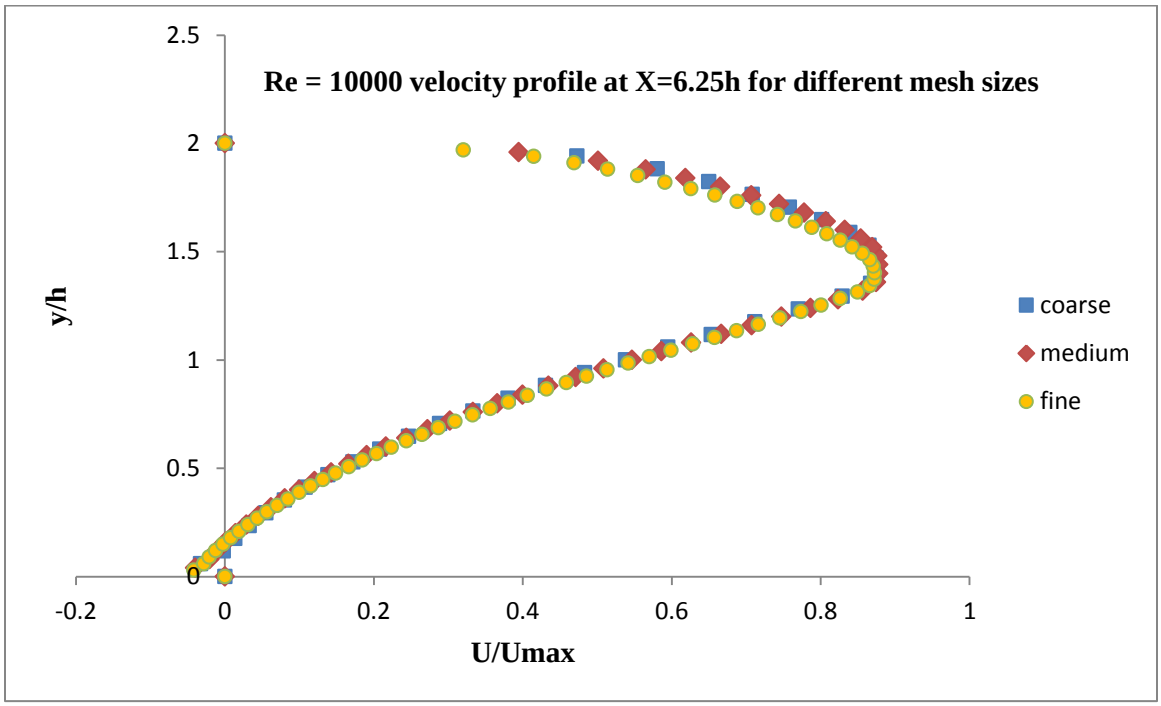

Figure 5.3: Comparison of velocity profiles at X = 6.25h for different mesh sizes for Re = 10000

5.2 Fully developed flow

The inlet channel length of 10h behind the step ensures that the flow just before the separation at the step is in a nearly fully developed condition. This is confirmed by comparing the velocity profile at the step with three different locations just behind the step. The velocity profiles at these locations match very well. Fully developed condition at the step is also verified by comparing the velocity profile with the power law.

The turbulent channel flow velocity profile is given by

$$\frac{U}{U_{max}} = \left(\frac{y}{h}\right)^{1/n}$$

Where

- U is the mean flow velocity
- U_{max} is the maximum velocity at the centerline
- y is the vertical distance from the wall
- h is the step height (half the channel height)
- n is the power law parameter

Variation of the power law parameter "n" is given in table 5.3

Re_D	$4x10^3$	$2.3x10^4$	$1.1x10^5$	$1.1x10^6$	$2.0x10^6$	$3.2x10^6$
n	6.0	6.6	7.0	8.8	10	10

Table 5.3: Variation of power law parameter with the Reynolds number - Schlichting (2000)

According to Table 5.3, n = 6.6 for both Re = 6550 and Re = 10000

Figures 5.4 to 5.7 shows the comparison of velocity profiles at the step with different locations behind the step and with the power law profile for Reynolds numbers 6550 and 10000

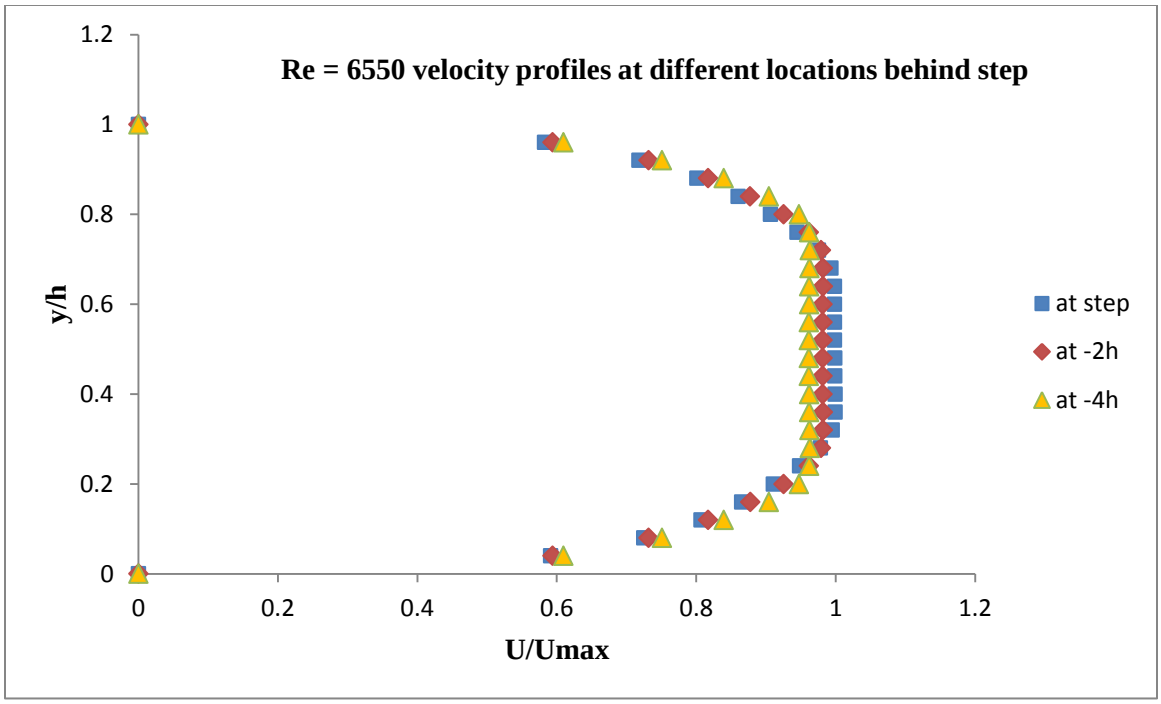

Figure 5.4: Velocity profile comparison at step with different locations behind step for Re = 6550

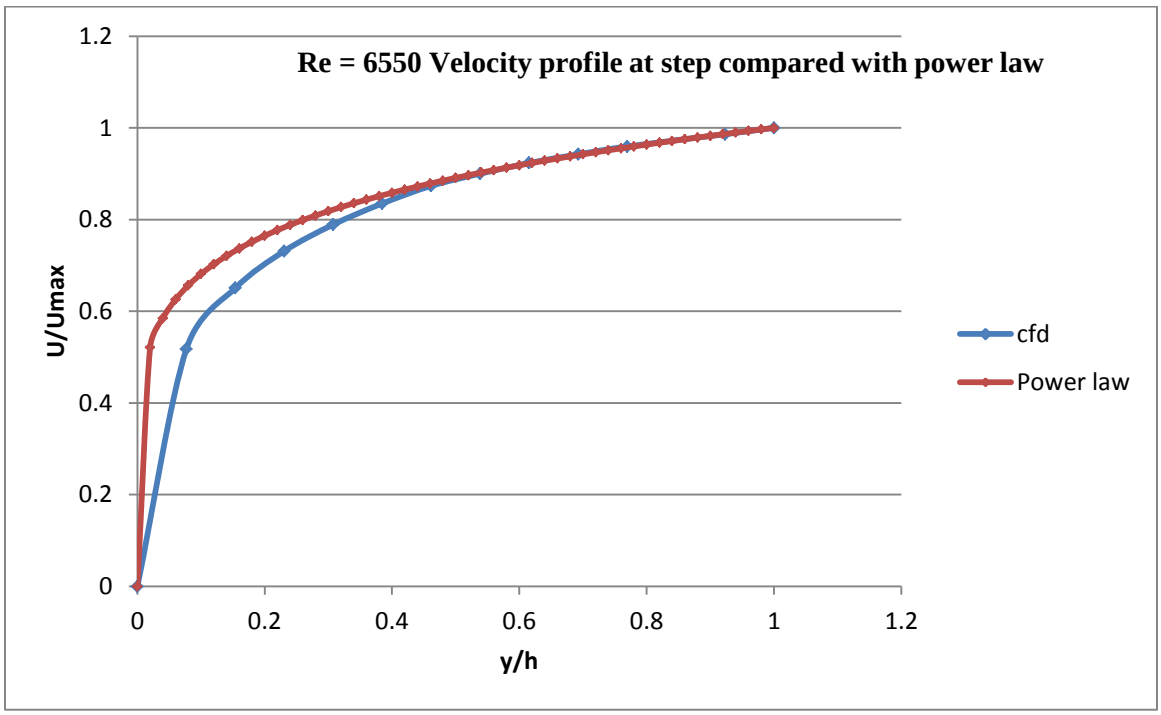

Figure 5.5: Velocity profile comparison at step with the power law profile for Re = 6550

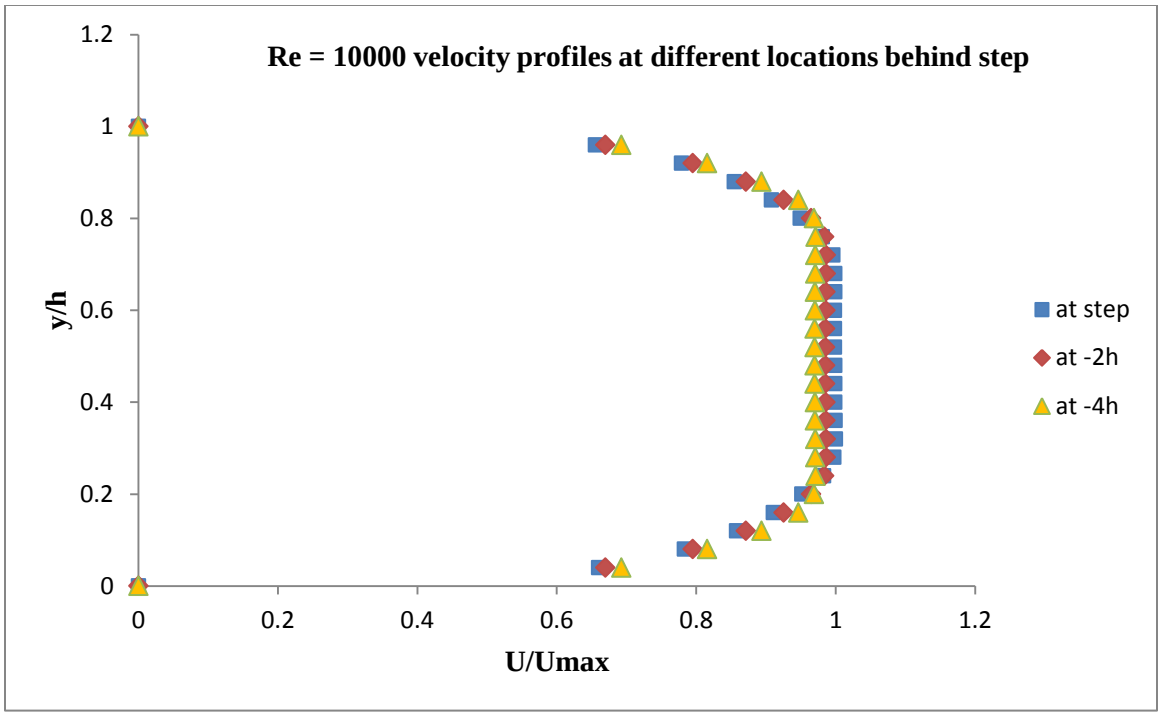

Figure 5.6: Velocity profile comparison at step with different locations behind step for Re = 10000

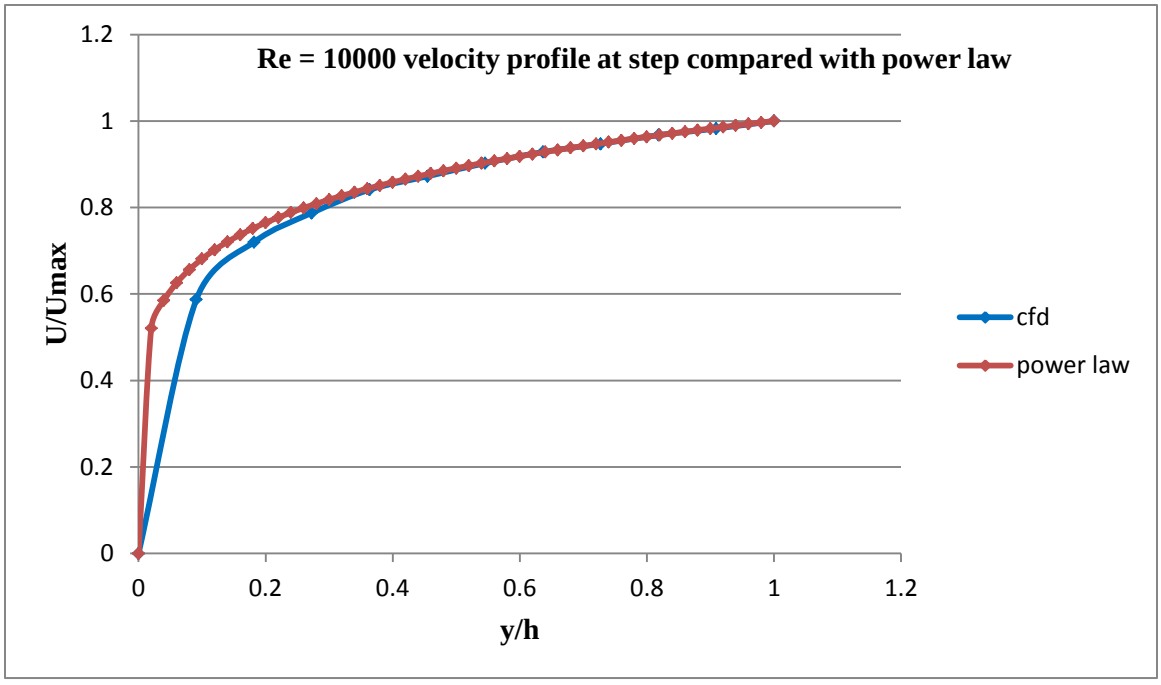

Figure 5.7: Velocity profile comparison at step with the power law profile for Re = 10000

5.3 Velocity field analysis for no filter case

5.3.1 Location at the step

Figure 5.8 shows the velocity profile for the Reynolds number of 6550 at the step, compared with experimental results of Yao (2000) and numerical results of Ravi (2010). The flow is nearly fully developed at this location, as described in the previous section.

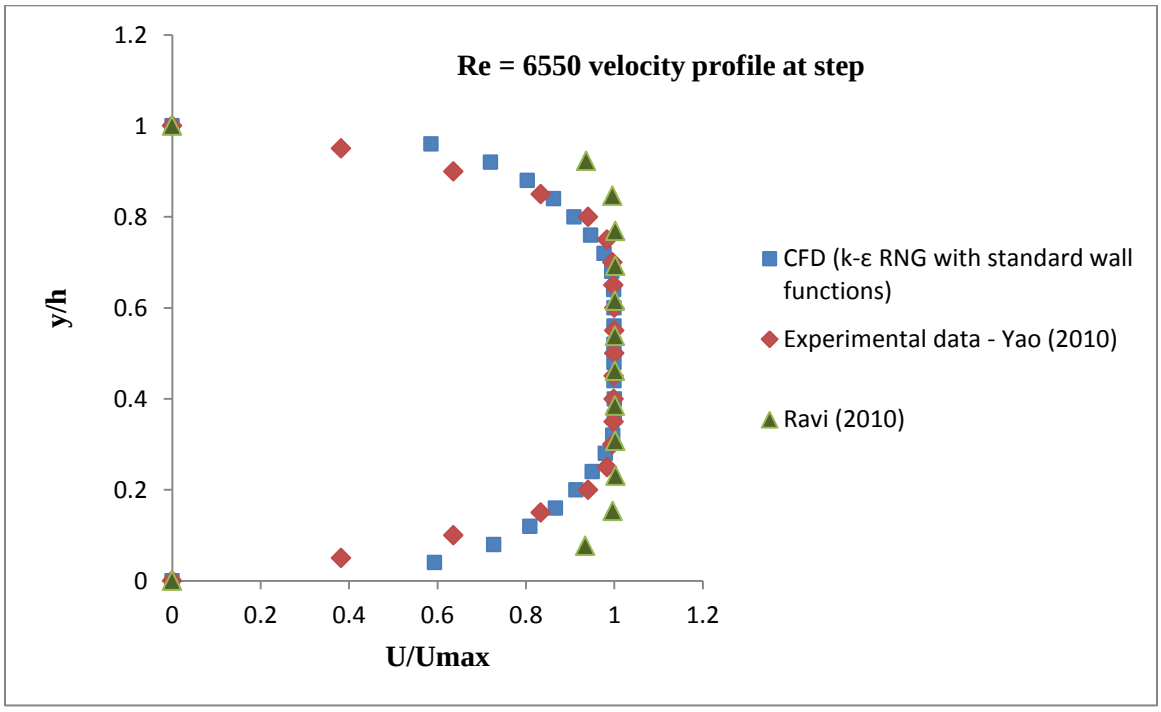

Figure 5.8 Comparison of velocity profiles at step for Re = 6550 for no filter case

From Figure 5.8, it can be seen that the profiles match well with the experimental data. The difference between numerical results of the current study and that of Ravi (2010) near the wall can be attributed to the difference in the inlet channel lengths before the step. Similar results can be found for the higher Reynolds number of 10000.

Figure 5.9 shows the velocity profiles at the step for Re = 10000

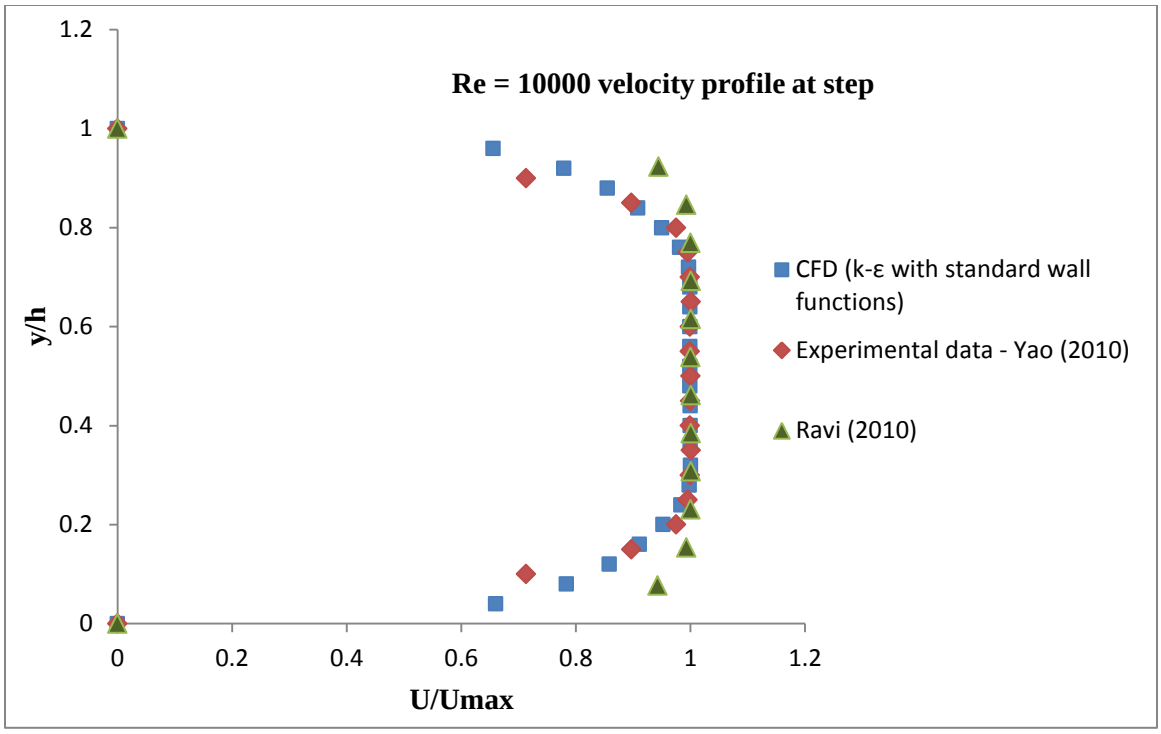

Figure 5.9: Comparison of velocity profiles at step for Re = 10000 for no filter case

Figure 5.9 shows good agreement between the numerical and the experimental results. The difference between the two numerical results can either be due to the different inlet channel lengths or due to the different wall functions used.

5.3.2 Location at X = 3.75h from the step

Figures 5.10 and 5.11 depict the velocity profiles at a horizontal distance of 3.75h from the step for Re = 6550 and Re = 10000, compared with experimental results of Yao (2000) and numerical results of Ravi (2010). The profiles match well in the middle region, but there is a slight variation near the wall region where the flow is reattached, even with the mesh adapted near the wall. This variation may be caused by the standard wall function used. The velocity drop is due to the recirculation zone produced by the sudden expansion just ahead of the step.

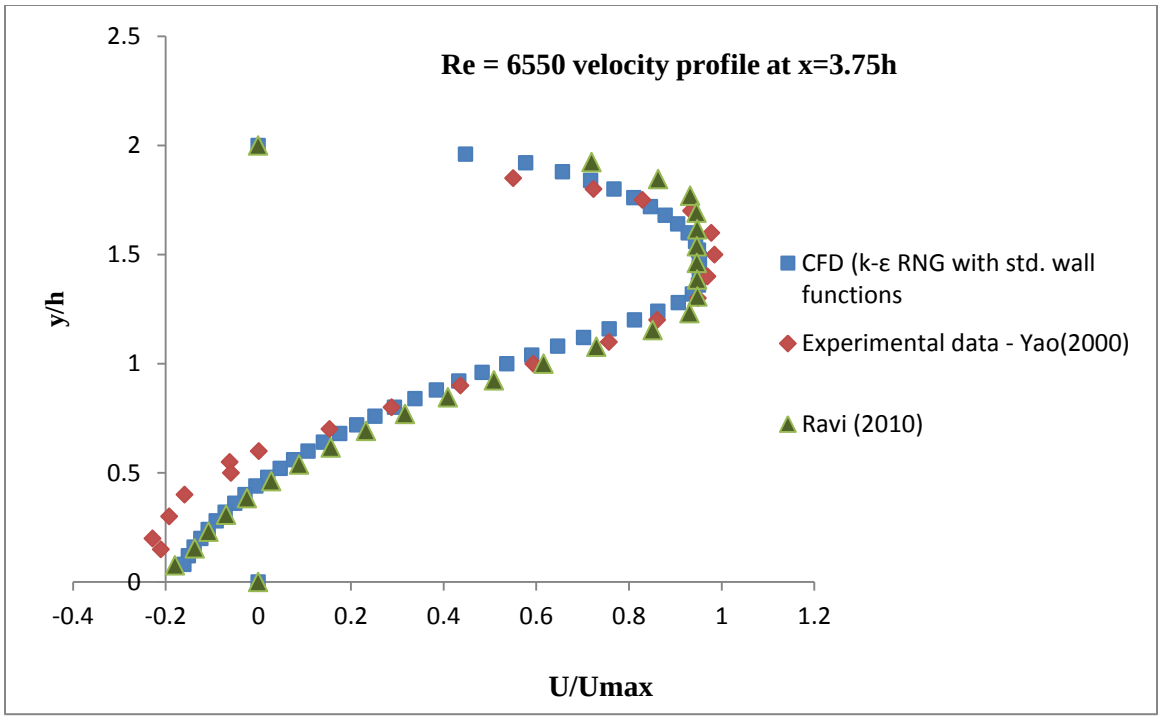

Figure 5.10: Comparison of velocity profiles at X = 3.75h for Re = 6550 for no filter case

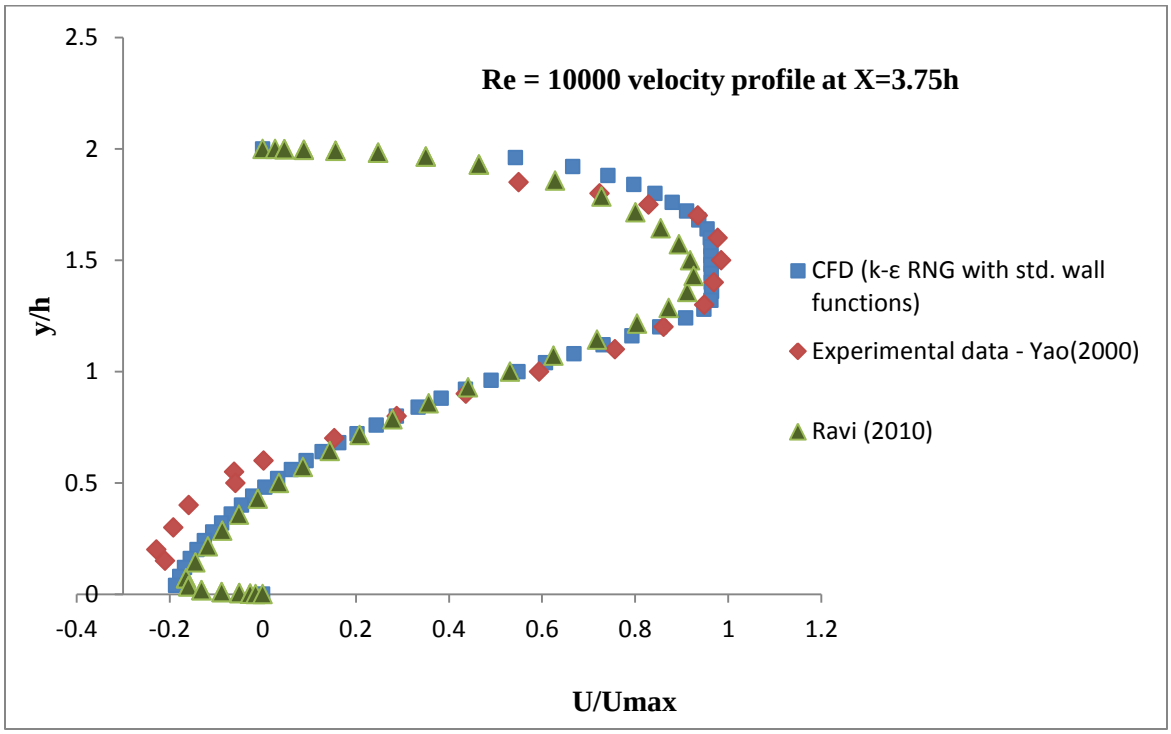

Figure 5.11: Comparison of velocity profiles at X = 3.75h for Re = 10000 for no filter case

5.3.3 Location at X = 6.25h from the step

Figures 5.12 and 5.13 show the velocity profiles further downstream at a distance of 6.25h from the step for Reynolds numbers 6550 and 10000. The profiles match very well with the experimental results in the middle as well as near the walls. This is due to the fact that the current location is near the reattachment section, and hence the turbulence models tend to perform better than with the previous case of X = 3.75h, which is right in the middle of the recirculation zone.

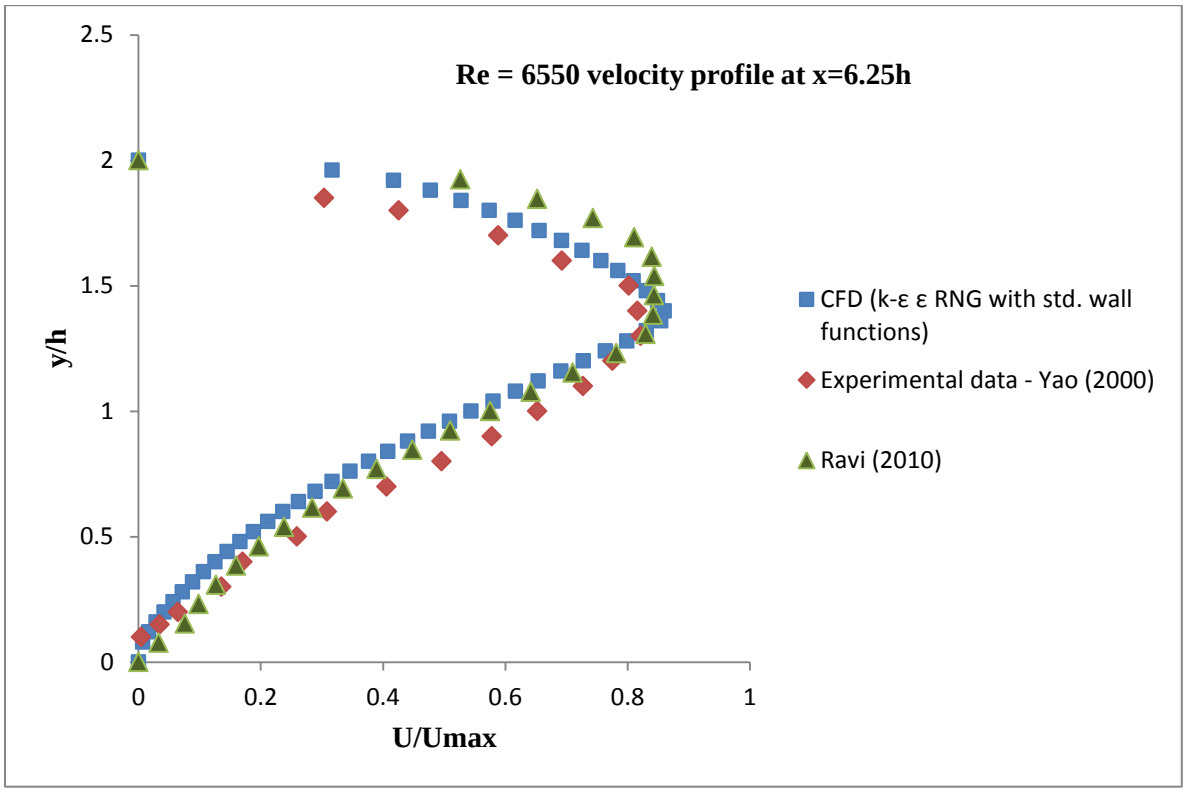

Figure 5.12: Comparison of velocity profiles at X = 6.25h for Re = 6550 for no filter case

As we can see from Figure 5.12, all the velocities are on the positive side, which suggests that the recirculation zone has ended. There is a slight deviation between the two numerical results, which may be due to the different wall functions used.

Similar results can be seen in Figure 5.13, which shows the profiles for Reynolds number of 10000.

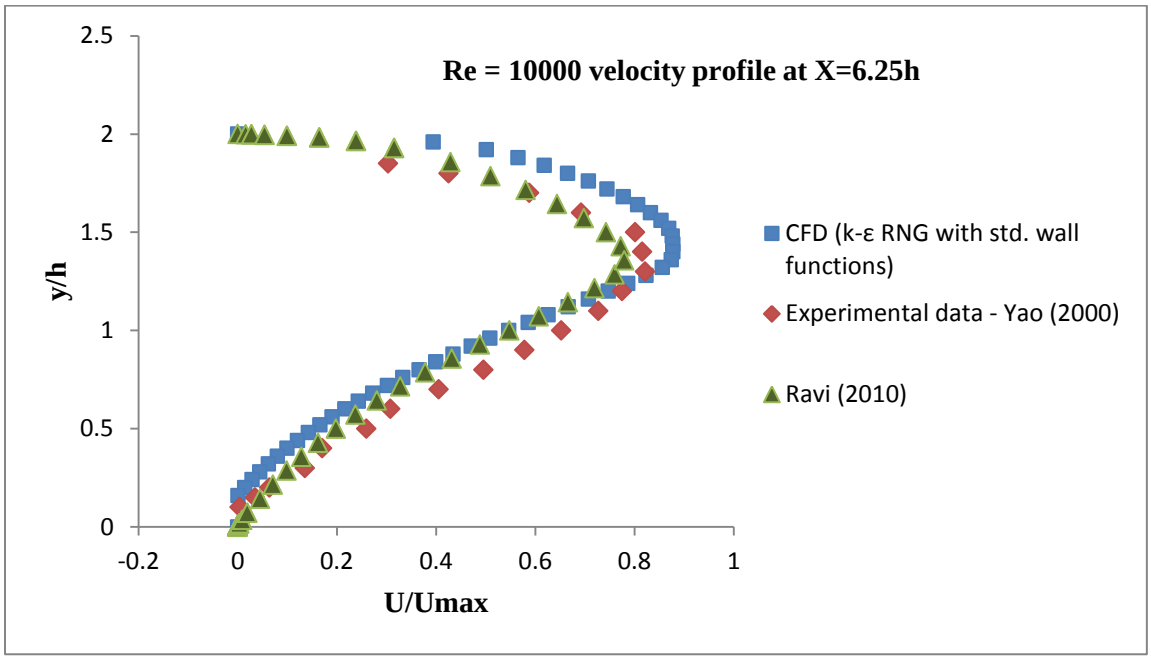

Figure 5.13: Comparison of velocity profiles at X = 6.25h for Re = 10000 for no filter case

5.3.4 Velocity contours

Good analysis of the flow field can be best made with flow velocity contours. Figures 5.14 and 5.15 show the velocity magnitude (in m/s) contours for Reynolds numbers 6550 and 10000 without the porous medium. The velocity contours help in analyzing the recirculation zone as well as the flow separation and reattachment. Figures 5.14 and 5.15 clearly show the flow separation due to sudden expansion at the step and the reattachment some distance downstream of the step. The reattachment lengths of "6.3h" for Reynolds number 6550 and "7.2h" for Reynolds number 10000 are in good agreement with the experimental results of Yao (2000) which give the lengths of "6.5h" for Reynolds number 6550 and "7h" for Reynolds number of 10000. The contours also show that the flow slowly starts developing downstream after the recirculation zone.

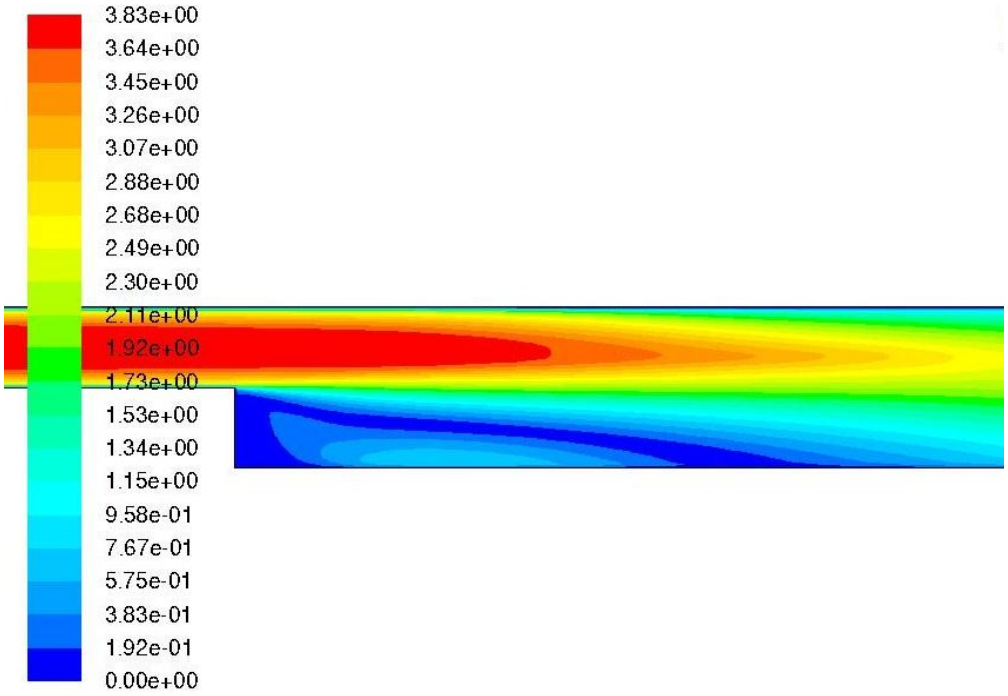

Figure 5.14: Velocity contours for Re = 6550 for no filter case

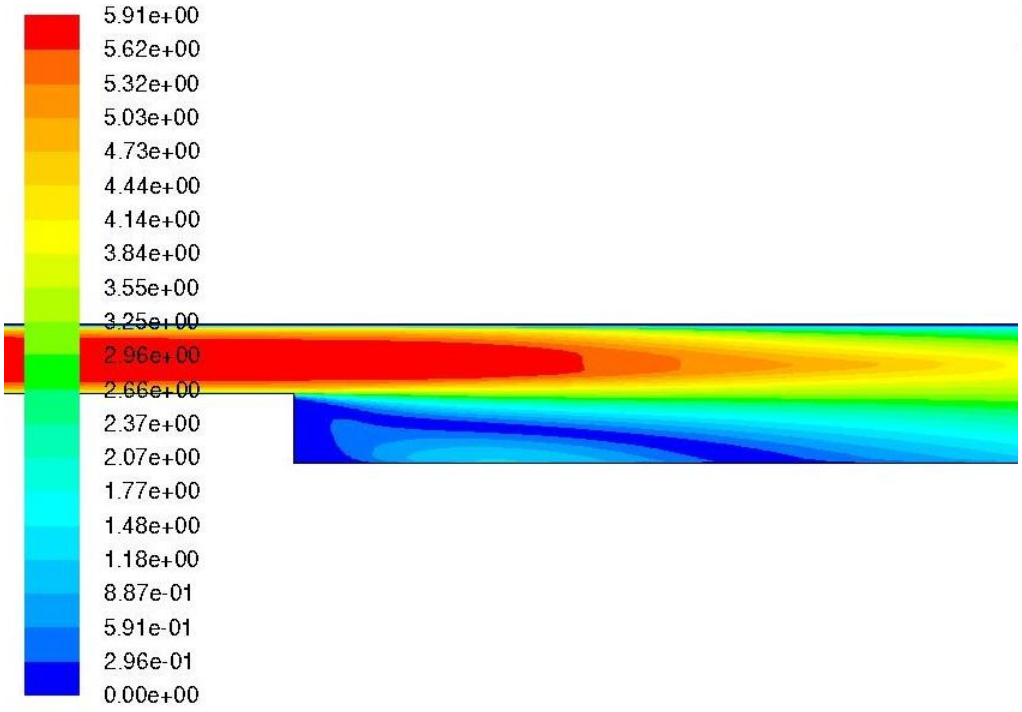

Figure 5.15: Velocity contours for Re = 10000 for no filter case

5.4 Velocity field analysis for filter at X = 4.25h

The velocity profiles and flow field analysis for the case of a pleated filter located at a distance of "4.25h" from the step is discussed in this section. Figures 5.16 and 5.17 show the velocity profiles for Reynolds numbers 6550 and 10000 respectively. The data is compared with the experimental results of Yao (2000) and with numerical results of Ravi (2010).

It is observed that when the filter is placed in the domain, the recirculation zone is shortened to a great extent and there is a big change in the flow field. The flow tends to reattach to the wall ahead of the filter location. The maximum velocity region is also shifted more towards the center of the channel as compared to the no filter case. The velocity profiles show a deviation from experimental results away from the wall. This can be due to the porous medium modeling. In the current study, the porous jump boundary condition is used to model the filter, which is a one-dimensional approximation of a full porous zone boundary condition. Because of the pleated design of a real air filter, the porous jump boundary condition does not accurately model the porous region, perhaps causing the deviation in velocity profiles from the experimental results. As compared to the region away from the wall, the near wall region and the flow reattachment are in good agreement with the experimental results.

The separation and early reattachment can be clearly seen in the velocity contours displayed in Figures 5.18 and 5.19 for Reynolds number 6550 and 10000 respectively. The contours are in m/s. The dark vertical line in the domain where the recirculation zone ends represents the porous medium, which is modeled using the porous jump boundary condition. After passing through the porous medium, the flow starts to develop downstream, becoming fully developed when it reaches the outlet. The velocity contours also show a prominent secondary recirculation zone at the top wall for both the Reynolds numbers due to the placement of the filter.

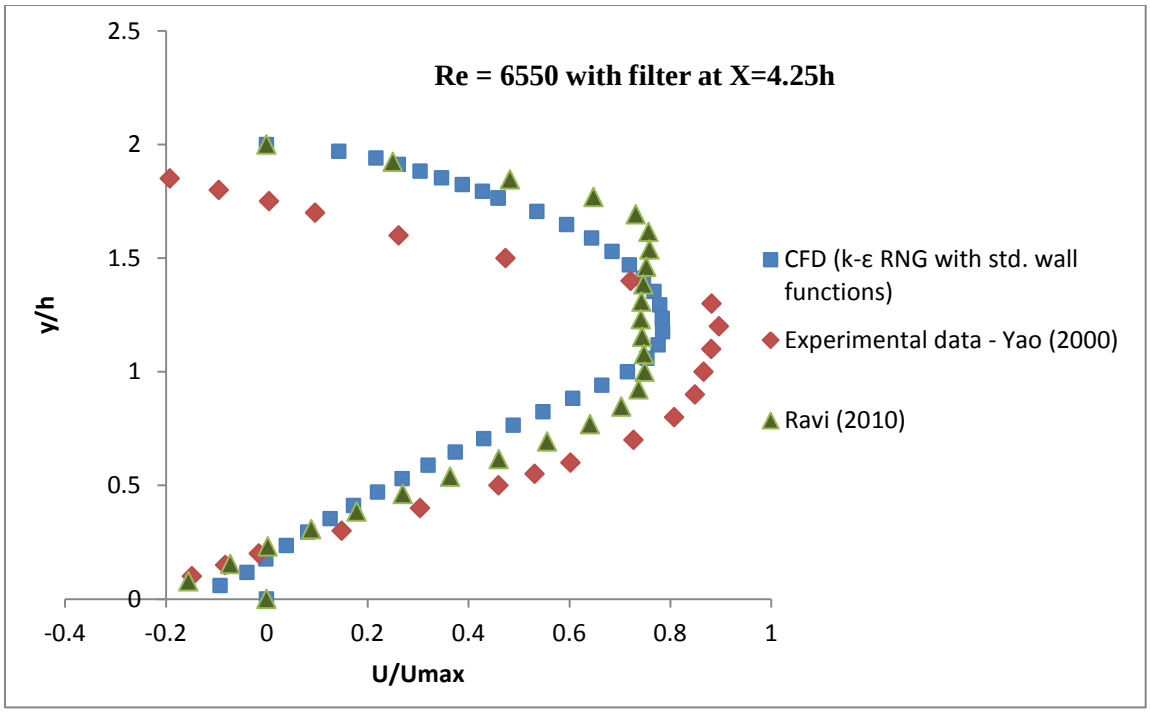

Figure 5.16: Comparison of Velocity profiles at X = 3.75h for Re = 6550 with filter at X = 4.25h

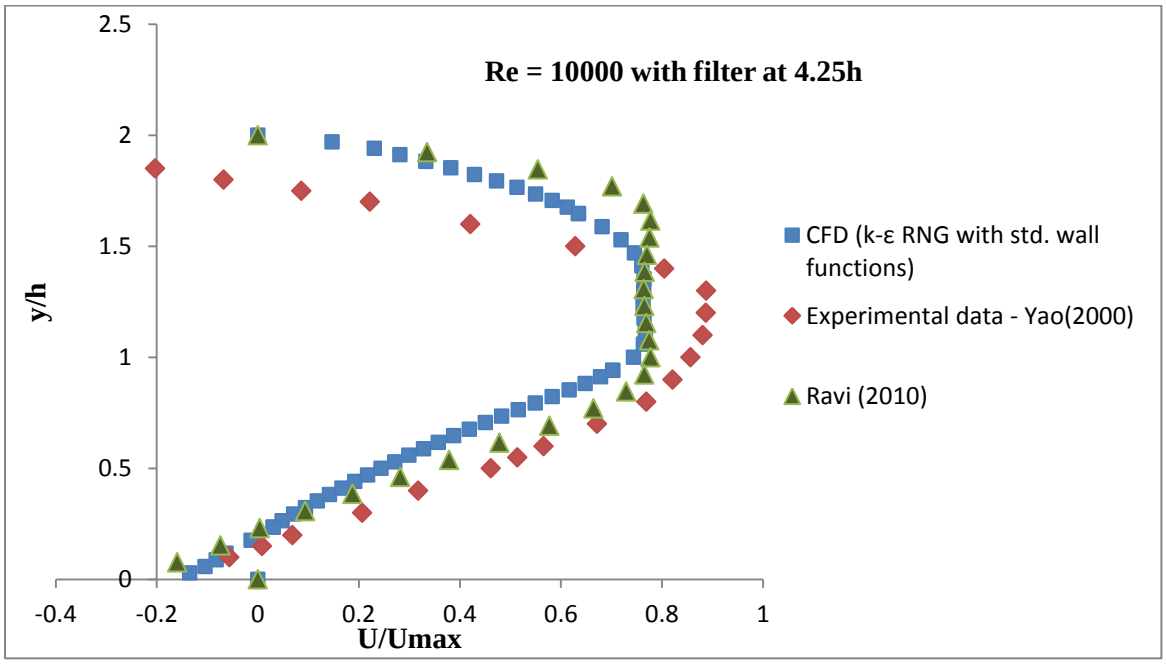

Figure 5.17: Comparison of velocity profiles at X = 3.75h for Re = 10000 with filter at X = 4.25h

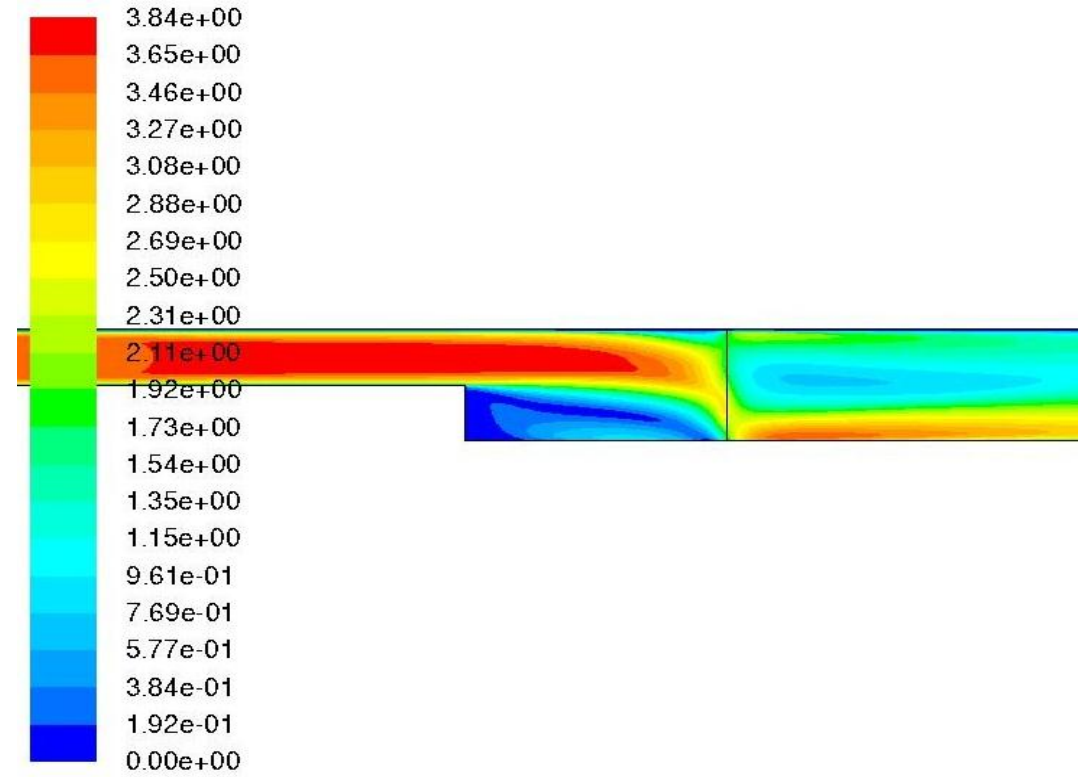

Figure 5.18: Velocity contours for Re = 6550 for filter at X=4.25h

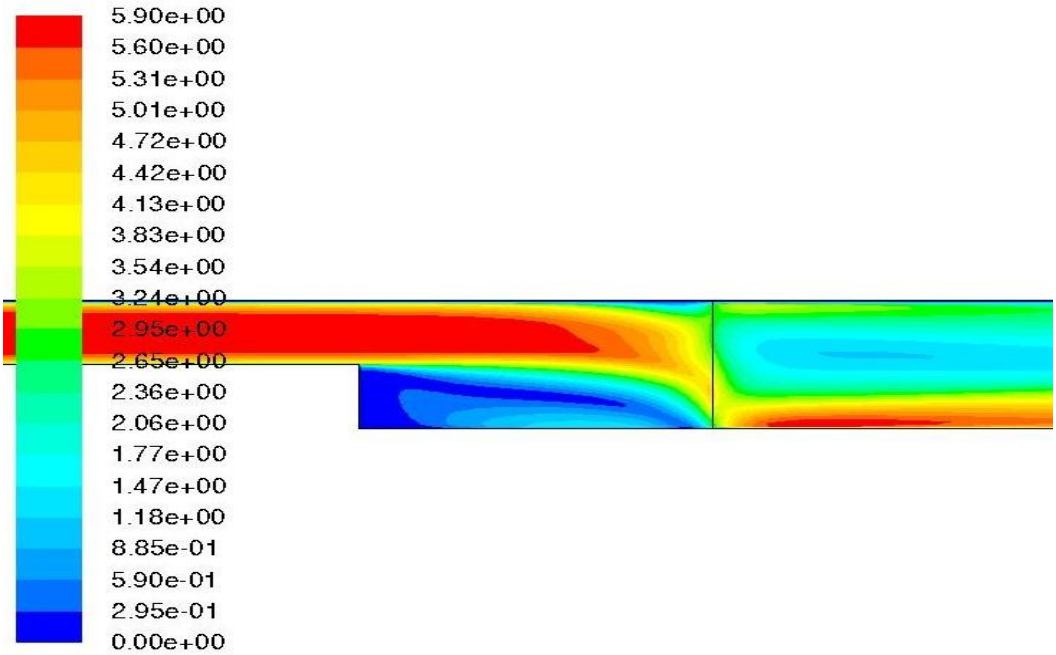

Figure 5.19: Velocity contours for Re = 10000 for filter at X=4.25h

5.5 Velocity field analysis for filter at X=6.75h

This section describes the velocity field when filter is placed further downstream at a distance of "6.75h" from the step. Figures 5.20 and 5.21 show the velocity profiles for Reynolds numbers 6550 and 10000 respectively. At this location, the filter has very little effect on the recirculation zone for both the Reynolds numbers. It can be seen that it agrees well with the trends displayed for the no filter case. The velocity profiles at X=6.25h are in good agreement with the experimental results, as compared to the velocity profiles at X=3.75h with the filter placed at "4.25h" from the step.

The slight deviation at the bottom wall may be due to the wall function effects.

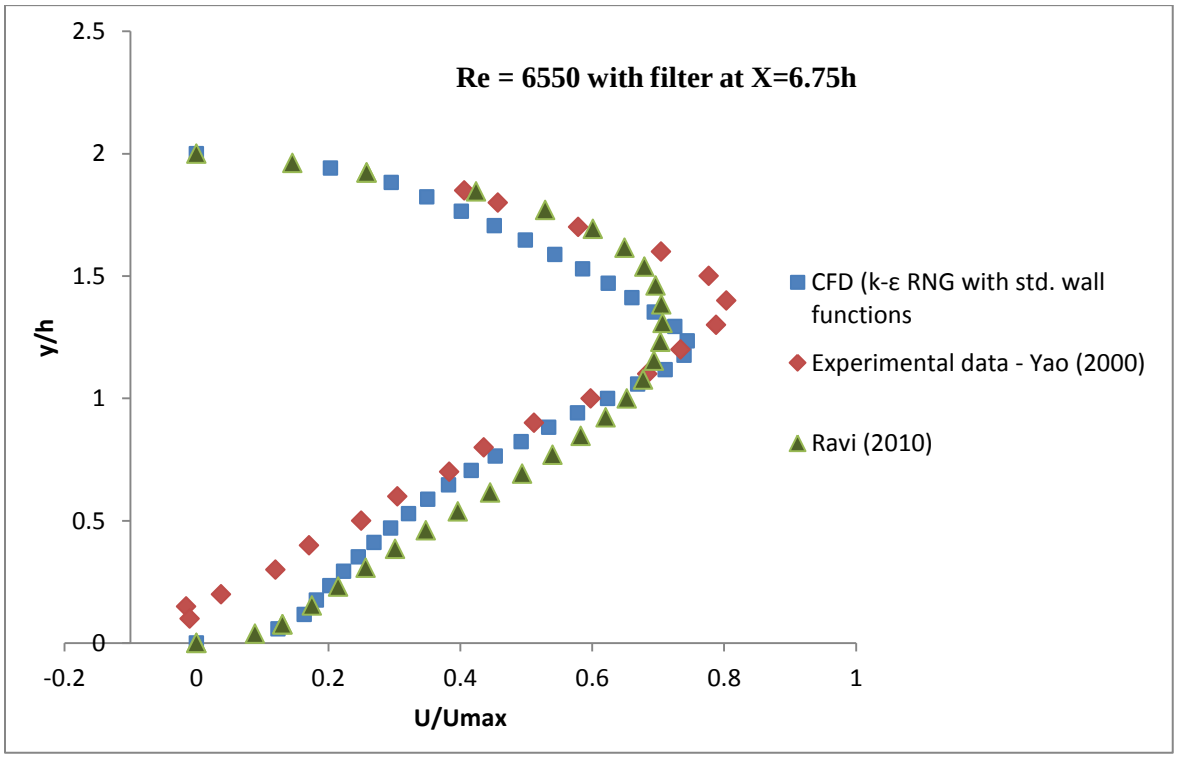

Figure 5.20: Comparison of velocity profiles at X = 6.25h for Re = 6550 with filter at X=6.75h

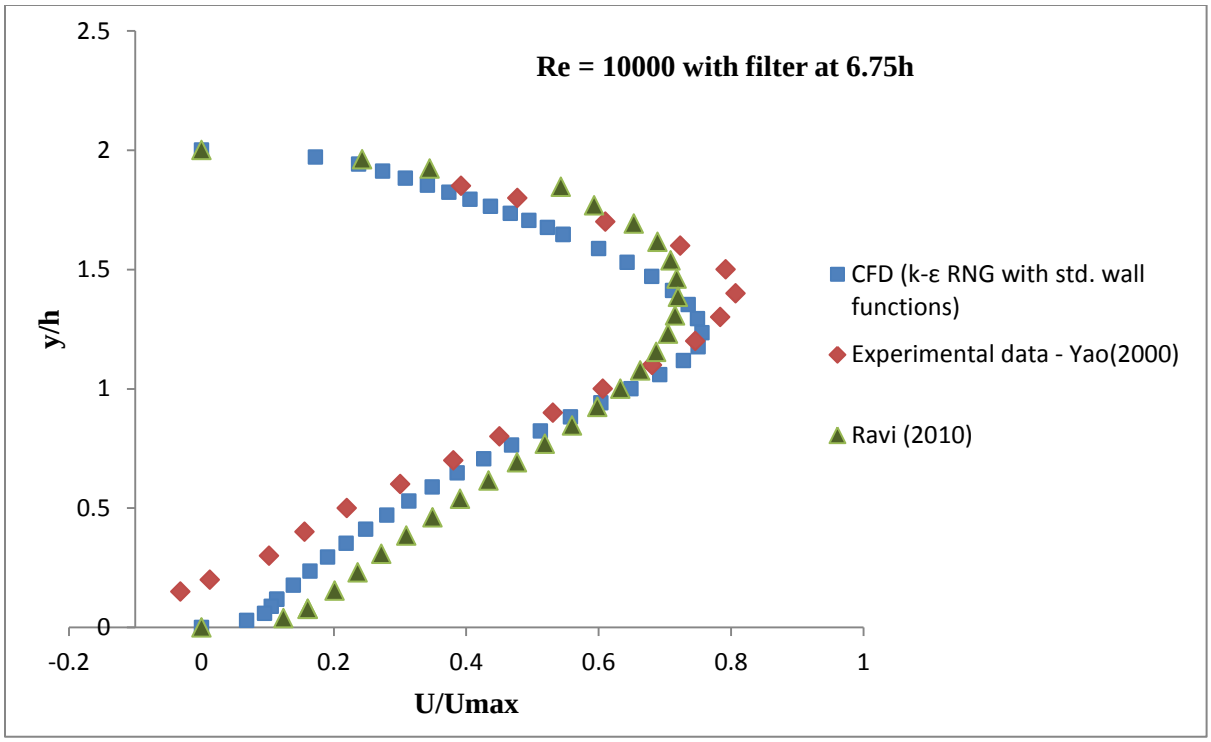

Figure 5.21: Comparison of velocity profiles at X = 6.25h for Re = 10000 with filter at X=6.75h

Figures 5.22 and 5.23 show the velocity contours for Reynolds number 6550 and 10000 at X = 6.25h when filter is placed at 6.75h from the step.

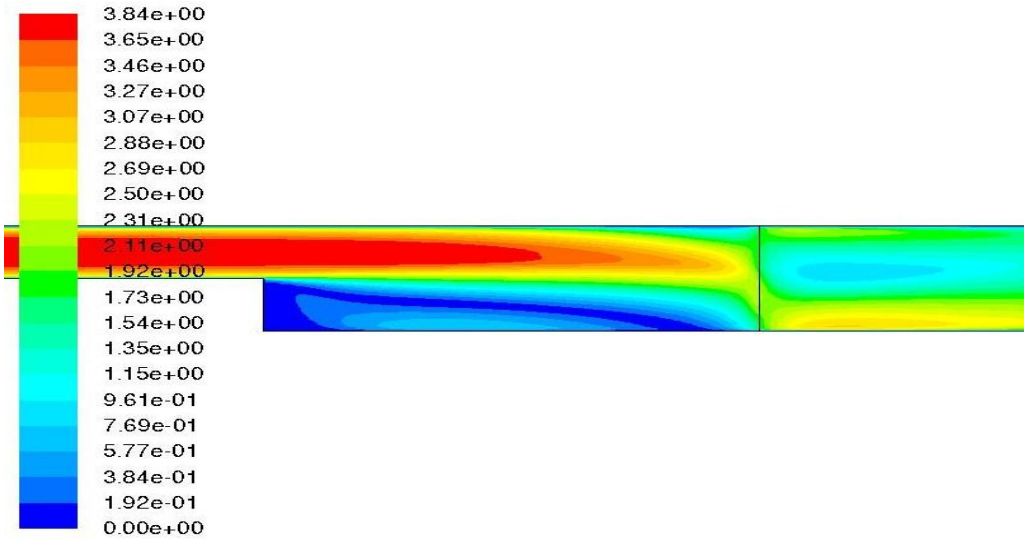

Figure 5.22: Velocity contours for Re = 6550 for filter at X=6.75h

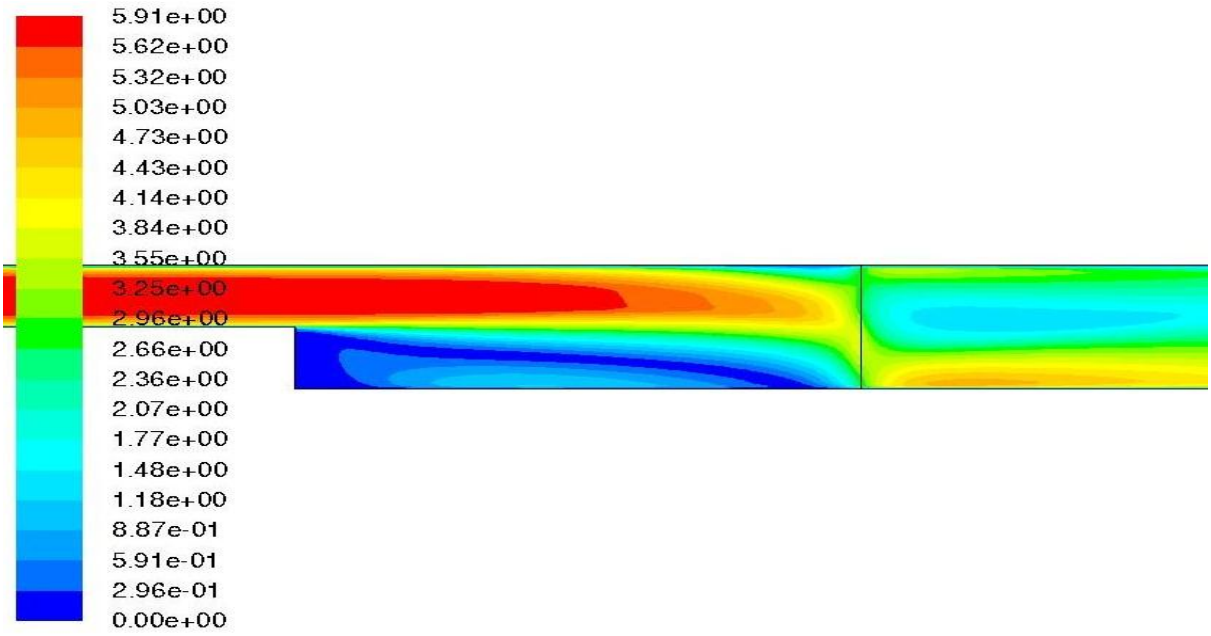

Figure 5.23: Velocity contours for Re = 10000 for filter at X=6.75h

The velocity contours again show a secondary recirculation zone near the top wall just behind the filter.

Figures 5.24 and 5.25 show the comparison of velocity profiles from the current study for “no filter” case and for the “filter case” for Reynolds number 6550 at the distances of “4.25h” and “6.75h” from step. It clearly shows the shift in the maximum velocity towards the channel center when the filter is placed at “4.25h” from the step. There is also a drop in the local maximum velocity because of the presence of the filter.

Very little effect is observed when filter is placed further downstream at “6.75h” from the step. The velocity profiles at this location for “filter case” and “no filter” case are almost identical. There is not much difference in the local maximum velocity as well.

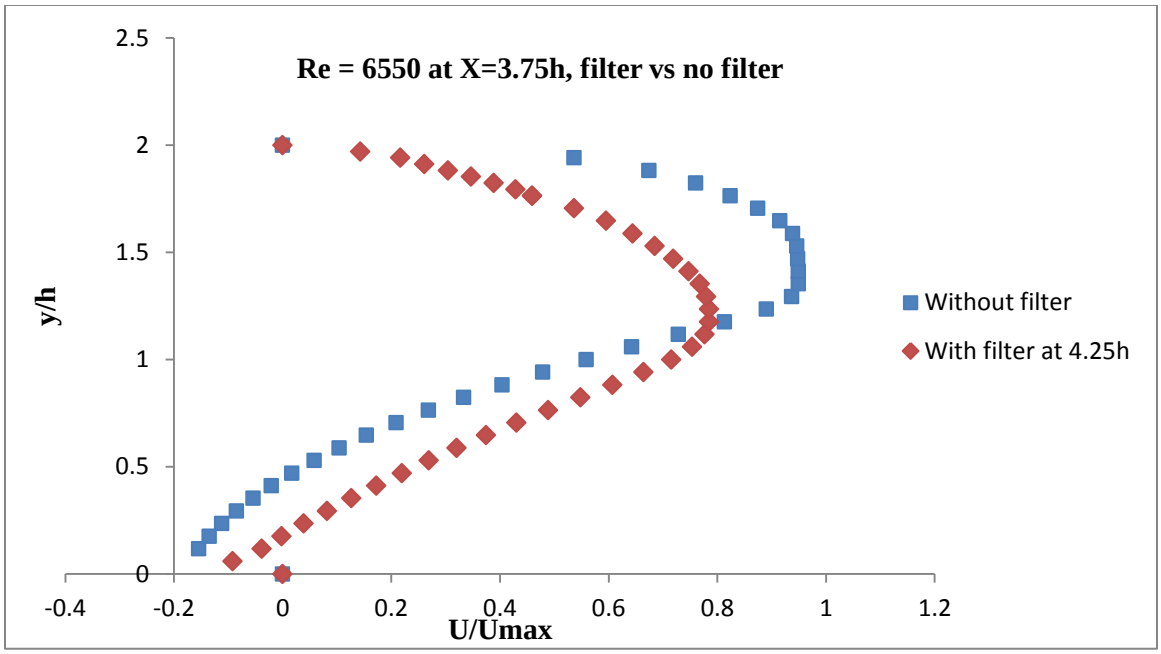

Figure 5.24: Comparison of velocity profiles for "no filter" and "filter" case at X=3.75h for Re = 6550

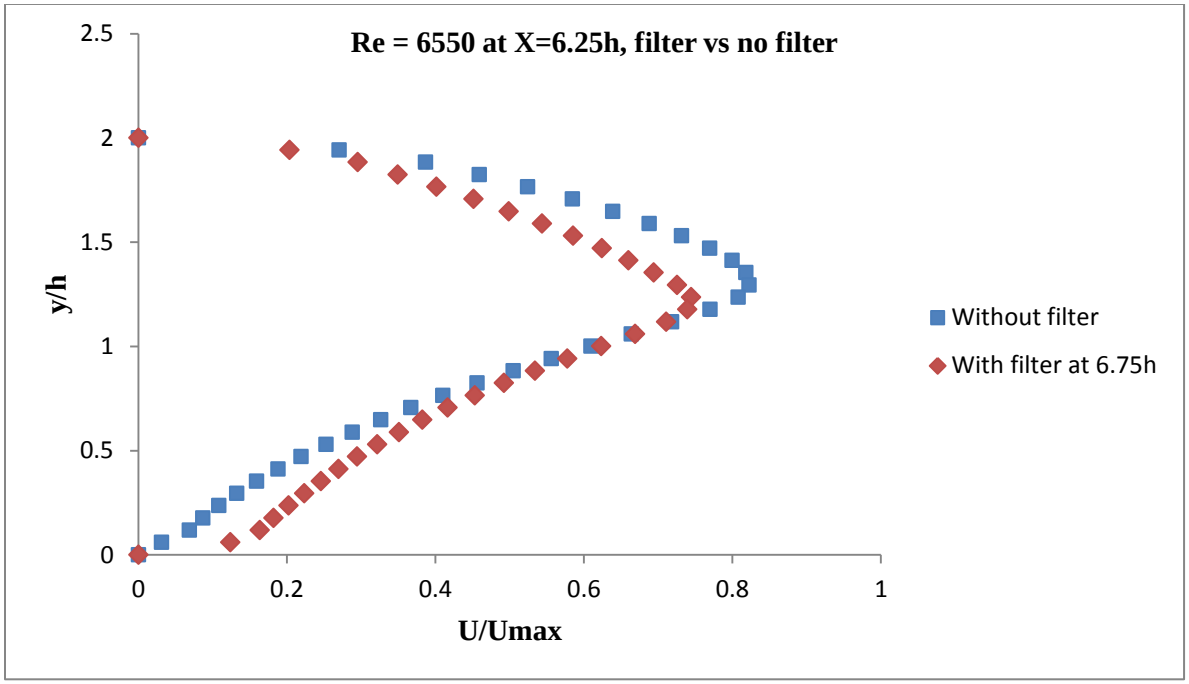

Figure 5.25: Comparison of velocity profiles for "no filter" and "filter" case

at X=6.25h for Re = 6550

5.6 Discrete phase modeling analysis

Steady state discrete phase model of FLUENT is used for studying the behavior of discrete particles when they are injected in a flow. The fundamental area to be analyzed within the domain is the recirculation zone. Monodispersed as well as polydispersed particles are studied for the Reynolds numbers of 6550 and 10000. The number of particles is set to 200 for the entire study and the particles are injected uniformly from the inlet.

5.6.1 Monodispersed particles

10µm and 40µm particles are injected in the domain and the filter is placed at "4.25h" and "6.75h" from the step. Trajectories for particle residence time, which is the time for which the particle is inside the domain before traveling to the filter, and velocities of the particle are plotted.

Particle tracks for filter at X = 4.25h

Figures 5.26 and 5.27 show the trajectories of 10µm particles for particle residence time and velocity for Reynolds number 6550. The legends have units of seconds for residence time and m/s for velocity

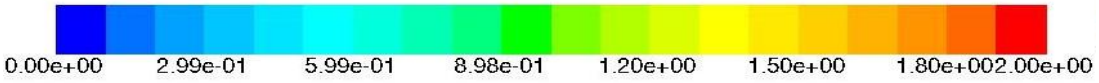

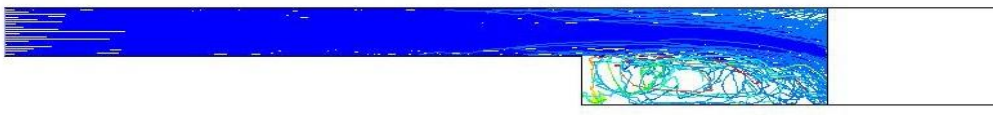

Figure 5.26: Particle residence time for 10µm particles for Re = 6550 with filter at X=4.25h

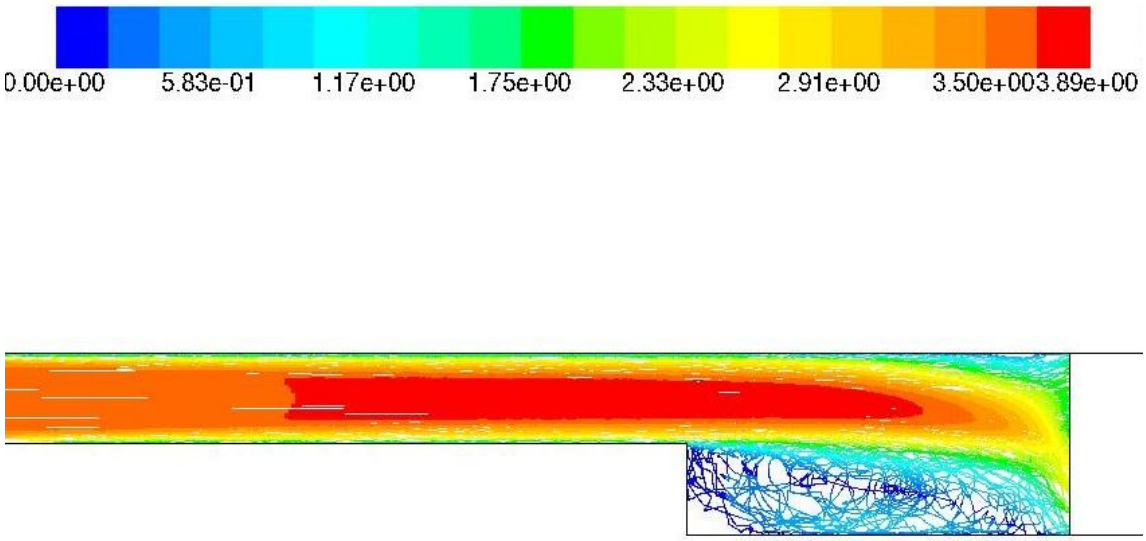

Figure 5.27: Velocity tracks for 10μm particles for Re = 6550 with filter at X=4.25h

Figures 5.28 and 5.29 show the trajectories of 40μm particles for particle residence time and velocity for Reynolds number 6550

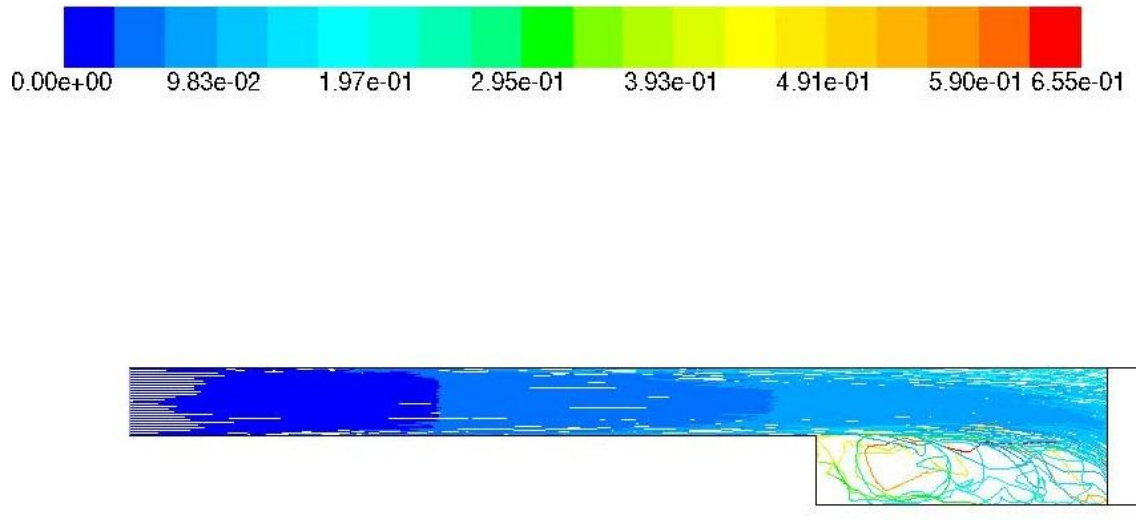

Figure 5.28: Particle residence time for 40μm particles for Re = 6550 with filter at X=4.25h

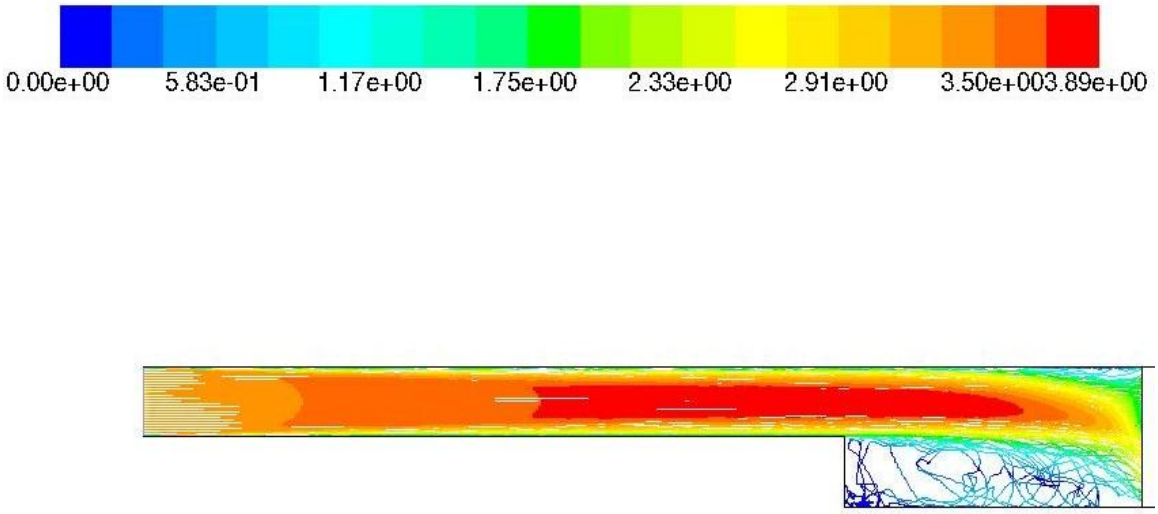

Figure 5.29: Velocity tracks for 40μm particles for Re = 6550 with filter at X=4.25h

It can be seen from Figures 5.25 – 5.29 that for 10μm particles, a large number of particles enter the recirculation zone compared to the case of 40μm particles. The higher Stokes number and thus higher momentum of the 40μm particles allows them to not enter the recirculation zone and directly enter the porous region. A prominent secondary recirculation zone can also be seen near the top wall just behind the filter. The recirculation zone tends to increase the filtration time because of the smaller particles entering the recirculation zone.

Similar results can be seen for Reynolds number 10000. Figures 5.30 – 5.33 show the particle residence time and velocity tracks for 10μm and 40μm particles with the filter located at 4.25h downstream of the step. Compared to Reynolds number of 6550, a smaller number of particles are observed in the recirculation zone. This is due to the fact that as the velocity of the continuous phase is increased, the Stokes number of the dispersed particles increases, and hence more particles directly reach the filter instead of entering the recirculation zone.

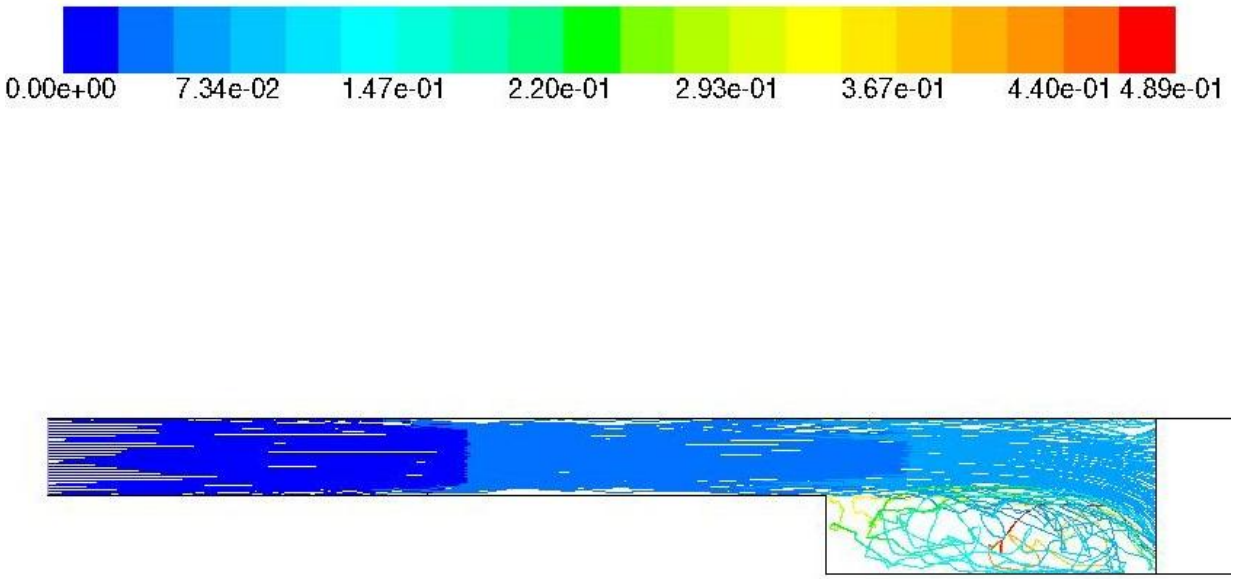

Figure 5.30: Particle residence time for 10μm particles for Re = 10000 with filter at X=4.25h

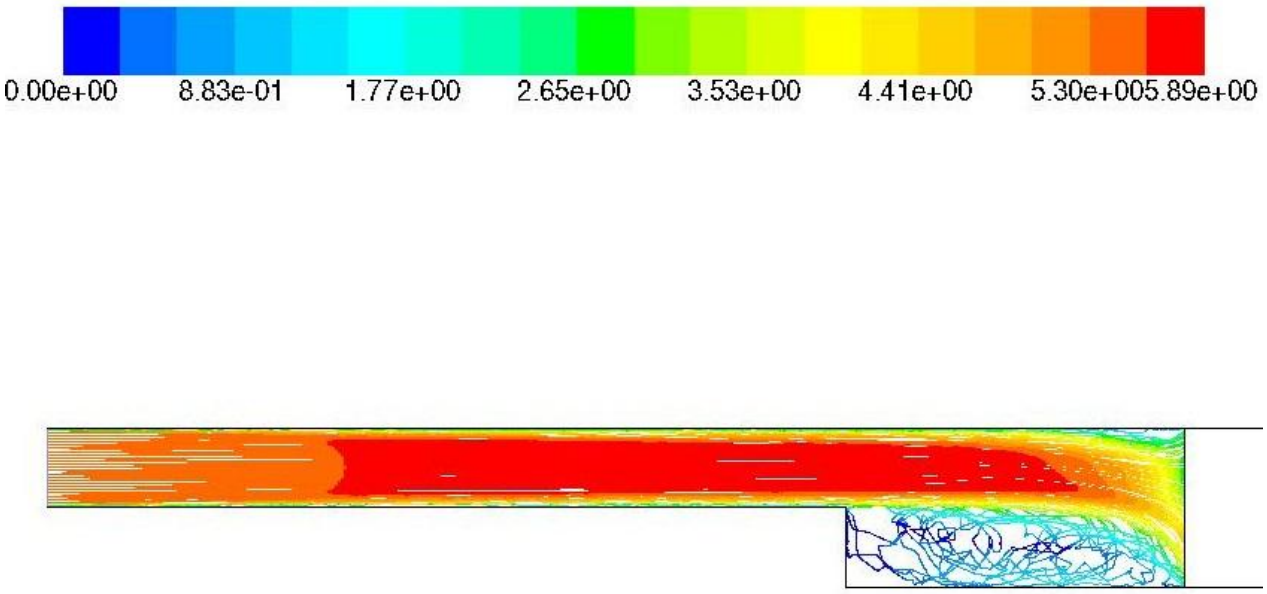

Figure 5.31: Velocity tracks for 10μm particles for Re = 10000 with filter at X=4.25h

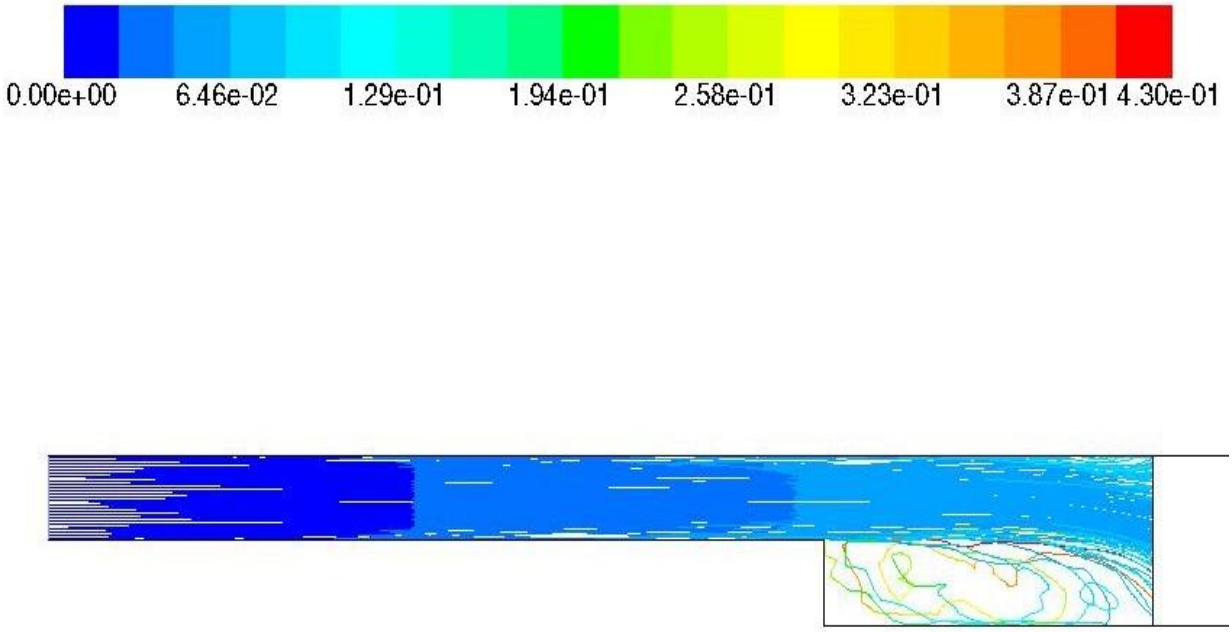

Figure 5.32: Particle residence time for 40μm particles for Re = 10000 with filter at X=4.25h

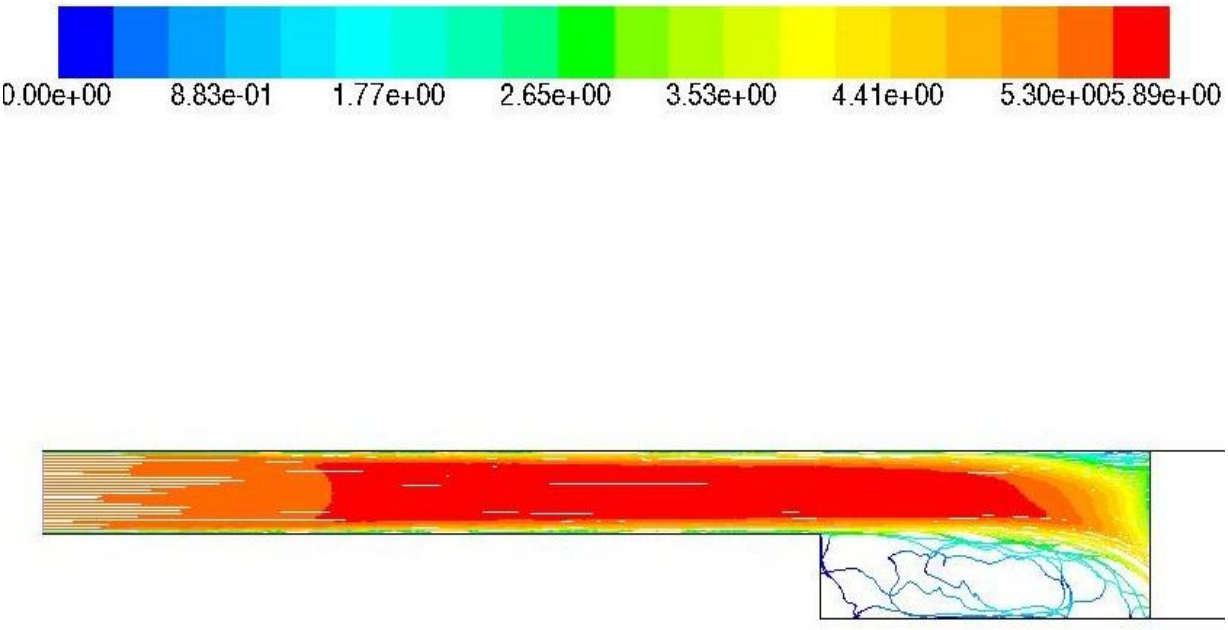

Figure 5.33: Velocity tracks for 40μm particles for Re = 10000 with filter at X=4.25h

Comparing the particle residence time for Reynolds number 6550 and 10000 clearly shows that as Reynolds number increases, the average particle residence time decreases and thus fewer particles are seen in the recirculation zone

Particle tracks for filter at X=6.75h

Figures 5.34 – 5.37 shows the particle tracks for Reynolds number 6550 when filter is placed farther downstream of the step at "6.75h" for 10μm and 40μm particles

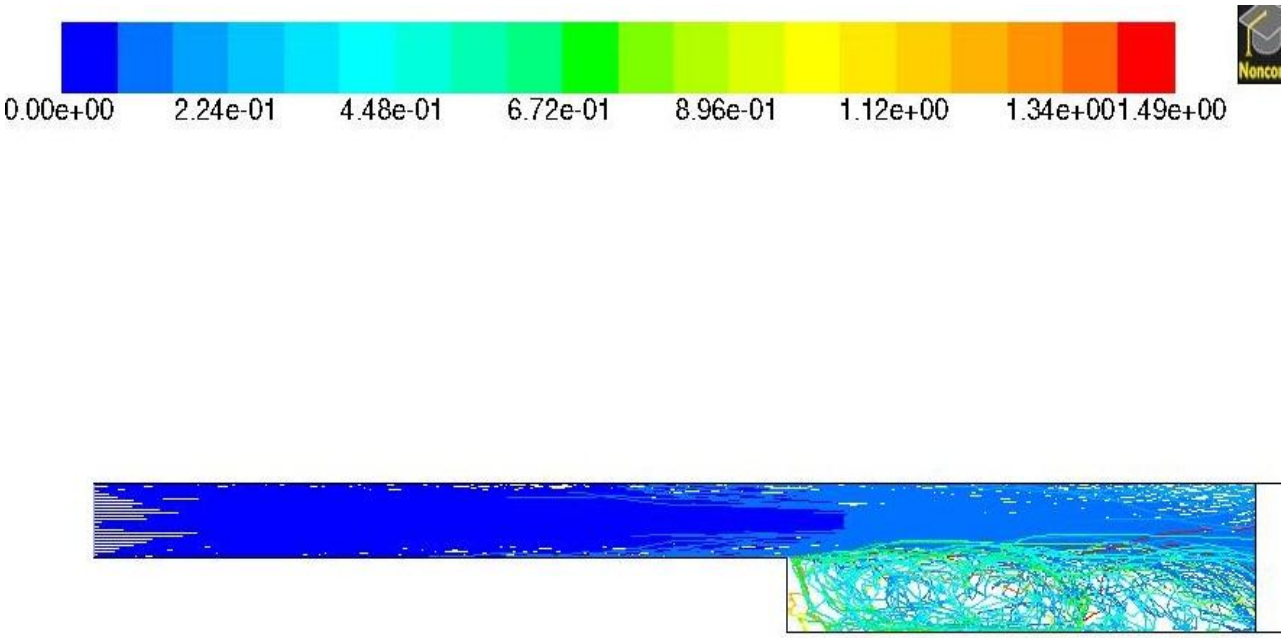

Figure 5.34: Particle residence time for 10μm particles for Re = 6550 with filter at X=6.75h

When the filter is placed farther away from step, there is a prominent increase in the recirculation zone. Due to this, more particles are trapped in the recirculation zone as compared to the previous case, when the filter was placed closer to the step. The longer recirculation zone results in the drop in centerline velocity and a significant momentum loss, thereby reducing the particle Stokes number. This results in more particles being trapped in the recirculation zone.

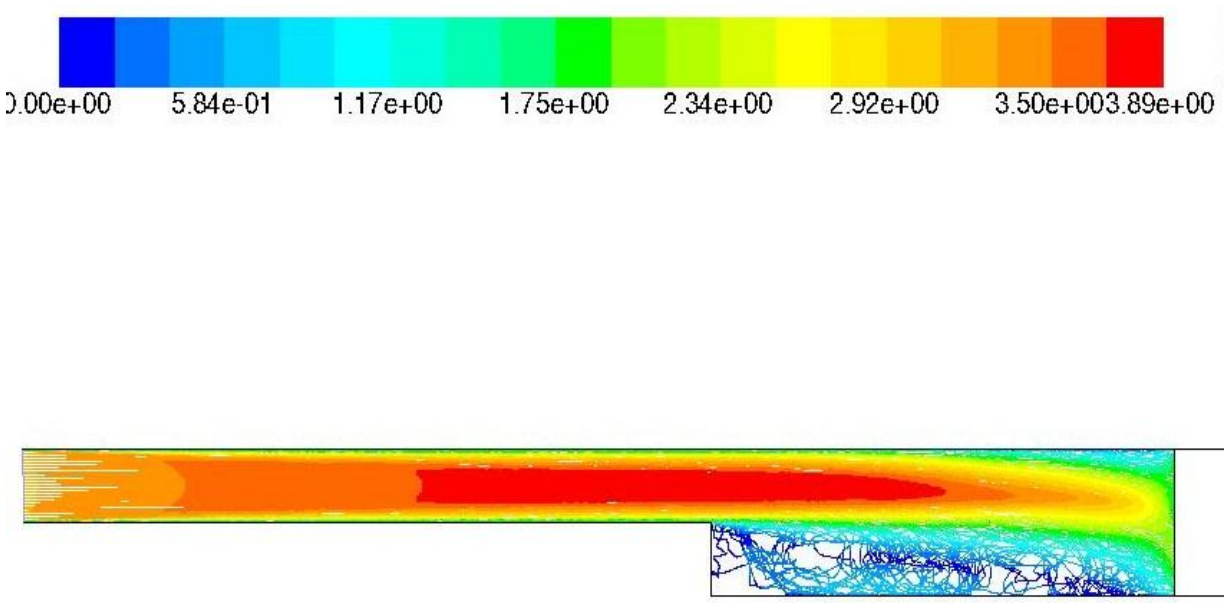

Figure 5.35: Velocity tracks for 10μm particles for Re = 6550 with filter at X=6.75h

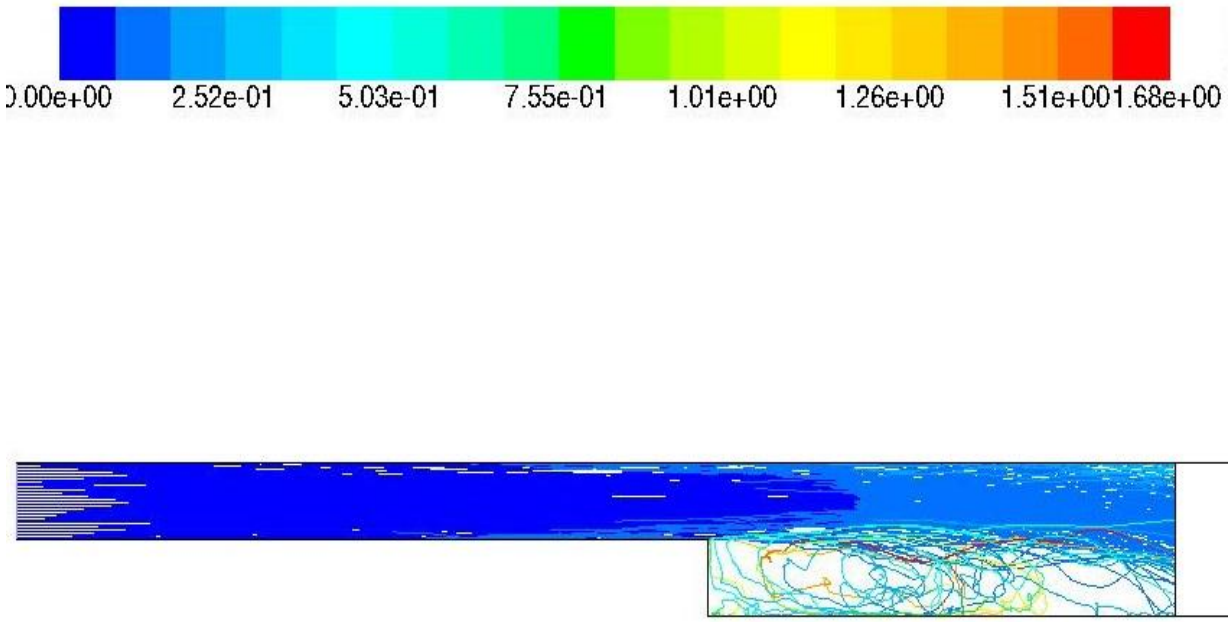

Figure 5.36: Particle residence time for 40μm particles for Re = 6550 with filter at X=6.75h

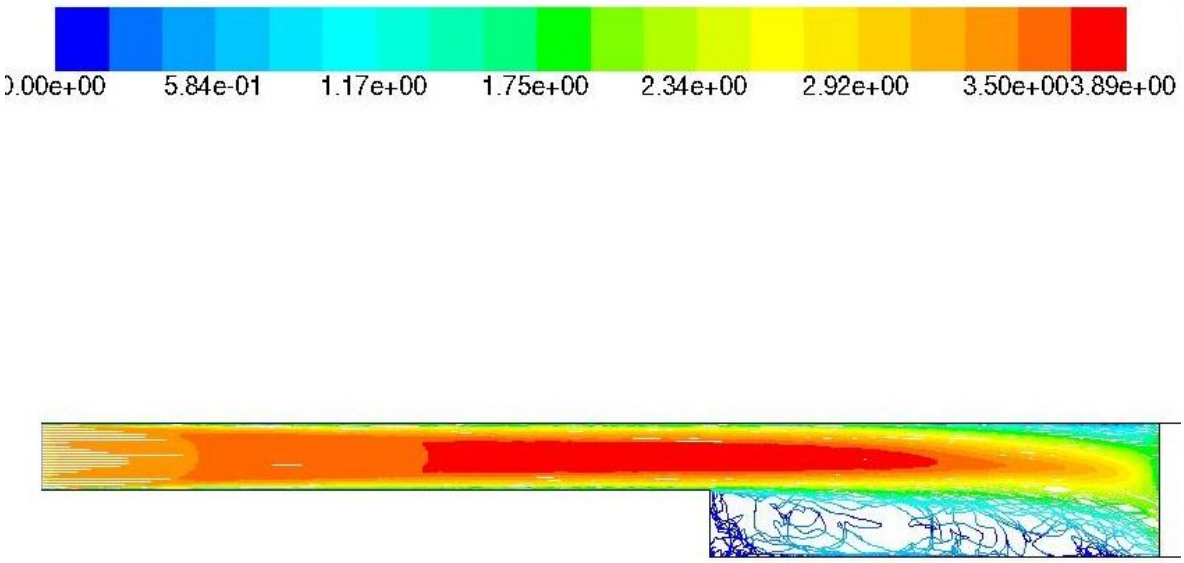

Figure 5.37: Velocity tracks for 40µm particles for Re = 6550 with filter at X=6.75h

Figures 5.38 – 5.41 show the particle tracks for Reynolds number 10000 with filter at "6.75h". Similar trend can be observed as with the filter at "4.25h".

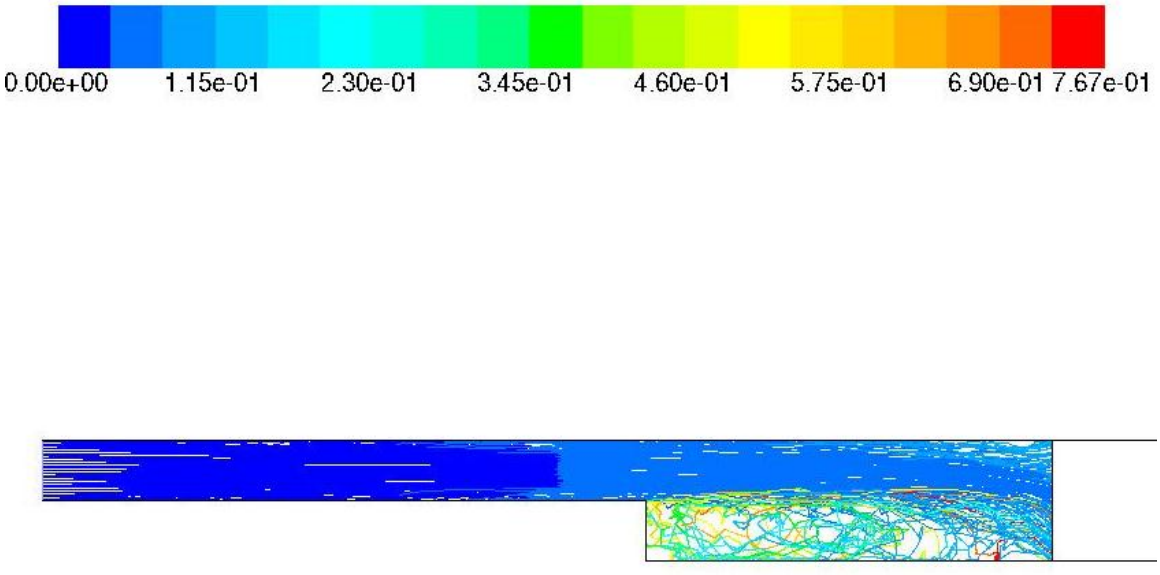

Figure 5.38: Particle residence time for 10µm particles for Re = 10000 with filter at X=6.75h

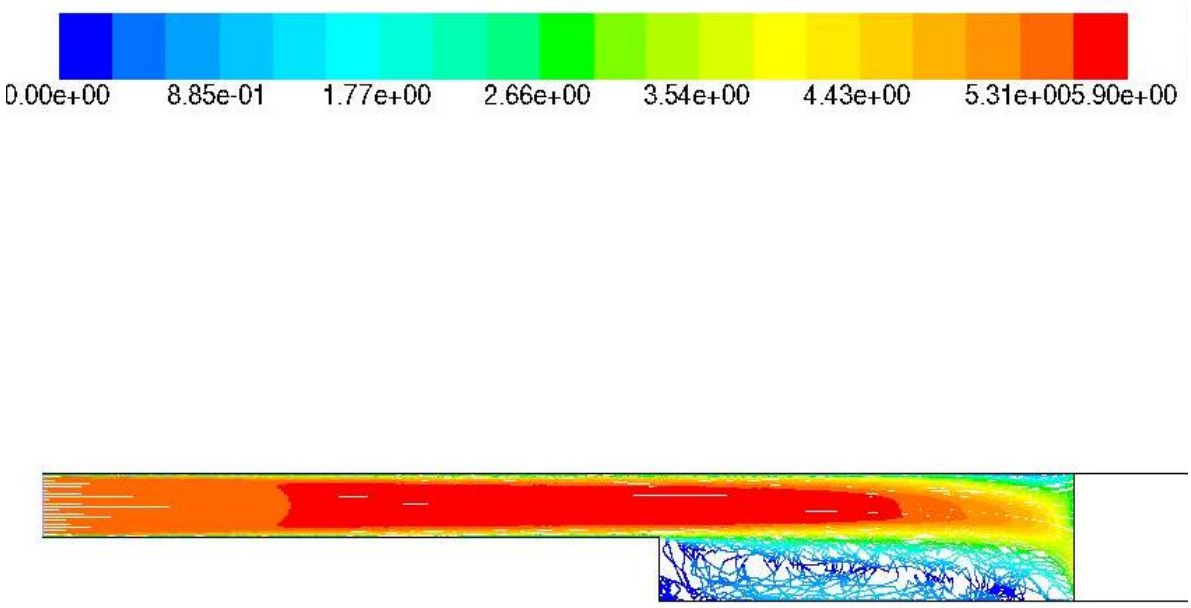

Figure 5.39: Velocity tracks for 10μm particles for Re = 10000 with filter at X=6.75h

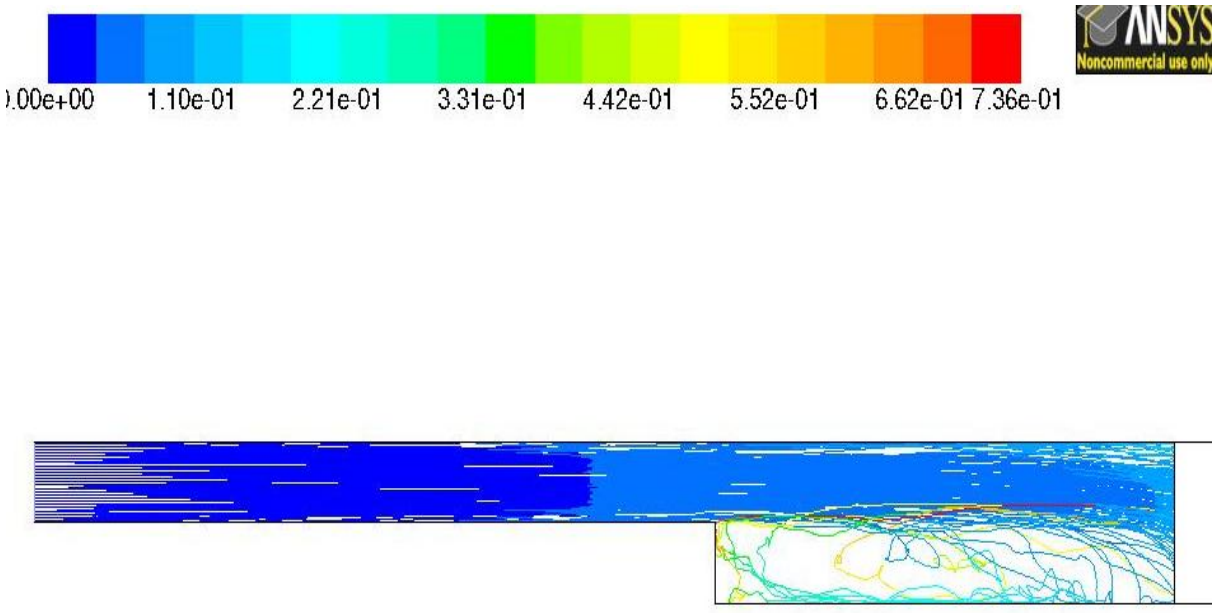

Figure 5.40: Particle residence time for 40μm particles for Re = 10000 with filter at X=6.75h

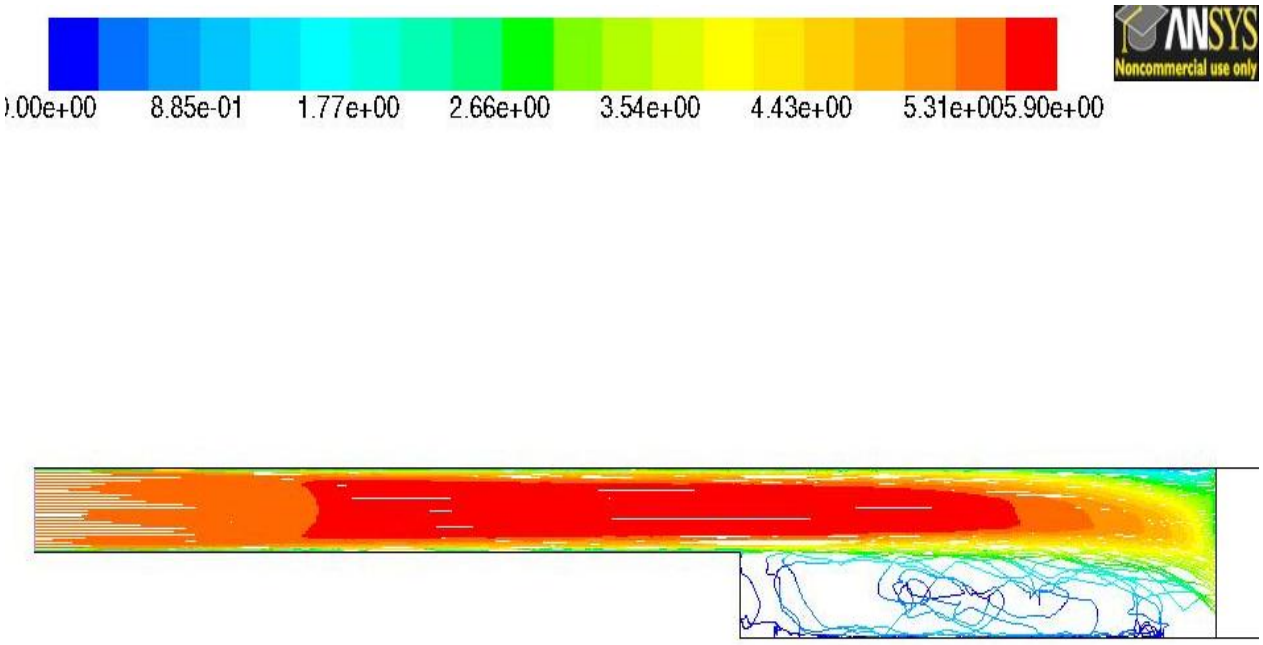

Figure 5.41: Velocity tracks for 40μm particles for Re = 10000 with filter at X=6.75h

Thus when the filter is moved farther downstream at 6.75h from the step, the recirculation zone is significantly increased which results in more particles entering the recirculation zone. The particle momentum is also considerably reduced. The secondary recirculation zone at the top wall also contributes to the momentum loss. Due to this, the particles require a longer time to reach the filter, thereby increasing the total filtration time. In practice, when the filters are used continuously over time, the smaller particles tend to increase the pressure drop across the filter more than large particles, reducing the filter life time. If these particles are permanently trapped in the recirculation zone, the filter life may be increased.

5.6.2 Polydispersed particles

Particles with varying diameters corresponding to varying Stokes numbers are injected together. FLUENT provides two options for variable diameter distribution. The first is the Rossin-Rammler diameter distribution which is based on the assumption that an exponential relationship exists between the particle diameter D, and the mass fraction of particles with diameter greater

than D. As described in FLUENT user manual (2010), the general form of the Rosin-Rammler distribution is given by $Y_d = e^{(\frac{-D}{\overline{D}})^n}$, where Y_d is the mass fraction and $\overline{D}$ is the mean particle diameter. The second type of distribution is the Rosin-Rammler logarithmic distribution, which is based on the natural logarithm of particle diameter. This is only used when the number of diameters is high and the mass flows of smaller particles are much higher in comparison with larger particles. The diameter range, as described in the user manual, for the Rossin-Rammler distribution is from 1μm to the maximum of 200μm. For the current study, the standard Rosin-Rammler distribution is used and the particle Stokes numbers are restricted to the range of 0.1 to 10. Particles with diameter 1μm correspond to Stokes number of about 0.1 while 50μm diameter particles correspond to Stokes number of about 10. Figures 5.42 and 5.43 show the polydispersed particles tracks for Reynolds number 6550 when the filter is placed at "4.25h" and "6.75h' respectively from the step, and Figures 5.44 and 5.45 show the polydispersed particle tracks for Reynolds number 10000 when filter is placed at "4.25h" and "6.75h' respectively from the step. The particle tracks are for the particle diameters ranging from 1μm to 50μm. It can be observed that only the particles with lower Stokes number of 0.1 enter the recirculation zone while the particles with higher Stokes numbers do not enter the recirculation zone and directly reach the filter. As described in the user manual, the Rosin-Rammler distribution predicts fewer particles with lower diameter compared to the particles with higher diameter and hence fewer particles are seen in the recirculation zone.

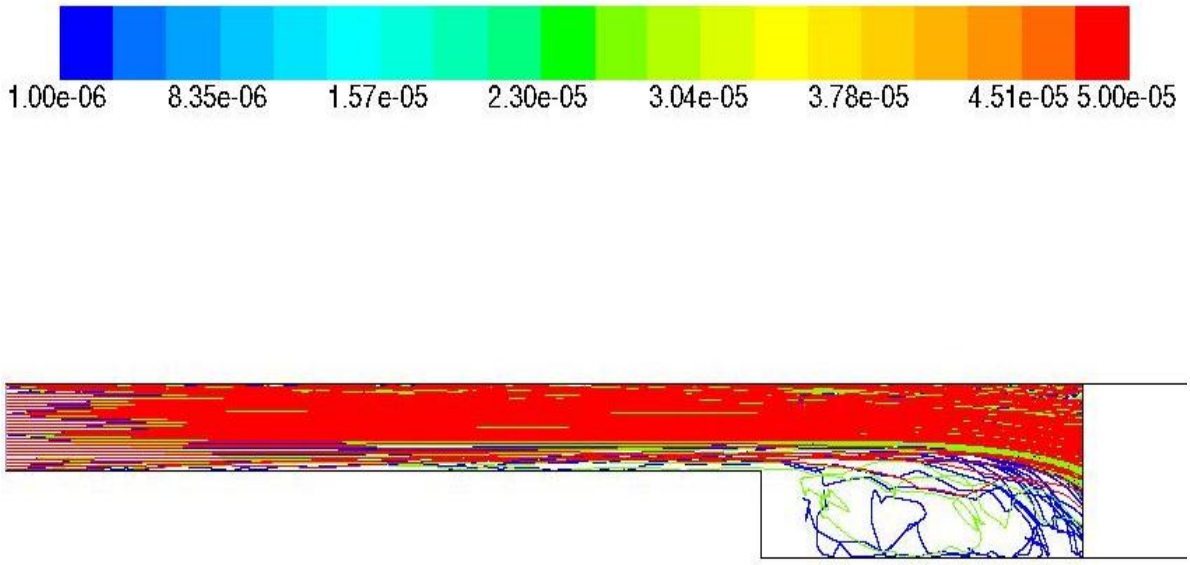

Figure 5.42: Trajectories for polydispersed particles based on diameter for Re = 6550 with filter at X=4.25h

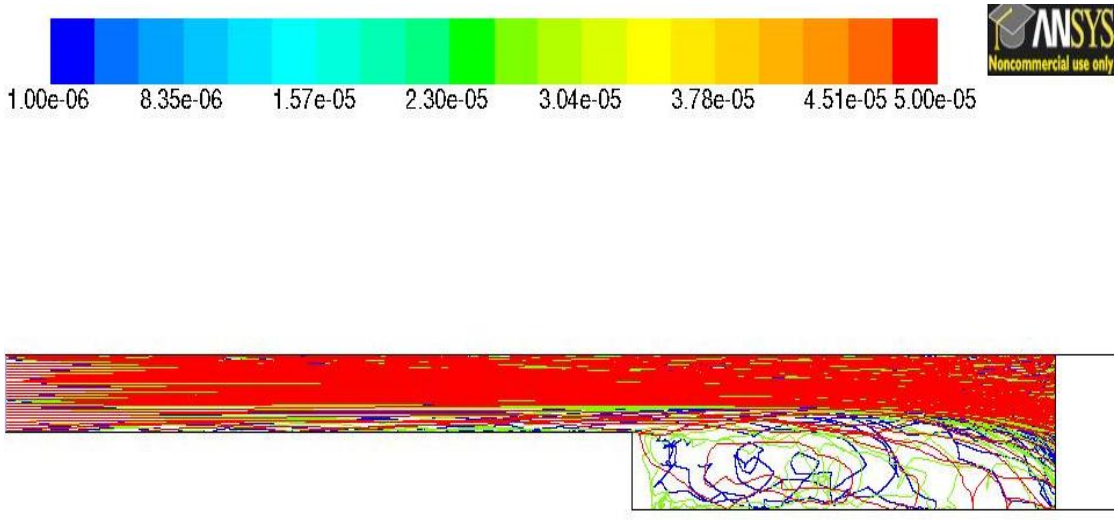

Figure 5.43: Trajectories for polydispersed particles based on diameter for Re = 6550 with filter at X=6.75h

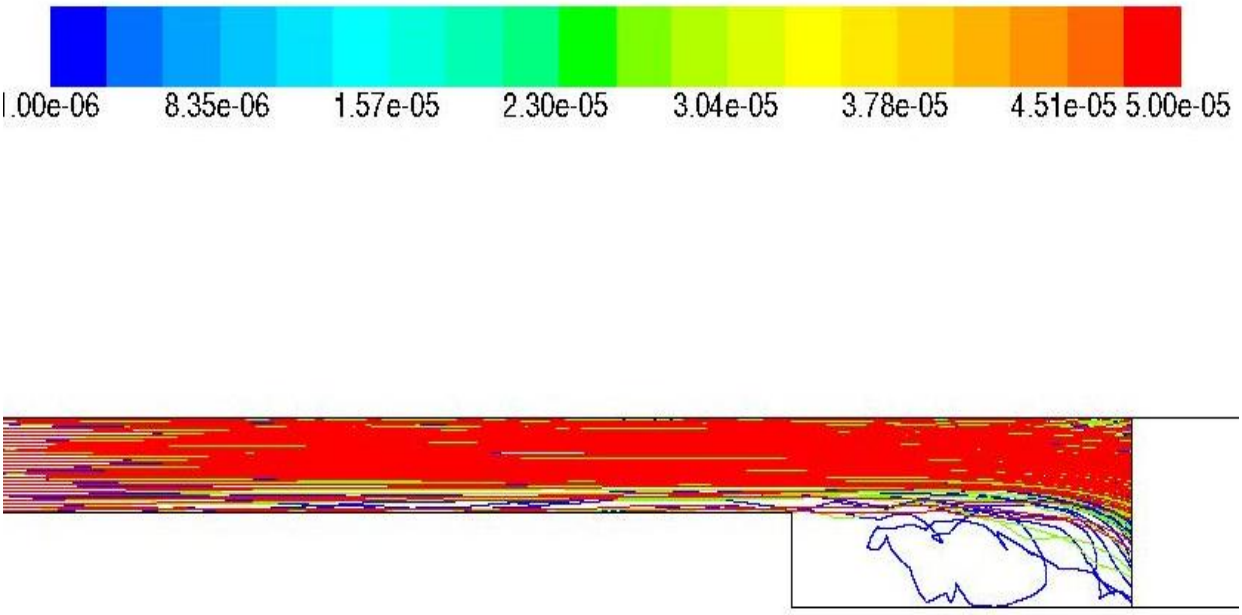

Figure 5.44: Trajectories for polydispersed particles based on diameter for Re = 10000 with filter at X=4.25h

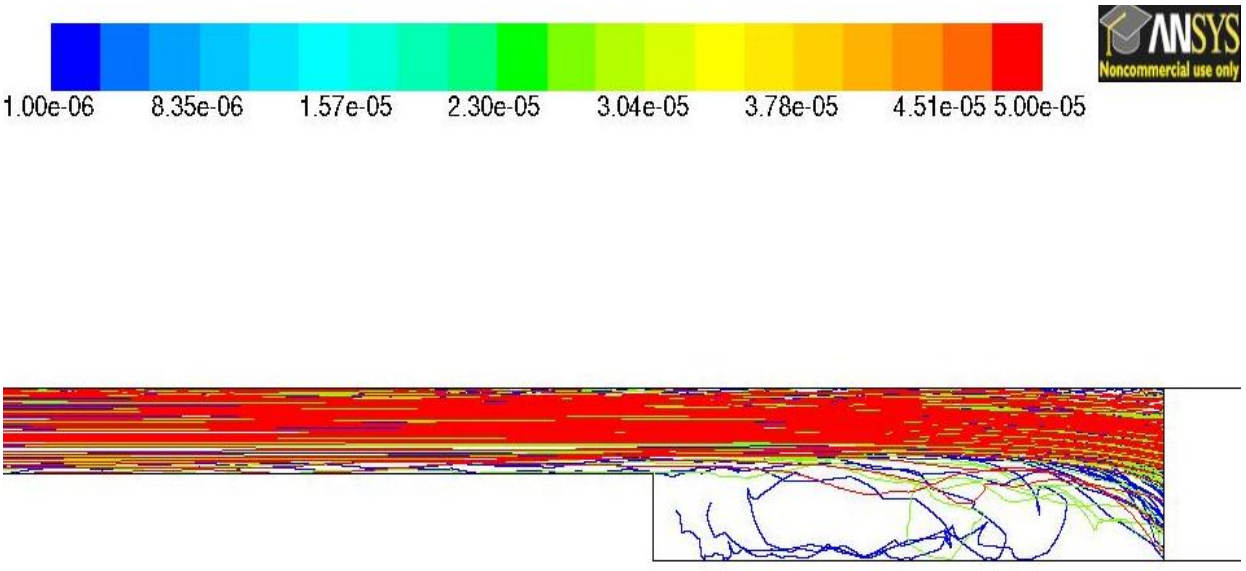

Figure 5.45: Trajectories for polydispersed particles based on diameter for Re = 10000 with filter at X=6.75h

A similar trend can be observed for polydispersed particles as was for the monodispersed particles. As Reynolds number increases, the number of particles in the recirculation zone decreases because of the increase in their Stokes number, and hence the momentum. Also, with the filter moved away from the step, more particles are trapped in the recirculation zone due to the increase in reattachment length and surface area between the recirculation zone and flow above.

Thus the discrete phase model tracks the injected particles in the domain and provides results which are qualitatively similar to the results of Ruck and Makiola (1988)

CHAPTER 6

CONCLUSIONS AND RECOMMENDATIONS

6.1 Conclusions

Two dimensional backward facing turbulent step flow with and without a porous medium was studied for Reynolds numbers 6550 and 10000. Discrete particles with varying diameters and correspondingly, Stokes number, were injected in the domain and the recirculation zone was analyzed. The *k*-ε RNG turbulence model with standard wall functions was used to solve the continuous phase and the discrete phase model of FLUENT was used to study the particle injections. The porous medium was located at two different locations in the domain. The monodispersed particles were tracked according to their residence time and velocity magnitude, while polydispersed particles were tracked according to their diameters.

The following conclusions were drawn:

- The numerical results are in good agreement with the experimental results of Yao (2000) for Reynolds number 6550 and 10000 and the *k*-ε RNG turbulent model with standard wall functions is able to capture the physics of recirculation zone well.
- The recirculation zone is highly affected by the presence of a porous medium, with a great reduction in reattachment length as compared to the case without filter. But when the porous medium is placed further downstream, it has little effect on the recirculation zone.
- The discrete phase model tracks injected particles inside the domain and provide results which are qualitatively similar to the literature.

- The particles get trapped in the recirculation zone depending on their Stokes number. Particles with higher Stokes number, and thus higher diameter and momentum, do not enter the recirculation zone and directly enter the porous region while the particles with lower Stokes number tend to follow the flow and get trapped in the recirculation zone. The particles thus require a longer time to reach the filter, thereby increasing total filtration time.
- The filter location plays a significant role in the behavior of particles. As the filter is moved away from the step, the reattachment length increases and more particles are trapped in the recirculation zone.

6.2 Recommendations for future work

- Porous zone boundary condition can be developed for a pleated filter instead of the porous jump, in order to account for pressure drop across the filter better, thereby increasing the accuracy of the results.
- Large eddy simulation can be performed to improve accuracy of the results.
- Flow field, along with the discrete particles can be studied for transient conditions, prevalent in a real flow field, which requires higher computational time.
- The discrete phase model can only handle particles with low volume fraction and low concentration. Particles with higher concentration which exhibit particle to particle interaction, prevalent in many multi-phase applications, need to be studied by developing new models.

REFERENCES

Abbott, D. E., and Kline, S. J. (1961). *Theoretical and experimental investigation of flow over single and double backward facing steps.* MD-5, Stanford University, Thermosciences Division, Department of Mechanical Engineering, Stanford, CA.

Adams, E. W., and Johnston, J. P. (1988). Effects of the separating shear layer on the reattachment flow structure. Part 1: Pressure and turbulence quantities. *Experiments in Fluids, 6*, 400 - 408.

Adams, E. W., and Johnston, J. P. (1988). Effects of the separating shear layer on the reattachment flow structure. Part 2: Reattachment length and wall shear stress. *Experiments in Fluids, 6*, 493 - 499.

Armaly, B. F., Durst, F., Pereira, J. C., and Schounung, B. (1983). Experimental and theoretical investigation of backward facing step flow. *Journal of Fluid Mechanics, 127*, 473-496.

Assato, M., Pedras, M. H., and De Lemos Marcelo, J. S. (2005). Numerical solution of turbulent channel flow past a backward facing step with a porous insert using linear and nonlinear k-epsilon models. *Journal of Porous Media, 8*(1), 13 - 29.

Bardina, J. E., Huang, P. G., and Coakley, T. J. (1997). *Turbulence modeling validation, testing and development.* NASA Technical Memorandum 110446.

Biswas, G., Breuer, M., and Durst, F. (2004). Backward facing step flows for various expansion ratios for low and moderate Reynolds numbers. *Journal of Fluids Engineering, 126*, 362 - 374.

Chan, E. C., and Lien, F.-S. (2005). Permeability effects of turbulent flow through a porous insert in a backward facing step channel. *Transport in Porous Media, 59*, 47 - 71.

Chandrsuda, C. (1975). *A reattaching turbulent shear layer in incompressible flow.* Ph.D. thesis, Imperial College of Science and Technology, Department of Aeronautics, London, UK.

Chung, K. B., and Sung, H. J. (1996). Control of turbulent separated flow over a backward facing step by local forcing. *Experiments in Fluids, 21*, 417 - 426.

Crowe, C. T., Sommerfeld, M., and Tsuji, Y. (1998). *Multiphase flows with droplets and particles.* CRC Press, Boca Raton, FL

Driver, D. M., and Seegmiller, L. H. (1985). Features of a reattaching turbulent shear layer in divergent channel flow. *AIAA Journal, 23*(2), 163 - 171.

Durst, F., and Tropea, C. (1981). Turbulent backward facing step flows in two dimensional ducts and channels. *Third International Symposium on Turbulent Shear Flows*, pp. 18.1 - 5. University of California, Davis, CA.

Fessler, J. R., and Eaton, J. K. (1997). Particle response in a planar sudden expansion flow. *Experimental, Thermal and Fluid Science, 15*(4), 413 - 423.

Fessler, J. R., and Eaton, J. K. (1999). Turbulence modification by particles in a backward facing step flow. *Journal of Fluid Mechanics, 394*, 97 - 117.

FLUENT user manual (2010). *FLUENT Inc., Lebanon, NH, USA.*

Goldstein, R. J., Eriksen, V. L., Olson, R. M., and Eckert, E. R. (1970). Laminar separation, reattachment and transition of the flow over a downstream backward facing step. *ASME Journal of Basic Engineering, 92*, 732 - 741.

Hanjalic, K., and Kenjeres, S. (2008). Some developments in turbulence modeling for wind and environmental engineering. *Journal of Wind Engineering and Industrial Aerodynamics, 96*, 1537 - 1570.

Johnston, J. P., and Eaton, J. K. (1980). *Turbulent flow reattachment: an experimental study of flow and structure behind a backward facing step.* MD-39, Stanford University, Thermosciences Division, Deptartment of Mechanical Engineering, Stanford, CA.

Jones, W. P., and Launder, B. E. (1972). The prediction of laminarization with a two-equation model of turbulence. *International Journal of Heat and Mass Transfer, 15*, 301 - 314.

Kim, J., and Moin, P. (1985). Application of a fractional step method to incompressible Navier-Stokes equations. *Journal of Computational Physics, 59*, 308 - 323.

Kim, J., Kline, S. J., and Johnston, J. P. (1980). Investigation of a reattaching turbulent shear layer: Flow over a backward facing step. *Journal of Fluids Engineering, 102*, 302 - 308.

Kim, J.-Y., Ghajar, A. J., Tang, C., and Foutch, G. l. (2005). Comparison of near-wall treatment methods for high Reynolds number backward facing step flow. *International Journal of Computational Fluid Dynamics, 19*(7), 493 - 500.

Krishnamoorthy, C. (2007). *Numerical analysis of backward facing step flow preceding a porous medium using FLUENT.* MS Thesis, Oklahoma State University, Stillwater, Oklahoma.

Krishnamoorthy, C., Ravi, K. C., Yao, S., and Chambers, F. W. (2009). Computational investigation of backward facing step flow preceding a porous medium. *Proceedings of the ASME 2009 International Mechanical Engineering Congress and Exposition.* Lake Beuna Vista, Florida. Paper IMECE2009-11228.

Launder, B. E., and Sharma, B. I. (1974). Application of the energy dissipation model of turbulence to the calculation of flow near a spinning disc. *Letters in Heat and Mass Transfer, 1*(2), 131 - 138.

Launder, B. E., and Spalding, D. B. (1974). The numerical computation of turbulent flows. *Computer methods in Applied Mechanics and Engineering, 3*, 269 - 289.

Lee, T., and Mateescu, D. (1998). Experimental and numerical investigation of 2-D backward facing step flow. *Journal of Fluids and Structure, 12*, 703 - 716.

Menter, R. F. (1994). Two equation eddy viscosity turbulence models for engineering applications. *AIAA Journal, 32*(8), 269 - 289.

Poinsot, T. J., and Lele, K. S. (1992). Boundary conditions for direct simulations of compressible viscous flows. *Journal of Computational Physics, 101*, 104 - 129.

Pope, S. B. (2000). *Turbulent Flows.* Cambridge University Press, Cambridge, UK

Ravi, K. C. (2010). *Numerical prediction of particulate flow over backward facing step preceding a filter medium.* MS Thesis, Oklahoma State University, Stillwater, Oklahoma.

Roache, P. (2002). Code verification by the method of manufactured solutions. *Journal of Fluids Engineering, 124*, 4 - 10.

Ruck, B., and Makiola, B. (1988). Particle dispersion in a single-sided backward facing step flow. *International Journal of Multiphase Flow, 14*(6), 787 - 800.

Schlichting, H., and Gersten, K. (2000). *Boundary Layer Theory*. McGraw-Hill, New York, NY.

Sinha, S. N., Gupta, A. K., and Oberai, M. M. (1981). Laminar separating flows over backsteps and cavities. *AIAA Journal, 19*, 1527-1530.

Tani, I., Luchi, M., and Komodo, H. (1961). *Experimental investigation of flow separation associated with a step or groove.* Report No. 364, Aeronautical Research Institute, University of Tokyo, Tokyo, Japan.

Wilcox, D. C. (2006). *Turbulence modeling for CFD.* DCW Industries Inc., La Canada, CA.

Yakhot, V., Orszag, S. A., Thangam, S., Gatski, T. B., and Speziale, C. G. (1992). Development of turbulence models for shear flows by a double expansion technique. *Physics of Fluids, 4*(7), 1510 - 1520.

Yao, S. (2000). *Two dimensional backward facing step flow preceding an automotive air-filter.* Ph.D. Thesis, Oklahoma State University, Stillwater, Oklahoma.

Yao, S., Krishnamoorthy, C., and Chambers, F. W. (2007). Experiments on backward facing step flows preceding a filter. *Proceedings of FEDSM2007, 5th Joint ASME/JSME Fluids Engineering Conference.* San Diego, CA. Paper FEDSM2007-37204.

VITA

Alok Dange

Candidate for the Degree of

Master of Sciences

Thesis: MODELING OF TURBUENT FLOW IN THE RECIRCULATION ZONE DOWNSTREAM OF A BACKWARD FACING STEP PRECEDING A POROUS MEDIUM

Major Field: Mechanical and Aerospace Engineering

Biographical:

Education:

Completed the requirements for the Master of Science in Mechanical and Aerospace Engineering at Oklahoma State University, Stillwater, Oklahoma in December, 2010.

Completed the requirements for the Bachelor of Science in Mechanical Engineering at University of Mumbai, Mumbai, India in 2005.

Experience: Graduate Trainee Engineer at Emerson Network Power India, Pvt. Ltd., from Jan. 2006 to May 2006. Quality Control Engineer at Godrej and Boyce Pvt. Ltd., from May 2006 to May 2007. Teaching assistant at Oklahoma State University in the Department of Mechanical and Aerospace Engineering, from Aug. 2008 to Dec. 2010

Name: Alok Dange Date of Degree: December, 2010

Institution: Oklahoma State University Location: Stillwater, Oklahoma

Title of Study: MODELING OF TURBULENT PARTICULATE FLOW IN THE RECIRCULATION ZONE DOWNSTREAM OF A BACKWARD FACING STEP PRECEDING A POROUS MEDIUM

Pages in Study: 78 Candidate for the Degree of Master of Science

Major Field: Mechanical and Aerospace Engineering

Scope and Method of Study: The current study focuses on flow characteristics and particle motion in the recirculation zone downstream of a backward facing step preceding a porous medium. A two dimensional backward facing step is created in ICEM CFD and the computations are performed in FLUENT. The numerical results for the velocity field are validated with the experimental results and with previous numerical results from the literature. A porous medium is placed at 4.25h and 6.75h from the step, where h is the step height, and its effect on the recirculation zone and the particle motion is analyzed. The Reynolds numbers used are 6550 and 10000. The *k*-ε RNG model with standard wall functions is used for modeling the continuous phase and the discrete phase is modeled using the discrete phase model of FLUENT. For the discrete phase, monodispersed particles of 10μm and 40μm diameter and polydispersed particles ranging from 1μm to 50μm, corresponding to the Stokes number ranging from 0.1 to 10 are used. The particle tracks are studied for the filter at 4.25h and 6.75h from the step.

Findings and Conclusions: It is observed that the numerical results for velocity are in agreement with the experimental results and with previous numerical results from the literature, except for the velocity profiles at X = 3.75h when the filter is placed at 4.25h from the step. This may be due to the porous jump boundary condition used to model the filter. The recirculation zone is highly affected by the placement of the filter at 4.25h from the step. But when the filter is moved farther downstream at 6.75h, the effect on the recirculation zone is negligible. The discrete phase model tracks injected particles inside the domain and provides results which are qualitatively similar to the literature. It is observed that the particles with lower Stokes number, and thus lower momentum, tend to follow the flow and enter the recirculation zone and the particles with higher Stokes number tend to reach the filter directly without entering the recirculation zone. The location of the filter also plays a significant role. When the filter is moved farther downstream at 6.75h, the recirculation zone is increased which results in more particles entering the recirculation zone. The results for the monodispersed and the polydispersed particles agree.

ADVISER'S APPROVAL: Dr. F. W. Chambers